NASA
Technical
Paper
3276

January 1993

Prediction of Rigid Silica Based Insulation Conductivity

Stanley D. Williams
and Donald M. Curry

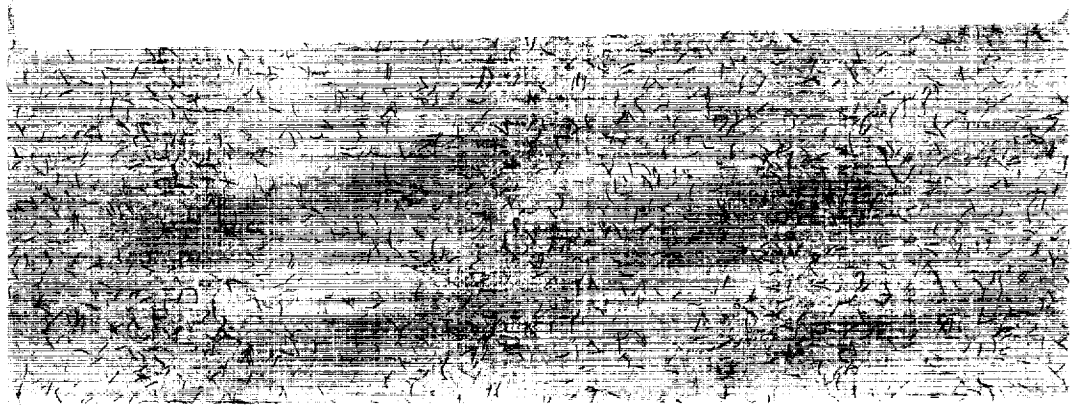

NASA

NASA Technical Paper 3276

1993

Prediction of Rigid Silica Based Insulation Conductivity

Stanley D. Williams
Lockheed Engineering & Sciences Company
Houston, Texas

Donald M. Curry
Lyndon B. Johnson Space Center
Houston, Texas

National Aeronautics and Space Administration

Office of Management

Scientific and Technical Information Program

Contents

Tables

Figures

Appendices

Nomenclature

a	Coefficient defined in Eq. 16 and Eq. 27
ABS	Alumina-boria-silica (Nextel 312)
Al	Alumina
b	Coefficient defined in Eq. 16 and Eq. 27
c	Coefficient defined in Eq. 16
D_{eff}	Effective pore or cell diameter (cm)
$\tilde{D}_{eff}$	Effective cell diameter, as defined by Eq. 10b
$\bar{D}_{eff}$	Effective cell diameter, as defined by Eq. 10c
d_i	Fiber diameter (cm)
d_g	Effective collision diameter of the gas (cm)
F_A	View factor between radiating ends
f_g	Gas conduction correction factor
F_i	Weight fraction of the fiber
$\tilde{F}_i$	Weight fraction of the fiber defined by Eq. 32
k	Conductivity (cal/cm-sec-K)
k_{air}	Conductivity due to air (cal/cm-sec-K)
k_{end}	Conductivity due of the cell end, as defined by Eq. 12d (cal/cm-sec-K)
k_g	Conductivity due to the gas (cal/cm-sec-K)
k_{gas}	Conductivity due to the gas (cal/cm-sec-K)
k'_g	Conductivity of the gas which permeates the structure (cal/cm-sec-K)
k'_{g_w}	Conductivity of the gas which permeates the structure in the weak direction (cal/cm-sec-K)
$k'_{g_{st}}$	Conductivity of the gas which permeates the structure in the strong direction (cal/cm-sec-K)
k_r	Conductivity due to the internal emission and absorption (cal/cm-sec-K)
k'_r	Conductivity of the infrared radiation and absorption in the pore spaces (cal/cm-sec-K)
k'_{rad}	Conductivity of the radiation in the cell as defined by Eq. 28 (cal/cm-sec-K)
k'_{r_w}	Conductivity of the emission in the weak direction (cal/cm-sec-K)
$k'_{r_{st}}$	Conductivity of the emission in the strong direction (cal/cm-sec-K)
k_{side}	Conductivity due of the cell side, as defined by Eq. 12d (cal/cm-sec-K)
k_{solid}	Conductivity due to the solid, as defined by Eq. 12 (cal/cm-sec-K)
k'_{so}	Conductivity of the bulk solid material from which the fibers are made (cal/cm-sec-K)
k'_{so_w}	Conductivity of the fibers in the weak direction (cal/cm-sec-K)
$k'_{so_{st}}$	Conductivity of the fibers in the strong direction (cal/cm-sec-K)
k''_{so}	Composite conductivity of the fibers (cal/cm-sec-K)
L	Thickness of material (cm)
L_{eff}	Effective fiber length (cm)
L_i	Fiber length (cm)
L_M	Effective (mean) cell length (cm)
$£_M$	Effective (mean) cell length in the strong direction (cm)
M	Molecular weight

N	Avogadro's number (molecules/gmole), also absorption cross section per unit mass (cm^2/gm)
n	Exponent or number of terms in series as defined in Eq. 16
N′	Density scaled absorption cross section (cm^{-1})
N_i	Total number of fibers per unit mass (fibers/gm)
n_i	Index of refraction for fiber i
N'_{st}	Number of fibers in the strong direction
N_T	Total fiber count (fibers/gm)
N'_w	Number of fibers in the weak direction
P	Pressure (atm), also Backscatter cross section per unit mass (cm^2/gm)
P′	Density-scaled backscatter cross section (cm^{-1})
P_0	Reference pressure for one atmosphere; equivalent to 1 when pressure is in atm
R	Universal gas constant (cm^3-atm)/(gmole)(K)
S	Solid volume fraction
S_i	Material solid volume fraction for fiber i
Si	Silica
SiC	Silicon Carbide
T	Temperature (K)
T′	Temperature, as defined by Eq. 20b (K)
u	Wall absorption coefficient
V_i	Volume fraction for each fiber
Z	Fraction of radiation stopped at each wall

Greek

β	Emissivity or emission scaling factor
ε	Emissivity
Γ	Emission term
Γ_ι	Emission term for the fiber
η	Conduction efficiency of fibers
η'_{st}	Conduction efficiency in the strong direction
η'_w	Conduction efficiency in the weak direction
$\eta_{g_{st}}$	Scaling factor for gas conduction in strong direction, Eq. 22
η_{st}	Solid conduction in the strong direction
η_w	Solid conduction in the weak direction
θ	Angle between fibers, 100°
λ	Mean free path, cm
μ	Viscosity of gas (cm^2/sec), also component of f_g as defined by Eq.20a
ν	Component of f_g as defined by Eq. 20a
ξ	Temperature compensation factor for f_g as defined by Eq. 20b
ρ	Density of gas (gm/cm^3)
ρ_i	Fiber density (gm/cm^3)
ρ_T	Total density of the insulation (gm/cm^3)

σ	Stefan-Boltzmann constant (cal/cm^2-sec-K)
σ_{st}	Tensile strength in the strong direction (N/m^2)
σ_w	Tensile strength in the weak direction (N/m^2)
σ'_w	Normalized tensile strength in the weak direction as defined by Eq. 11b
τ_{st}	Solid volume power in the strong direction as defined by Eq. 12c
τ_w	Solid volume power in the weak direction as defined by Eq. 12c

Subscripts

i	Belonging to the set containing the materials (fibers)
st	Strong direction
w	Weak direction

ABSTRACT

A method is presented for predicting the thermal conductivity of low density, silica based fibrous insulators. It is shown that the method can be used to extend data values to the upper material temperature limits from those obtained from test data. It is demonstrated that once the conductivity is accurately determined by the analytical model the conductivity for other atmospheres can be predicted. The method is similar to that presented by previous investigators, but differs significantly in the contribution due to gas and internal radiation.

INTRODUCTION

A nonlinear least squares technique was used to determine the effective thermal conductivity of an insulating material from a transient thermal response test.[1] In this analysis it was assumed that the material would have several in-depth thermocouples, with constant surface temperature at constant pressure test conditions. The objective of this analysis was to calculate coefficients to a polynomial expression representing the thermal conductivity at the specified pressure condition that was valid over the test temperature range. A cubic was selected since this would permit the approximation of the conductivity due to conduction of the solid, collision of the gas molecules with the cell walls in the porous media, and internal radiation. The disadvantages of this approach are that it requires accurate placement of the thermocouples, thermal/vacuum test facilities, sophisticated data acquisition equipment, and that it cannot be used for predicting conductivity values at other conditions. The advantages are that it is relatively inexpensive, reliable, can produce results in a short time frame, and agrees well with data obtained from conventional test techniques.

Other techniques have been developed that are more analytical in nature. In 1971 Dresher and Pike[2] proposed a model that was a linear function of solid, gas conduction and radiation. This model considers the solid volume fraction of the fiber bundle and uses this to proportion the contribution to each component.

In 1975 Klett[3] developed a model and computer program that would aid in the design of an insulating material. Through the use of this program, the analyst can investigate the effects of density, cell size, and cell structure. This model may be classified as a parallel network model, as opposed to the series network model proposed by Dresher and Pike.[2] This model also assumes that the conductivity can be segregated into three components: solid conduction, gas conduction, and radiation. The gas conduction term is expressed as a function of the effective cell size and mean free path of the gas. The main disadvantage in using this method is the use of an absorption coefficient for the material used for predicting the contribution due to radiation. The data for the absorption coefficient is not readily available, which makes conductivity relatively difficult to determine. Data for material properties and gases were entered in tabular form.

In 1977 Striepens[4] presented a series network model used for approximating the thermal conductivity of refractory blown fibrous insulations. It was assumed that the solid conductivity could be considered a constant. The gas conduction term, similar to most techniques, was a function of the effective pore size and mean free path of the gas. The radiation term was expressed as a function of backscattering cross section, thickness of the insulation, and the emittance of the bounding surfaces. The main disadvantages of this method were due to a poor estimation to the solid conductivity, and radiation contribution dependent on material thickness and backscattering cross section. A subsequent modification removed the dependence on material thickness. However, backscattering data is not readily available and requires detailed experimental data collection and analysis.

In 1985 Stewart and Leiser[5] presented a technique for characterizing rigid fibrous reusable insulation materials based on the model proposed by Dresher and Pike.[2] The advantage of this approach is in developing the model from morphological data to establish parameters for predicting conductivity values. In particular, they were able to approximate the solid conductivity in two directions based on the measured tensile strength. The gas conduction term was a function of the effective pore size, and mean free path of the gas. The radiation term, based on the derivation by Dresher and Pike,[2] is a function of effective pore size and solid volume fraction.

The initial effort in this investigation was based on a computer program supplied by Stewart and Leiser.[5] The primary approach in the proposed method, as distinct from previous methods are: the use of solid conductivity approximation in the weak direction proposed by Stewart and Leiser,[5] but modified for predictions in the strong direction; a correction term for gas conduction; and the characterization of the radiative contribution from the separate components that constitute the insulation material. This permits the effective emittance for each class of fibers to be determined independently of other fiber components.

DISCUSSION

The study of heat flow through porous insulating materials has been an ongoing effort for over 100 years. This effort has included experimental and analytical investigations used to develop the theory and application for thermal insulation. Good insulators are classified into different categories, but for thermal modeling the most convenient classification is based on the physical structure of the insulator. Fibrous insulations can be made of loose or bonded fibers in either a random or preferential orientation, i.e., fiberboard, mats, and wools. Granular insulations can be in either a loose or bonded form, i.e., pumice, sand, diatomaceous powders, and microspheres. Cellular insulation is a continuous solid containing either open or closed cells. Closed cells are completely enclosed and are highly resistant to air movement, i.e., wood and cork. Open cells permit the movement of gas more readily than closed cells, and the voids are connected and allow gases to flow through the material. Fiber reinforced foam, Min-K, LI-900, and FRCI-12 are examples of materials made from granular powders and fibers. LI-900 is a porous material composed of silica fibers, while FRCI-12 is a porous material composed of silica and alumina-boria-silica (Nextel) fibers.

The proposed mathematical model is similar to that presented by Dresher and Pike.[2] It is assumed that the conductivity can be expressed as a linear function of the contributions due to solid, gas, and radiation:

$$k = k_{so} + k_g + k_r \quad , \tag{1}$$

where k_{SO} is the conductivity due to the solid, k_g is the conductivity due to the gas, and k_r is the conductivity due to the internal radiation and absorption. This can be rewritten as

$$k = S\,k'_{so} + (1-S)\,k'_g + S^{-1}\,k'_r \quad , \tag{2}$$

where S is the solid volume fraction. This expression treats the insulating material as a composite in which a solid phase interacts with a gaseous phase and radiative phase to yield an overall performance in the transmission of heat. In this formulation, the three modes of heat transfer which are of importance at high temperatures are clearly separated. The functions which depend on the solid fraction, S, go very roughly as S, 1 - S, and 1/S, depending on the geometric structure of the porous material. k'_{SO} is the conductivity of the bulk solid material from which the fibers are made; k'_g is the conductivity of the gas which permeates the

structure; and $k'_r \sim 4d\sigma\varepsilon T^3$ is the thermal conductivity of the infrared radiation and absorption in the pore spaces, with d representing the pore size, fiber diameter or other morphological consideration of the insulating material. Several other investigators have presented expressions similar to Eq. 2, see for example references 2 - 6.

EFFECTIVE CELL SIZE

The derivation for the parameters defining the effective cell size is taken from Stewart and Leiser [5] and is repeated for continuity. The concept is to define the insulation material based on fiber characteristics and pore size from measured physical properties of the fibers that go into defining material structure. It is assumed that each fiber can be represented as a cylinder. The total number of fibers per unit mass can be defined as

$$N_i = \frac{F_i}{\frac{1}{4}\pi d_i^2 L_i \rho_i}, \qquad i \in \{\text{Si, Al, ABS, SiC}\}, \tag{3a}$$

where F_i denotes the weight fraction of the fiber, ρ_i the fiber density, L_i the fiber length, and d_i is the diameter for each respective fiber. The abbreviations for the fibers are Si for silica, Al for alumina, ABS for alumina-boria-silica (Nextel 312), and SiC for silicon carbide. In particular for silica the representation given in Eq. 3a would be

$$N_{Si} = \frac{F_{Si}}{\frac{1}{4}\pi d_{Si}^2 L_{Si} \rho_{Si}} \quad . \tag{3b}$$

The total fiber count is the simple sum

$$N_T = \sum_i N_i \quad , \qquad i \in \{\text{Si, Al, ABS, SiC}\} \quad . \tag{4}$$

The effective fiber length may be calculated as

$$L_{eff} = \frac{1}{N_T} \sum_i N_i L_i \quad , \qquad i \in \{\text{Si, Al, ABS, SiC}\} \quad , \tag{5}$$

The solid volume fraction of each material can be calculated from

$$S_i = \frac{F_i \rho_T}{\rho_i} \quad , \qquad i \in \{\text{Si, Al, ABS, SiC}\} \quad , \tag{6}$$

where ρ_T is the total density of the porous insulation. The solid volume fraction is then defined as

$$S = \sum_i S_i \quad , \qquad i \in \{\text{Si, Al, ABS, SiC}\} \quad . \tag{7}$$

This permits the total volume for each fiber component to be defined by

$$V_t = S_t / S \quad , \qquad t \in \{\mathrm{Si, Al, ABS, SiC}\} \quad . \tag{8}$$

Using the definition given by Stewart and Leiser,[5] the effective pore or cell diameter may be calculated as

$$D_{eff} = \sqrt{\frac{S}{\frac{1}{4}\pi \rho_T L_{eff} N_T}} \quad , \tag{9}$$

although this may also be considered equivalent to the effective fiber diameter.

The effective (mean) length of the cell may be approximated by

$$L_M = \frac{D_{eff}}{\sqrt{S/3}} \quad . \tag{10a}$$

In contrast, Klett [3] defined the interior cell dimension, L_M, as

$$L_M = \tilde{D}_{eff} \, (1-S)^{1/3} \, , \tag{10b}$$

where $\tilde{D}_{eff}$ is the effective cell diameter, and S is the effective volume fraction defined in a manner similar to Eq. 6, *i.e.,* the ratio of the bulk density to the fiber density.

Striepens defined the effective pore size as

$$L_M = \frac{\pi \overline{D}_{eff}}{4S} \, , \tag{10c}$$

where this effective diameter is the ratio of the mean square diameter to the mean diameter of the fibers, and S as the ratio of the bulk density to the fiber density. For LI-900 and LI-2200, this was effectively d_{Si}.

To obtain a better concept of what we are attempting to model, it is interesting to look at the material in more detail using Scanning Electronic Microscopy (SEM). Figure 1 shows microphotographs of some of the fibrous insulation materials used in this investigation. It is interesting to note that even though 320 grit or 600 grit silicon carbide particles are included in the fiber mixture for all materials except LI-900, no silicon carbide particles are observed in these microphotographs.

SOLID CONDUCTIVITY

Stewart and Leiser [5] were able to relate the anisotropic nature of this class of insulators by approximating the number of fibers in the weak and strong directions. The weak and strong directions of the insulation are defined by tensile strength measurements. The assumption is made that the number of fibers under load is directly

proportional to the tensile strength. It is also assumed that the conductivity in the strong and weak directions are related to the number of fibers in the walls and the orientation of the fibers in the insulation. The ratio of fibers in the weak or strong direction may be expressed as a function of the tensile strength and average angle between the fibers and may be represented by

$$N'_w = \frac{2\sigma'_w}{\left[\sigma'_w + 2(1-\sigma'_w)\tan(\theta/2)\right]} \quad , \quad \text{and} \quad N'_{st} = 1 - N'_w \quad , \tag{11a}$$

where

$$\sigma'_w = \frac{\sigma_w}{(\sigma_w + \sigma_{st})} \tag{11b}$$

with respect to the solid fiber conductivity, k_{solid}, where σ_w and σ_{st} are the tensile strengths in the weak and strong directions, respectively.

Unfortunately, this still provides too high of an estimate to the contribution by solid conductivity since not all of the fibers provide direct conduction paths. This means that somehow the contribution of the conductivity in each direction must be scaled. By calculating the "conduction efficiency" of the fibers, η, Stewart and Leiser [5] were able to approximate the contribution of the solid conductivity in the weak and strong directions as

$$\eta_w = \eta N'_w, \quad \text{and} \quad \eta_{st} = \eta N'_{st} \quad . \tag{12a}$$

As was mentioned earlier, Striepens assumed the solid conductivity could be represented by a constant scaling factor of the density, i.e.,

$$k_{solid} = C\,\rho_T \quad , \tag{12b}$$

This may have been adequate for the limited temperature range investigated at that time, but with the LI-900 and LI-2200 series of low density rigid insulation materials, the equation was modified by Striepens and Reeves[6] to the form

$$k_{solid_w} = S^{\tau_w} k_{fiber} \quad , \quad k_{solid_{st}} = S^{\tau_{st}} k_{fiber} \quad , \tag{12c}$$

where $S^{\tau w}$ and $S^{\tau st}$ represent the solid conduction efficiency in the weak and strong directions, respectively. The value of τ_w was calculated to be 1.56 (weak direction) and τ_{st} was calculated as 1.39 (strong direction) for LI-900. For LI-2200 the values were calculated as 1.83 to 1.62, respectively. To maintain consistency with the formulation outlined in Eq. 2, a value of one would be subtracted from each of the exponents of S (τ_w or τ_{st}) since solid conductivity will be multiplied by the solid volume fraction. Thus, τ_w - 1 and τ_{st} - 1 are fairly similar to η_w and η_{st} proposed by Stewart and Leiser.[5]

Klett defined the conductivity of the cell side and end as

$$k_{side} = \frac{k_{solid}\left(\tilde{D}_{eff}^2 - L_M^2\right)}{\tilde{D}_{eff}}, \quad k_{end} = \frac{K_{solid}\, L_M^2}{\tilde{D}_{eff} - L_M} \ . \tag{12d}$$

Klett [3] did not directly address bidirectional conductivity, but did consider cell orientation with respect to heat flow for compressed and crushed cell structures. Thus, with minor modification his model could readily be adapted to conduction in the strong and weak direction.

It has been observed that a separate conduction efficiency factor, determined from analysis of experimental data, is required for each direction since Eq. 12a overpredicts the contribution in the strong direction. Thus, if η'_w is used for the weak direction then η'_{st} can be used for the strong direction which modifies Eq. 12a as

$$\eta_w = \eta'_w N'_w \ , \quad \text{and} \quad \eta_{st} = \eta'_{st} N'_{st} \ . \tag{13}$$

In general, η'_{st} ranges from 50% to 80% of η'_w. It will be shown later, however, that η_{st} is still approximately twice as large as η_w.

Since the solid conductivity for different fibers is represented as

$$k''_{so} = \sum_i V_i k_i \ , \qquad i \in \{\text{Si, Al, ABS, SiC}\} \ , \tag{14}$$

one can calculate the contribution in both directions by

$$k'_{so_w} = \eta_w k''_{so} \ , \quad \text{and} \quad k'_{so_{st}} = \eta_{st} k''_{so} \ . \tag{15}$$

The fiber conductivities used in this analysis are from the Thermophysical Properties of Matter series on thermal conductivity by Touloukian, Powell, Ho, and Klemens[7] (see figure 2).

GAS CONDUCTION

Many estimation procedures for the thermal conductivity of monatomic and simple molecule gases have been developed in parallel with methods used for estimating the viscosity of gases. All such methods are based on the expressions of thermal conductivity derived from theory and take on one of the following forms:

$$k_{gas} = aT^n \ , \tag{16a}$$

$$k_{gas} = \frac{aT^n}{1 + (b/T)} \ , \tag{16b}$$

$$k_{gas} = \frac{a(1+bT)T^{1/2}}{1+(c/T)} \quad , \tag{16c}$$

$$k_{gas} = \frac{a\sqrt{T}}{1+\left\{(b/T)10^{c/T}\right\}} \quad , \tag{16d}$$

$$k_{gas} = \sum_{i=0}^{n} a_i T^i \, , \tag{16e}$$

where the constants a, b, c, and n are determined in each case by forcing a particular equation to best fit the experimental data as a function of temperature.

Stewart and Leiser [5] calculated the conductivity of air with the approximation

$$k_{air} = a\sqrt{T} \quad , \tag{16f}$$

with $a = 6.325 \times 10^{-6}$ (units for conductivity are cal/cm-sec-°C, and T is in K). This is a variation of Eq. 16a, however, it tends to overpredict reference values. Ivy and Striepens[8] approximated the conductivity of air with the expression

$$k_{air} = \frac{a\sqrt{T}}{1+\left(\frac{b}{T\ 10^{c/T}}\right)} \, , \tag{16g}$$

where $a = 6.3225 \times 10^{-6}$, b = 245.4, and c = 12 (T in K), which is from a NBS report,[9] and can also be found in the reference for the 1976 U. S. Standard Atmosphere.[10] This expression tends to closely approximate the reference values and is a modified form of Eq. 16d. On the other hand, Klett simply performed a linear interpolation on tabular values for any gas. In this paper a least squares approximation was made to the recommended reference values used by Touloukian, Liley, and Saxena.[11] For air this takes the form

$$k_{air} = \sum_{i=0}^{3} a_i T^i \, . \tag{16h}$$

These coefficients ($a_0 = 1.26129 \times 10^{-6}$, $a_1 = 2.228759 \times 10^{-7}$, $a_2 = -7.988213 \times 10^{-11}$, $a_3 = 4.1917306 \times 10^{-14}$) are selected to provide conductivity units in cal/cm-sec-°C or cal/cm-sec-K for values of T in K. Below 150 K a straight line approximation is used ($k = 8.577777 \times 10^{-8} + 2.190195 \times 10^{-7}\ T$). A comparison of the different approximating techniques to reference data values can be seen in figure 3.

Typically, the gas conduction term in a closed container is modified by the effects of the mean free path. The equation most investigators use for gas conduction in the cell is

$$k_g' = k_{gas}\left[\frac{L_M}{L_M + \lambda}\right], \tag{17}$$

where λ is the mean free path of the gas.

The mean free path, λ, is the average distance traveled by an atom or molecule of a gas between collisions. It is dependent on the gas state and frame of reference from which the system is observed. For a gas at rest in local thermodynamic equilibrium, it may be defined by the equation

$$\lambda = \frac{\mu}{\rho}\sqrt{\frac{\pi M}{2RT}}\quad , \tag{18a}$$

where μ is the viscosity, ρ the density, T the temperature, R the universal gas constant, and M the molecular weight. Typically, these values should be within a few percent of measured values.

For a gas whose molecules are represented by rigid spheres of diameter d_g, the mean free path may be represented more conveniently as a function of temperature and pressure as

$$\lambda = \frac{RT}{\sqrt{2}\pi \mathrm{N P} d_g^2}\quad , \tag{18b}$$

where R is the universal gas constant, T is the temperature, N is Avogadro's number, P is the pressure, and d_g is the effective collision diameter of the gas. This is the form used in this analysis.

Stewart and Leiser calculated the mean free path as

$$\lambda = 2.303 \text{ X } 10^{-8}\ \mathrm{T/P}, \tag{18c}$$

which is equivalent to using a collision diameter of $3.64908 \text{ X } 10^{-8}$ cm for air. Hughes[12] (and subsequently Striepens [4]) calculated the mean free path coefficient based on the Boltzmann mean free path of O_2 and N_2 of $8.6 \text{ X } 10^{-6}$ cm at 0°C and 750 mm Hg. The equivalent expression is

$$\lambda = 3.102631579 \text{ X } 10^{-8}\ \mathrm{T/P}, \tag{18d}$$

which uses a collision diameter of $3.14388 \text{ X } 10^{-8}$ cm for air. Klett [3] used a collision diameter of $3.64998 \text{ X } 10^{-8}$ cm for air. Calculations based on sea level values of ICAO atmosphere[13] give a collision diameter of $3.65009 \text{ X } 10^{-8}$ cm and this is the value of d_g used in this analysis.

Eq. 17 may be an adequate representation for bulk insulation materials (blanket insulation). Later Striepens and Reeves [6] found it desirable to negate the effects of porosity on air conduction by using $(1 - S)^m$, with

m = 0. Thus, to be consistent with other formulations (e.g., Eq. 2) his formulation for air conductivity should be divided by the porosity (1 - S).

In this investigation however, it was found desirable to modify Eq. 17 to account more for the open cell concept required for the class of insulators under investigation. If one observes the nature of the fiber bundles and fiber endings in figure 1, it becomes obvious that the cells are not closed and that the ends are frequently free. This implies that the collision diameters and pressure effects would have a greater influence on the conductivity. Thus, it was decided to incorporate an additional factor that would more closely approximate the effects of the temperature and pressure effects on mean free path. The variation of mean free path for air as a function of temperature and pressure can be seen in figure 4. The form of the additional factor proposed for the open cell is

$$\left[1+f_g\ \nu\xi\left(\frac{P}{P_0}\right)\right] \quad , \tag{19}$$

for rigid insulation materials where ν is defined as

$$\nu=2^{\mu}\ , \quad \text{with} \quad \mu=-1-3\log_{10}\left(\frac{P}{P_0}\right) \quad . \tag{20a}$$

In this formulation, f_g is a gas conduction correction factor *that is density dependent*, and P_0 is the reference pressure in the appropriate units for one atmosphere. Since the behavior is markedly different at lower temperatures where radiation is not so dominant, an additional compensation, x, is made to account for temperature dependent effects.

$$\xi = \begin{cases} 1 \ , \ \text{for} \quad T>T' \\ \\ T'/T, \ \text{for} \quad T\le T' \end{cases} \quad . \tag{20b}$$

A typical value for T′ was found to be 500 K for this study. Thus, the gas conduction term used in this analysis in the weak direction is

$$k'_{g_w}=k_{gas}\left[\frac{L_M}{L_M+\lambda}\right]\left[1+f_g\ \nu\xi\left(P/P_0\right)\right]. \tag{21}$$

A comparison of the correction of the gas conductivity for LI-900 for the open and closed cell terms can be seen in figure 5. This figure shows the expressions used to multiply the gas conductivity, k_{gas}, in Eq. 17 and Eq. 21. In this figure it is clear that the gas conduction effects are greater for an open cell as a function of pressure than for the closed cell. In addition, Eq. 21 tends to give a slightly greater influence to gas conduction than the other models; for example, the open cell correction term is approximately 1.5 at 1 atmosphere for temperatures above 500 K.

As with the solid conductivity, it was found that a slightly different scaling factor is required for each direction. An appropriate scaling factor for the strong direction, based on morphological properties, was found to be

$$\eta_{g_{st}} = \frac{\eta_{st}}{\eta_w}, \tag{22}$$

which primarily increases the pore size from L_M to £M,

$$£_M = \eta_{g_{st}} L_M \quad , \tag{23}$$

and the gas conduction term in the strong direction becomes

$$k'_{g_{st}} = k_{gas}\left[\frac{£_M}{£_M + \lambda}\right]\left[1 + f_g\, \nu\, \xi\left(P / P_0\right)\right]. \tag{24}$$

Typically, £M ranges from 1½ to 2½ cm. In comparison to the contribution by Eq. 19, the influence of Eq 23 produces only second or third order effects.

EMISSION AND ABSORPTION

The contribution due to emission and absorption used by Stewart and Leiser [5] is

$$k'_r = 4\,\Gamma\,\sigma\,\varepsilon\,T^3 \quad , \tag{25}$$

where the term Γ, derived by Dresher and Pike [2] is

$$\Gamma = D_{eff}\,\frac{\left(1-\gamma^2\right)}{\left[\gamma^2(2-\gamma)\right]} \quad , \quad \text{with} \quad \gamma = \sqrt{S/3} \quad . \tag{26}$$

This represents the bulk radiation term for the insulation in terms of the cell parameters defined earlier. Stewart and Leiser [5] were then able to approximate, by analysis of experimental data, the bulk emissivity:

$$\varepsilon = \beta\ a\ \ln\left(\frac{b}{T}\right) \quad , \tag{27}$$

where β is an emissivity scaling factor (dependent on density and material composition). (Our preference is to include β in Eq. 25 instead of Eq. 27, which makes it an emission scaling parameter.) The two constants, a and b, were defined as 0.473 and 3000, respectively.

For convenience, the terminology used by other investigators will be adopted and the effects of emission and absorption will be described only as emission. Similarly, in this discussion emissivity will be used collectively for emissivity/absorptivity.

The expression used by Klett [3] is

$$k'_{rad} = \frac{L_M^2 F_A \varepsilon \sigma}{Z}\left[4T^3 + \left(\frac{\Delta T}{2}\right)^2\right] \quad , \quad \text{with} \quad Z = 1 - e^{-u\left(\tilde{D}_{eff} - L_M\right)} \quad , \tag{28}$$

where L_M and $\tilde{D}_{eff}$ are defined in Eq. 11, Z is the fraction of radiation stopped at each wall, u is the wall absorption coefficient, ΔT is the temperature gradient across the cell, and F_A is the view factor between radiating ends. A value of 0.53 was used for F_A. As was mentioned earlier, it is difficult to obtain values of u.

As a matter of contrast, the expression used by Striepens [4] is

$$k'_{rad} = \frac{4\sigma T^3 L}{\frac{2}{\varepsilon} - 1 + N'L} \quad , \tag{29a}$$

where L is the thickness of the material (test specimen), N' is obtained by scaling the effective backscatter cross section per unit mass, N, by the bulk density ($N' = \rho_T N$), and e is the effective emittance of the bounding surfaces. However, this was later simplified by Striepens and Reeves [6] as

$$k'_{rad} = \frac{8\sigma T^3}{(P' + 2N')} \quad , \tag{29b}$$

where P' is obtained by scaling the absorption cross section per unit mass, P, by the bulk density ($P' = \rho_T P$). The values for N and P are obtained from the experimental data. They recommended values of N for both LI-900 and LI-2200 of 204.816 cm^2/gm, while the recommended values of P are 0 cm^2/gm and 81.926 cm^2/gm for LI-900 and LI-2200, respectively. It should be noted that assuming N and P are constant is equivalent to assuming the emissivity is constant (independent of temperature).

The approach used for Eq. 25 and Eq. 26 appears to be more attractive than Klett's or Striepens' since data are readily available from the previous calculations. However, it was found that Eq. 26 provides an adequate representation for the emission scaling factor, Γ, for LI-900; the computed value of Γ decreases in magnitude for the higher density LI-2200 when it should increase in magnitude.

In each of the representations for the radiative term presented above, the assumption is made that the emission can be treated collectively for all of the fibers. No attempt was made to determine if the emission was selective with respect to the individual class of fibers. In this paper, however, it is proposed that the radiative contribution of each fiber type, as a distinct class, can be characterized. That is, the silica fibers have a characteristic emission behavior that is distinct from any other group of fibers, such as alumina. With this approach it is reasonable to assume that, like the solid conductivity, the contribution would be related to the relative amounts of the different fibers in the insulation. Likewise, the preferential orientation and fiber count for that orientation would influence the emission in that respective direction.

The approach taken is to utilize the index of refraction n_i, $i \in \{\text{Si, Al, ABS}\}$, and fiber diameter, d_i, in computing the emission scaling factor, Γ. In this formulation the contribution due to emission/absorption may be defined as

$$k_r' = 4\beta\sigma T^3 \sum_l \tilde{F}_l \Gamma_l \varepsilon_l \quad , \quad l \in \{\text{Si, Al, ABS}\}, \tag{30}$$

where Γ_i is defined as

$$\Gamma_l = d_l \, 10^{n_l} \quad , \quad l \in \{\text{Si, Al, ABS}\} \quad . \tag{31}$$

The parameter β is reserved for scaling the emission term, if required, but not the apparent fiber emissivity. The values selected for the index of refraction are 1.487, 1.768, and 1.642 for silica, alumina, and mullite (Nextel), respectively. The term, $\tilde{F}_l$, is essentially a switching parameter that either takes on the value of the weight fraction, F_i, or is set to zero if no emission contribution is desired for a selected material. Since SiC grit may be ignored with respect to the contribution to emission, it may be expressed as

$$\tilde{F}_l = \left\{ \begin{array}{ccc} F_l & , & F_{\text{SiC}} = 0 \\ \dfrac{F_l}{1-F_{\text{SiC}}} & , & F_{\text{SiC}} \neq 0 \end{array} \right\} \quad , \quad l \in \{\text{Si, Al, ABS}\}. \tag{32}$$

While ignoring the contribution of silicon carbide may sound strange, especially since it is added to enhance the surface emittance, its addition provides no observable contribution to the effective conductivity[14] for the lower density materials. It does, however, effect the effective surface emittance from approximately 0.2 to 0.8 if the coating is breached.

Thus, Eq. 30 and Eq. 31 can be used to calculate the internal conduction due to emission/absorption in the weak and strong directions as

$$\begin{aligned} k'_{r_w} &= 4\beta\sigma T^3 \sum_l \tilde{F}_l \Gamma_l \varepsilon_{w_l} \, , \\ & \qquad\qquad l \in \{\text{Si, Al, ABS}\} \\ k'_{r_{st}} &= 4\beta\sigma T^3 \sum_l \tilde{F}_l \Gamma_l \varepsilon_{st_l} \, , \end{aligned} \tag{33}$$

where the appropriate apparent emittance factor for each fiber is a function of temperature and direction for that particular material.

COMBINED MODEL

Thus substituting Eq. 15, Eq. 21, Eq. 24, and Eq. 33 into Eq. 2 gives the combined equation for both directions as

$$k_w = S k'_{so_w} + (1-S)k'_{g_w} + S^{-1} k'_{r_w} ,$$
$$k_{st} = S k'_{so_{st}} + (1-S)k'_{g_{st}} + S^{-1} k'_{r_{st}} . \tag{34}$$

DATA CORRELATION

To correlate the mathematical model with test data, a basic set of criteria is assumed to be known: the conductivities and collision diameters of the molecules or atoms that constitute the gas or atmosphere, the densities and conductivities of the various fibers, and miscellaneous ingredients that are used to form the insulation. Touloukian, Liley, and Saxena[11] provide recommended conductivity values for several gases. A third order least squares fit to this data provides a reasonable approximation to the gas conductivity or standard models, such as those proposed by Hilsenrath, et al.[15] for selected gases, can be used. A comparison of different equations used to approximate the conductivity of air can be seen in figure 3. The collision diameters for air and CO_2 are provided in table I.

With respect to the various fibers used in the insulation, Touloukian, Powell, Ho, and Klemens [7] provided recommended values for silica (SiO_2) and alumina (Al_2O_3), but no data are available for Nextel ($3\ Al_2O_3 \cdot BO_3 \cdot 2\ SiO_2$). However, Mullite conductivity values ($3\ Al_2O_3 \cdot 2\ SiO_2$) can be found in the literature, which appears to closely resemble Nextel except for the lack of the boria molecule. Nextel has a density of 2.7 gm/cm^3 as opposed to the reported density of 3.15 gm/cm^3 for Mullite, but conductivity values were found for Mullite with a fiber density of 2.79 gm/cm^3. For this analysis, it was decided to use these values of Mullite as a substitute for Nextel 312. All of the materials except LI-900 have a small amount of silicon carbide (SiC) added to enhance the emissivity in case the coating is breached during the mission. Typically, only two or three percent silicon carbide (320 or 600 grit) is added in the manufacturing process. For this analysis, it was assumed that a grit particle could mathematically be represented by a cylindrical particle whose length and diameter are of the same dimensions. The equations and coefficients used to approximate these data are provided in table II, while the representative values can be seen in figure 2.

METHOD EMPLOYED

In this section, the method and philosophy used to determine the various parameters required to predict the conductivity of a class of insulators is discussed. The basic assumption is that if the density (ρ), tensile strength (σ_w and σ_{st}), and fiber composition (length, diameter, type of fiber, and fiber mixture) are known, then only the relative binding efficiencies (η'_w and η'_{st}), gas conduction factor (f_g), and apparent fiber emissivity (ε) need to be determined in order to characterize the material conductivity. The empirical conductivity data are available as results obtained through standard ATSM test procedures. The data used in this paper are for the silica-based materials designated as LI-900 (all silica), LI-2200 (silica and SiC), FRCI-12 (silica, Nextel, and SiC), HTP-12, HTP-9, and HTP-6 (silica, alumina, and SiC).

It should be observed that η'_w and η'_{st} are essentially scaling parameters for influencing the solid conductivity contribution in the weak and strong directions. It would be highly desirable to determine these values with minimal influence due to gas conduction and emission. The gas conduction effects can be minimized by using data at 10^{-4} atmospheres or below, while emission effects can be minimized by using data below 300 K.

Two or three temperature values are selected and an optimization program is used to calculate an η'_w or η'_{st} that allows the conductivity to approximate the data in either the weak or strong direction.

Once the appropriate values for η'_w and η'_{st} have been selected then the process can be repeated, only in this case for the ε_i and f_g in the weak direction, and the ε_i in the strong direction. Typically, the variables must be bound such that

$$0.025 \le \eta'_w \le 1, \qquad 0.025 \le \eta'_{st} \le 1, \qquad 0 \le \varepsilon_i \le 1, \text{ and} \qquad 0.5 \le f_g \le 2.5.$$

At this stage, it should be intuitively obvious that the ε_i are selected to correspond with the conductivity values at a given temperature. The basic assumption is that the apparent fiber emissivity is a function of temperature only, thus all of the temperature and pressure data can be used to obtain this fit. The gas conduction factor, f_g, is used to make minor adjustments due to material binding characteristics with respect to gas pressure. In general, f_g is very close to one for the low density materials. It is assumed that f_g is unchanged when using different gases in the model.

A sketch of the calculation procedure for conductivity prediction can be found in Appendix A. In this sketch, the equation numbers that apply to a particular process are identified.

BASELINE REFERENCE DATA

Excellent data are available for LI-900,[16] an all silica material, from 116.67 K through 1922.22 K in the weak direction and from 116.67 K through 1533.33 K in the strong direction. Average values for the length and diameter of the silica fibers used in the manufacture of LI-900 are 1.27 cm and 1.4 μm, respectively. It has a density of 0.144 gm/cm^3 and measured tensile strength values of $\sigma_w = 1.655 \times 10^5$ N/m^2 and $\sigma_{st} = 4.619 \times 10^5$ N/m^2. The average angle between fibers is estimated to be 100°. The values for η'_w, η'_{st}, and f_g were calculated to be 0.45513, 0.38492, and 1.04799, respectively. After the ε_i values were calculated for both directions, it was determined that a quadratic approximation could be made to represent the apparent fiber emissivity values over the entire temperature range. The relative agreement to the baseline data using this approximation can be seen in figures 6 and 7 for the weak and strong directions. The predicted values in the strong direction have been extended to 1922.22 K to be consistent with the data presented in the weak direction. The ratio η_{gst} was calculated as 2.39088 for this data. The percentages of error in the predicted values are shown in figures 8 and 9, where it can be seen that most of the errors are within ±10 percent. For reference purposes, the apparent fiber emissivity values used for all materials are shown in figures 10a – 10c. In these figures the silica emissivity values obtained from the LI-900 analysis are shown. It is interesting to observe that for silica the emissivity values in the strong direction were almost double those in the weak direction at the higher temperatures. Apparent reflection in emissivity is observed at approximately 0.42 for the weak and strong directions. The predicted apparent fiber emissivity values ranged from approximately 0.33 at 116.67 K to 0.63 at 1922.22 K in the strong direction, and from approximately 0.49 at 116.67 K to 0.29 at 1922.22 K in the weak direction.

FRCI-12 [16,17] is a silica-based material consisting of a weight ratio of 78 percent silica and 22 percent alumina-boria-silica (Nextel) with a density of 0.192 gm/cm^3. This material has three percent 320 grit silicon carbide added. The silica fibers are 1.27 cm long with an average diameter of 1.4 microns. Nextel fibers have

a diameter of 11 microns and are also 1.27 cm long. Measured tensile strength values of FRCI-12 are σ_w = 5.585 X 10^5 N/m^2 and σ_{st} = 1.772 X 10^5 N/m^2. The average angle between fibers is estimated to be 100°. The values for η'_w, η'_{st}, and f_g were calculated to be 0.30993, 0.17315, and 1.06574, respectively. After the ε_i values were calculated for both directions, it was determined that the apparent fiber emissivity could be represented in quadratic form similar to silica. The relative agreement to the baseline data using this approximation can be seen in figures 11 and 12 for the weak and strong directions. As with the LI-900 comparison, the predicted data have been extended to 1922.22 K. Similarly, data are predicted at all five decades of pressure (1, 10^{-1}, 10^{-2}, 10^{-3}, and 10^{-4} atmospheres) in the strong direction. The ratio η_{gst} was calculated as 1.83315 for this data. The percentages of error in the predicted values are shown in figures 13 and 14, where it can be seen that most of the errors are within ±10 percent, except for the low temperatures, where errors of approximately 40 percent are observed. Due to the rather excellent agreement in the strong direction, the assumed mullite and silicon carbide data may be suspect at temperatures below 400 K (see figure 2). The greatest variation for the weak direction was for the data at 10^{-4} atmosphere pressure, with rather excellent agreement at all other pressures. The predicted apparent fiber emissivity values for Nextel emission contribution are shown in figure 10a along with the silica emissivity values as a function of the temperature. In the weak direction, these values range from 0.35 at 116.67 K to 0.0039 at 1922.22 K. In the strong direction, the apparent fiber emissivity ranges from 0.78 at 116.67 K to 0.078 at 1922.22 K. It should be pointed out that this is extrapolating data above 1200 K to the higher temperatures in both cases.

The HTP ceramics are silica-based materials consisting of 78 percent silica and 22 percent alumina with 3 percent 600 grit SiC added. The silica fiber are 1.27 cm long with an average diameter of 1.4 microns, and the alumina fibers have a diameter of 3 microns and are also 1.27 cm long. The densities used in this investigation were 0.096 gm/cm^3, 0.144 gm/cm^3, and 0.192 gm/cm^3. The materials are appropriately designated as HTP-6, HTP-9, and HTP-12 corresponding to density in lb/ft^3. Measured tensile strength values are 3.172 X 10^5 N/m^2 in the weak direction and 9.101 X 10^5 N/m^2 in the strong direction for HTP-6; 4.619 X 10^5 N/m^2 in the weak direction and 1.558 X 10^6 N/m^2 in the strong direction for HTP-9; and 6.067 X 10^5 N/m^2 in the weak direction and 2.206 X 10^6 N/m^2 in the strong direction for HTP-12. The average angle between fibers is estimated to be 100°, the same as used for the other materials.

Limited experimental data exists for the HTP materials. HTP-6 data[18] are available only in the weak direction for two pressures, 1 atmosphere and 10^{-4} atmosphere. HTP-9 data [18] are available for both strong and weak directions, but only at 10^{-4} atmosphere and the data span a limited temperature range (94.44 K to 922.22 K). The HTP-12 data[19] are reported for all five pressure levels in the weak direction, but not for temperatures below 297.22 K. The compromise reached was to use the ratio between η'_w and η'_{st} calculated from HTP-9 to calculate η'_{st} for HTP-6 and HTP-12. Likewise, HTP-6 data were used to calculate the gas correction factor, f_g, for HTP-6, but f_g values for LI-900 and FRCI-12 were used for HTP-9 and HTP-12, respectively. The computed values for η'_w and η'_{st} were 0.12574 and 0.08136, respectively for HTP-6; 0.10802 and 0.06989 for HTP-9; and 0.26164 and 0.16928 for HTP-12. The computed gas correction factor, f_g, was computed to be 0.95861 for HTP-6 while the values computed for LI-900 and FRCI-12 were used for HTP-9 and HTP-12, respectively.

The comparison of the predicted and baseline values for HTP-6 in the weak direction can be seen in figure 15. Predicted values in the strong direction are shown in figure 16. In both plots, predicted data are extended to 1922.22 K at all five pressure levels. Only predicted data in the strong direction are shown in figure 16 since no comparison can be made with measured data. The ratio η_{gst} was calculated as 1.88926 for this data. The percentages of error in the predicted values in the weak direction are shown in figures 17a and 17b, with most of the errors between -13% to 24% if the low temperature (94.44 K) values are ignored. The alumina apparent fiber emissivity values can be seen in figure 10b.

The comparison of the predicted and baseline values for HTP-9 can be seen in figures 18 and 19. The ratio η_{gst} was calculated as 2.27744 for this data. In these plots the predicted data are extended to 1922.22 K at all five pressure levels. The percent error in the predicted values are shown in figures 20a and 20b with most of the errors within ±5 percent. Identical to HTP-6, the alumina apparent fiber emissivity values can be seen in figure 10b.

The comparison of the predicted and baseline values for HTP-12 can be seen in figure 21. In this plot, predicted data are extended to range from 116.67 K to 1922.22 K at all five pressure levels. Predicted values in the strong direction are shown in figure 22. The ratio η_{gst} was calculated as 2.48035 for this data. The percent error in the predicted values are shown in figure 23, with most of the errors within ±10 percent. The alumina predicted apparent fiber emissivity values for HTP-12 are presented in figure 10b.

Predicted conductivity values for all three HTP materials were higher than the measured data in both directions at low temperatures. This can be directly attributed to the rapid increase in conductivity with decreasing temperature of the alumina fibers (see figure 2). At this time it is not know if the fibers used in the construction of the HTP materials differ significantly from those reported by Touloukian, et al.[7] Nonetheless, if an attempt were made to be closer at the cryogenic temperatures, the values of η'_w and η'_{st} would decrease significantly.

Predicting the material conductivity for LI-2200 was difficult since the standard reference data[20] were unreliable. Test data from the Ivy and Striepens report [8] were used in this LI-2200 analysis. In this model, it was necessary for both β and f_g to depart from approximately one. In addition, while the apparent fiber emissivity values computed for LI-900 in the weak direction could be used with a fair degree of accuracy, it was necessary to compute different apparent fiber emissivity values in the strong direction. Similar to LI-900, LI-2200 consists of 98 percent silica with 2 percent 320 grit SiC particles included to enhance emissivity in case the coating is breached during entry. The average length and diameter of the silica fibers are the same as those used in all of the other materials. This material has a density of 0.35241 gm/cm^3 and measured tensile strength values of $\sigma_w = 5.033 \times 10^5$ N/m^2 and $\sigma_{st} = 1.241 \times 10^6$ N/m^2. As with the other materials the average angle between fibers is estimated to be 100°. The values calculated for η'_w, η'_{st}, and f_g were 0.46581, 0.26359, and 1.59464, respectively. The ratio η_{gst} was calculated as 1.37992 for this data. The estimated value of β was 2.48429. The relative agreement to the baseline data using this approximation can be seen in figures 24 and 25 for the weak and strong directions. The predicted values in the strong direction have been extended to 1922.22 K to be consistent with the LI-900 data. The percentages of error in the predicted values are shown in figures 26 and 27, where it can be seen that most of the errors are within ±10 percent. As would be expected, the relative errors in the strong direction are slightly better than those in the weak direction since the apparent fiber emissivity was fit to this data instead of using data for LI-900. The apparent fiber emissivity values for the silica fibers used for this analysis can be seen in figure 10c. It is interesting to note that the shape of the emissivity curves in the strong direction are diametrically opposed. The shape of the LI-2200 curve is similar to all other materials, except for LI-900, in the strong direction.

As with the other materials at cryogenic temperatures, the agreement with measured data appears to be poor. However, the excellent agreement at higher temperatures in the weak direction (see figures 26 and 27) does tend to support the independent contribution of the fibers. Additionally, in the weak direction, this tends to support the view that apparent fiber emissivity is invariant with respect to density for a particular fiber. Further substantiation of this concept is the relative close agreement between the three HTP materials, with respect to variations in density and invariance with respect to apparent fiber emissivity.

Only one data point exists to illustrate that the emission scaling factor, β, is a function of density (see figure 28). Substantial data exists to confirm the dependence of the gas conduction correction factor on density (see figure 29).

A tabulation of the experimental and predicted conductivity values for these materials is provided in Appendix B.

ADDITIONAL OBSERVATIONS

After this investigation was completed, it was brought to our attention that a branch report* containing additional HTP-6 test data was available for comparison.[21] As with the baseline data, the calculated conductivity values were available only in the weak direction. The radiant test data are available for temperatures from 294 K to 1644 K at pressures of 10^{-1}, 10^{-2}, and 10^{-3} atmospheres. A comparison of this calculated conductivity data with the baseline data can be seen in figure 30. For temperatures up to 1000 K, the calculated values are in fairly close agreement with baseline data when comparing 10^{-3} and 10^{-4} atmosphere pressure data. Above 1000 K, the data appeared to rapidly depart from the baseline data. A comparison of the predicted values and the values calculated from the branch report in the weak direction can be seen in figure 31. In this figure, the data appear to be relatively close except for midrange temperatures for the 10^{-1} atmosphere data. This is better illustrated in figure 32 which shows a comparison of the percent error in predicting this data. For the two lowest pressure levels, the predictions are within 20 percent of the calculated values.

The relative contribution of the three components of conductivity provides an insight into the dependency of the composite conductivity as a function of temperature and pressure. This is illustrated in figure 33 which shows the percent contribution of the solid, gas, radiative components as a function of temperature for LI-900 in the weak direction at 10^{-2} atmospheres. In this figure, it can be seen that at low temperatures the solid and gas components are the more dominant contributing factors. However, above 800 K emission dominates the other two components. In direct contrast, the actual conductivity values for the same conditions, which indicate the low, almost constant values attributed to solid and gas conductivity, may be seen in figure 34. Similar results can be seen in the strong direction in figures 35 and 36. In these figures, however, the contributions due to solid and gas components are nearly equal throughout the temperature range.

Another interesting result of using this analysis is the prediction of the relative improvement in FRCI-12 conductivity achieved by reducing the Nextel fiber diameter from 11 mm to 3 mm. Figures 37 and 38 illustrate this improvement in the weak and strong direction. In these figures, the reference baseline values are also shown in order to make a direct comparison. Of more interest is the percent variation between the predicted values using the 3 μm fiber diameter to the predicted values using the 11 μm fiber diameter. Of particular interest is the influence of pressure, as well as temperature on the variation in conductivity due to this fiber diameter change (reduction). This reduces the emission scaling factor, Γ_{ABS}, by a factor of 27 percent (see Eq. 31), which reduces the contribution due to emission/absorption, but also produces a minor change in the effective cell dimensions. In the weak direction, the peak reduction (approximately 35 percent) occurs around 900 K at the lowest pressure where gas conduction is negligible (10^{-4} atmospheres) (see figure 39). Very little change occurs at the lowest and highest temperature extremes where solid conduction and emission effects are dominant in both models. At one atmosphere approximately 18 percent reduction can be obtained at 1100 K. These variations are dominated by the apparent fiber emissivity change due to fiber diameter (see Eq. 31 and Eq. 33). This is better illustrated in figure 40 where the individual components of conductivity (solid, gas, and emission) are compared for the two fiber diameters at a pressure of 10^{-2} atmospheres. In this figure, the solid and gas conductivity are essentially the same, and the only change is between the radiative components. This could also be implied from figure 39 since gas conduction is negligible at 10^{-4} atmospheres. In contrast, for the strong direction almost no change occurs above 1500 K, although it is similar at lower temperatures (see figure 41). As would be expected, less improvement can be obtained in the strong direction

*Copies of this report are available through the Lyndon B. Johnson Space Center, Structures and Mechanics Division, Thermal Branch.

than in the weak direction. This is primarily due to the slightly greater influence of the solid and, to a lesser extent, to gas conductivity components (see Eq. 13 and Eq. 22). In general, there is a 5 percent greater reduction in the weak direction than in the strong direction. It is also interesting to note that the maximum change in the strong direction occurs approximately 300 K lower than for the weak direction.

PREDICTIONS IN A CO_2 ATMOSPHERE

Due to the demands placed on modern hypersonic spacecraft there is a need to be able to predict the thermal conductivity of a material from basic morphological data prior to development and testing of the material candidates. It is also desirable to be able to determine the suitability of existing materials for uses other than those for which they were originally designed, and to predict their properties in environments in which they have not been tested. As opposed to the effects of changing the fiber diameter described in the previous section, this analysis would be directed towards the effects due to changes in gas conductivity and its associated collision diameter.

This analysis has been extended for prediction in a CO_2 atmosphere similar to that for Mars. The technique selected is similar to that previously employed, namely comparing to baseline values in air, followed by percent variation plots from the predictions in air. It is felt that this would provide an insight into errors that could be encountered for porous materials whose properties are not known in an exotic atmosphere.

A comparison of different approximation techniques for CO_2 can be seen in figure 42, and the coefficients are listed in table I. In this analysis, it should be noted that conductivity values for this gas are not tabulated below 200 K (it becomes a solid). However, for continuity between the analysis for air and carbon dioxide, values were estimated such that the conductivity would be zero at absolute zero. The comparison between air and CO_2 conductivity can be seen in figure 43. In this plot, it can be seen that the conductivity for air is greater than CO_2 for temperatures below 1000 K, and the role reverses above 1000 K. Thus, just due to gas conductivity alone, the conductivity of a porous material would be expected to be less than those predicted in air at temperatures below 1000 K where emission effects are minimal. The collision diameter used for CO2, $d_g = 4.59241 \times 10^{-8}$ cm, is based on the value for the mean free path of 4.19×10^{-6} cm reported by Kennard.[22] The surface pressure on Mars is approximately 10^{-2} atmospheres, so more interest is directed at predicted data above 200 K in the 10^{-2} to 10^{-4} atmosphere pressure range.

Predicted values of LI-900 conductivity in the weak and strong direction compared to baseline values in air can be seen in figures 44 and 45, respectively. From these plots, the predicted data above 500 K appear to be in reasonable agreement with baseline values. For values below 500 K, it appears that using air-derived conductivity values would produce large errors except at the lowest pressure. Percent variation plots of the predicted values in CO_2 with the values predicted in air can be seen in figures 46 and 47. These indicate that at 10^{-4} atmospheres the data are in excellent agreement over the entire temperature range. At 10^{-3} and 10^{-2} atmospheres, the conductivity values predicted in CO_2 are lower than those predicted in air for temperatures less than 500 K. While the percent variation values are greater for temperatures above 500 K for these pressure levels, the variation is within 5 percent. For pressures of 10^{-1} and 1 atmospheres, the negative variation occurs below 1000 K and, similar to data at other pressures, tends to be in close agreement at temperatures above 1000 K where emission is dominant.

Due to the similarity in trends for the other materials to that observed for LI-900, the individual characteristics of each material will not be discussed. Predicted values of FRCI-12 conductivity in the weak and strong direction compared to baseline values in air can be seen in figures 48 and 49, respectively. The corresponding percent variation plots of the predicted values in CO_2 with the values predicted in air can be seen in figures 50 and 51. Predicted values of HTP-6 conductivity in the weak direction compared to baseline values in air

can be seen in figure 52. Predicted values in the strong direction (no baseline values are available for air) can be seen in figure 53. The corresponding percent variation plots of the predicted values in CO_2 with the values predicted in air can be seen in figures 54 and 55. Predicted values of HTP-9 conductivity in the weak and strong direction compared to baseline values in air can be seen in figures 56 and 57, respectively. The corresponding percent variation plots of the predicted values in CO_2 with the values predicted in air can be seen in figures 58 and 59. Predicted values of HTP-12 conductivity in the weak direction compared to baseline values in air can be seen in figure 60. Predicted values in the strong direction (no baseline values are available for air) can be seen in figure 61. The corresponding percent variation plots of the predicted values in CO_2 with the values predicted in air can be seen in figures 62 and 63. Predicted values of LI-2200 conductivity in the weak and strong direction compared to baseline values in air can be seen in figures 64 and 65, respectively. The corresponding percent variation plots of the predicted values in CO_2 with the values predicted in air can be seen in figures 66 and 67. A tabulation of these predicted values are provided in Appendix C.

CONCLUDING REMARKS

- A mathematical model has been developed to predict the thermal conductivity of low density, silica-based, fibrous composite insulation materials. This model, while based on a mathematical formulation, is correlated with experimental data.

- The contribution due to silica is consistent for all temperatures in the weak direction.

- The contribution due to individual fibers in the composite insulation appear to be independent of one another.

- Once the parameters have been defined for one atmosphere they can be used to predict conductivities for other atmospheres. Conductivity values were predicted for a carbon dioxide atmosphere for all of the materials analyzed.

- A technique has been developed for assessing properties at other densities and compositions.

- The effects of density variation influence on gas conduction and emission have been identified.

- Conductivity predictions are better at high temperatures than at cryogenic temperatures.

- Effects due to fiber diameter have been analyzed. An analysis of reducing the fiber diameter of Nextel from 11 μm to 3 μm indicate that the conductivity could be reduced by up to 30 percent at 700 K for FRCI-12.

REFERENCES

1. Curry, D. M.; and Williams, S. D.: Nonlinear Least Squares-An Aid to Thermal Property Determination, AIAA Journal, Vol. 11, No. 5, May 1973, pp. 670-674.

2. Dresher, W. H.; and Pike, J. N.: Ceramic Fibrous Materials for High-Temperature Insulation, Metals Engineering Quarterly, Vol. 11, No. 3, August 1971, pp. 32-35.

3. Klett, Robert D.: Analytical Thermal Design of Cellular Insulations and Laminated Composites, SAND74-0232, Sandia Laboratories, Albuquerque, NM, February 1975.

4. Striepens, A. H.: Review of Thermal Conductivity Data for 8 lb/ft^3 Thermoflex Insulation, LTR 1263-4413, Laboratory Test Report, Downey, CA, Rockwell International, April 1976.

5. Stewart, David A.; and Leiser, Daniel B.: Characterization of the Thermal Conductivity for Fibrous Refractory Composite Insulations, Ceramic Engineering Science Proceedings, Vol. 6, No. 7-8, July-August 1985, pp. 769-792.

6. Striepens, A. H.; and Reeves, R. D.: Predicted Thermal Performance of LI900 and LI2200 Reusable Surface Insulations, LTR 1207-4551, Laboratory Test Report, Downey, CA, Rockwell International, September 1980.

7. Thermophysical Properties of Matter, Thermal Conductivity of Nonmetallic Solids, Volume 2, Edited by Touloukian, Y., S.; Powell, R. W.; Ho, C. Y.; and Klemens, P. G.: IFI/Plenum, New York - Washington, 1970.

8. Ivy, R. G.; and Striepens, A. H.: Thermal Conductivity of High-Temperature Bulk Insulation for Shuttle TPS Applications, LTR 1848-4438, Laboratory Test Report, Downey, CA, Rockwell International, February 1977.

9. Tables of Thermal Properties of Gases, NBS Circular 564, 1955.

10. U. S. Standard Atmosphere, 1976, National Oceanic and Atmospheric Administration, National Aeronautics and Space Administration, United States Air Force, Washington, D.C., October 1976.

11. Thermophysical Properties of Matter, Thermal Conductivity Nonmetallic Liquids and Gases, Volume 3, Edited by Touloukian, Y. S.; Liley, P. E.; and Saxena, S. C.: IFI/Plenum, New York – Washington, 1970.

12. Hughes, T. A.: A Technique for Estimating the Thermal Conductivity of Insulations at Low Pressures, MDC E0285, McDonnell Douglas Astronautics Company - East, St. Louis, MO, January 1971.

13. CRC Handbook of Chemistry and Physics, Ed. by Robert C. West, 60th Edition, 1981, p. F-206.

14. Williams, S. D.: Thermal Conductivity Analysis of LI-900 Tiles Impregnated with Silicon Carbide, LEMSCO-15768, Lockheed Engineering and Management Services Co., Houston, TX, November 1980.

15. Hilsenrath, Joseph; Beckett, C. W.; Benedict, W. S.; Fano, L.; Hoge, H. J.; Masi, J. F.; Nuttall, R. L.; Touloukian, Y. S.; and Woolley, H. W.: Tables of Thermodynamic and Transport Properties of Air, Argon, Carbon Dioxide, Carbon Monoxide, Hydrogen, Nitrogen, Oxygen, and Steam, Pergamon Press, Oxford, London, New York, Paris, 1960.

16. Williams, S. D.; and Browning, R. E.: PathFinder Thermophysical Property Data—Thermal Protection Materials For High Energy Aerobraking Vehicles, Volume 1, LESC–27438, Lockheed Engineering and Sciences Co., Houston, TX, August 1989.

17. McCormick, M. J.: Undocumented FRCI-12 Thermal Conductivity Test Results, transmitted by R. P. Banas, Lockheed Missiles & Space Company, Sunnyvale, CA, October 10, 1981.

18. McCormick, M. J.: Undocumented Test Results for HTP-6-22 & HTP-9-22 Apparent Thermal Conductivity, transmitted by R. P. Banas, Lockheed Missiles & Space Company, Sunnyvale, CA, April 14, 1988.

19. Data Sheet, HTP High Thermal Performance, Lockheed Missiles & Space Company, April 1987.

20. Space Shuttle Program Thermodynamic Design Data Book, Penetrations, Volume 3E, Rockwell International, Downey, CA, January 1981.

21. Kowal, T. J.: Radiant Thermal Testing and Conductivity Analysis of HTP-6 Tile Material, Thermal Branch Internal Report, Johnson Space Center, Houston, TX, April 1991.

22. Kennard, E. H.: Kinetic Theory of Gases with an Introduction to Statistical Mechanics, McGraw-Hill Company, Inc., New York and London, 1938.

Table Ia - Collision Diameters for Air and Carbon Dioxide

Gas	T (K)	P (atm)	λ (cm)		d_g (cm)	Reference
Air	288.16	1.0	6.6317223	X 10^{-6}	3.65035 X 10^{-8}	13
CO_2	288.16	1.0	4.19	X 10^{-6}	4.59241 X 10^{-8}	22

Table Ib - Equations Used to Approximate Air and CO_2 Conductivity

$$k_{air} = \sum_{i=0}^{n} a_i T^i \,, \quad n = 1 \text{ for } T < 100\,K \,, \quad n = 3 \text{ for } 100\,K \le T \le 2000\,K$$

$$k_{CO_2} = \sum_{i=0}^{n} a_i T^i \,, \quad n = 2 \text{ for } T < 200\,K \,, \quad n = 2 \text{ for } 200\,K \le T \le 2000\,K$$

Table Ic - Coefficients Used to Approximate Air and CO_2 Conductivity

	Air < 100 K	Air ≥ 100 K
a_0	8.577777 X 10^{-8}	1.26129 X 10^{-6}
a_1	2.190195 X 10^{-7}	2.228759 X 10^{-7}
a_2		-7.988213 X 10^{-11}
a_3		1.5816405 X 10^{-14}

	CO_2 < 200 K	CO_2 ≥ 200 K
a_0	-8.777165 X 10^{-10}	-2.7224489 X 10^{-5}
a_1	7.601161 X 10^{-8}	2.3923836 X 10^{-7}
a_2	1.891736 X 10^{-10}	-5.0480815 X 10^{-11}

Table IIa - Equations Used to Approximate Solid Conductivity for Silica, Alumina, Mullite (Nextel), and Silicon Carbide

Silica $$k = \sum_{i=0}^{8} a_i T^i \quad , 50\ \text{K} < \text{T} \leq 2000\ \text{K}$$

Alumina $$k = 10^z \ , z = -1 + \cos\left(\sum_{i=0}^{9} a_i T^i \right) \quad , 100.277195\ \text{K} \leq \text{T} \leq 2000\ \text{K}$$

$$k = \sum_{i=0}^{2} a_i T^i \quad , 50\ \text{K} < \text{T} < 100.277195\ \text{K}$$

Mullite $$k = \sum_{i=0}^{3} a_i T^i \quad , 50\ \text{K} < \text{T} \leq 2000\ \text{K}$$

Silicon Carbide $$k = \sum_{i=0}^{1} a_i T^i \quad , 50\ \text{K} < \text{T} \leq 2000\ \text{K}$$

Table IIb - Coefficients Used to Approximate Solid Conductivity for Silica, Alumina, Mullite (Nextel), and Silicon Carbide

	SiO_2	Al_2O_3	
		50 K < T < T_{crit}	T_{crit} ≤ T ≤ 2000 K
a_0	$1.11335958 \times 10^{-4}$	$-7.88248123 \times 10^{-2}$	3.7054204×10^{-2}
a_1	$1.55188268 \times 10^{-5}$	$7.73371359 \times 10^{-3}$	$1.5349288469 \times 10^{-2}$
a_2	$3.82441377 \times 10^{-9}$	$-3.799585256 \times 10^{-5}$	$-6.7582406126 \times 10^{-5}$
a_3	$-1.35737925 \times 10^{-10}$		$1.77289023438 \times 10^{-7}$
a_4	$3.21058986 \times 10^{-13}$		$-2.8013704328 \times 10^{-10}$
a_5	$-3.43568691 \times 10^{-16}$		$2.77132827779 \times 10^{-13}$
a_6	$1.92130034 \times 10^{-19}$		$-1.73085249 \times 10^{-16}$
a_7	$-5.46480792 \times 10^{-23}$		$6.6277947001 \times 10^{-20}$
a_8	$6.25315816 \times 10^{-27}$		$-1.4203766279 \times 10^{-23}$
a_9			$1.304374531 \times 10^{-27}$

	$3\,Al_2O_3 \cdot 2\,SiO_2$	SiC
a_0	$1.79893598 \times 10^{-2}$	2.7769927×10^{-2}
a_1	$-1.7863805 \times 10^{-5}$	-2.89519×10^{-6}
a_2	1.1463903×10^{-8}	
a_3	$-2.565216 \times 10^{-12}$	

Alumina — T_{crit} = 100.277195 K

Fig. 1a Micrograph of LI-900 Surface Parallel to the Mold Line.

ORIGINAL PAGE
BLACK AND WHITE PHOTOGRAPH

Fig. 1b Micrograph of FRCI-12 Surface Parallel to the Mold Line.

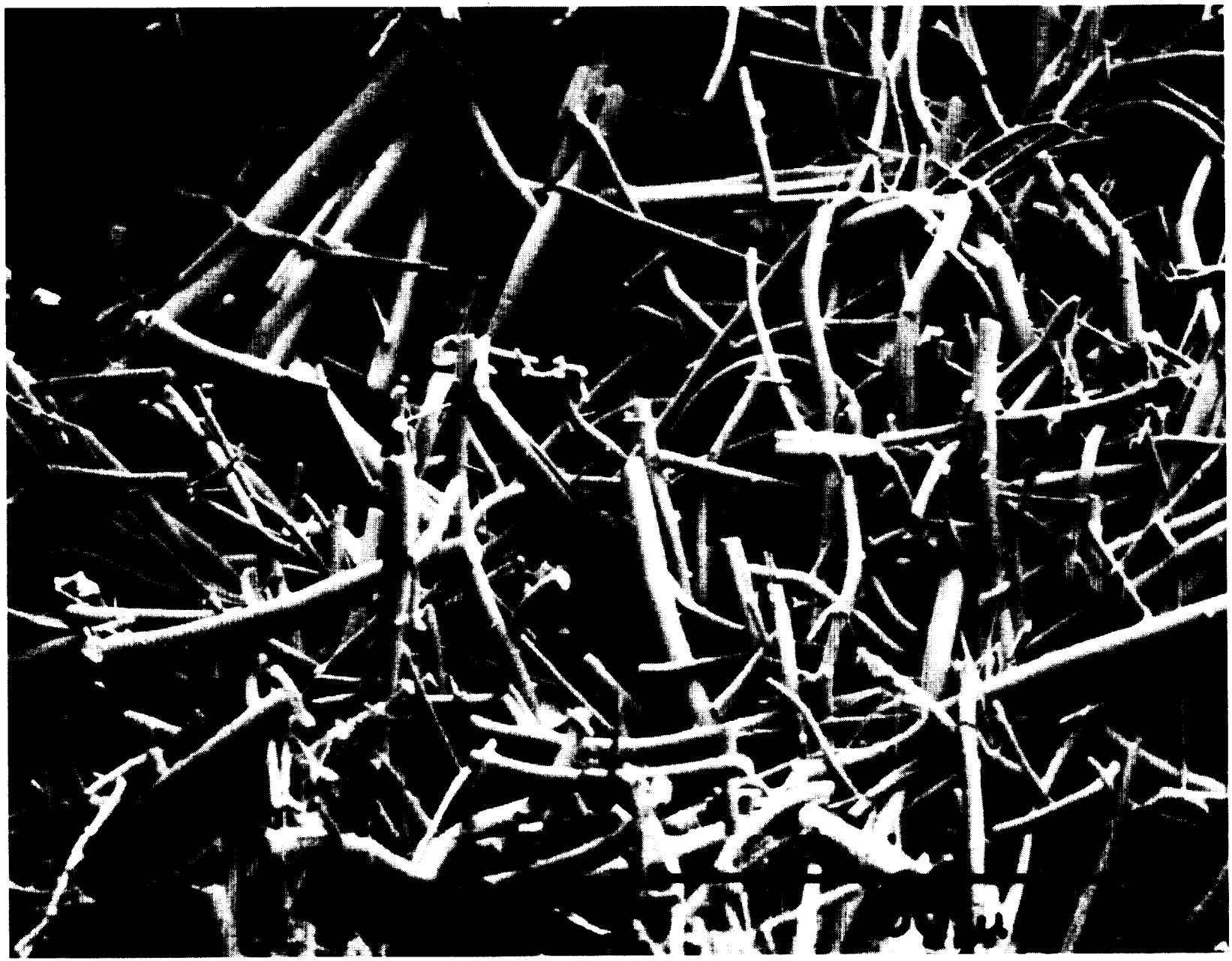

Fig. 1c Micrograph of LI-2200 Surface Parallel to the Mold Line.

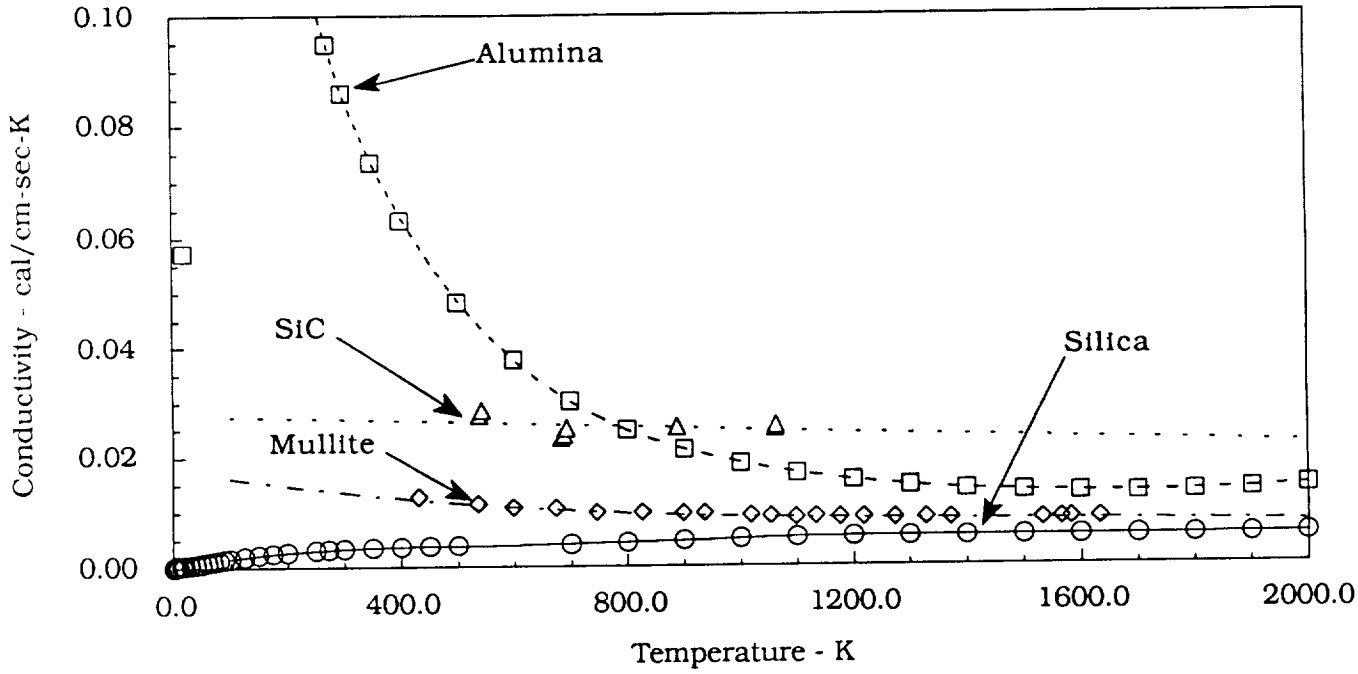

Fig. 2 Conductivity for Silica, Alumina, Mullite, and Silicon Carbide.

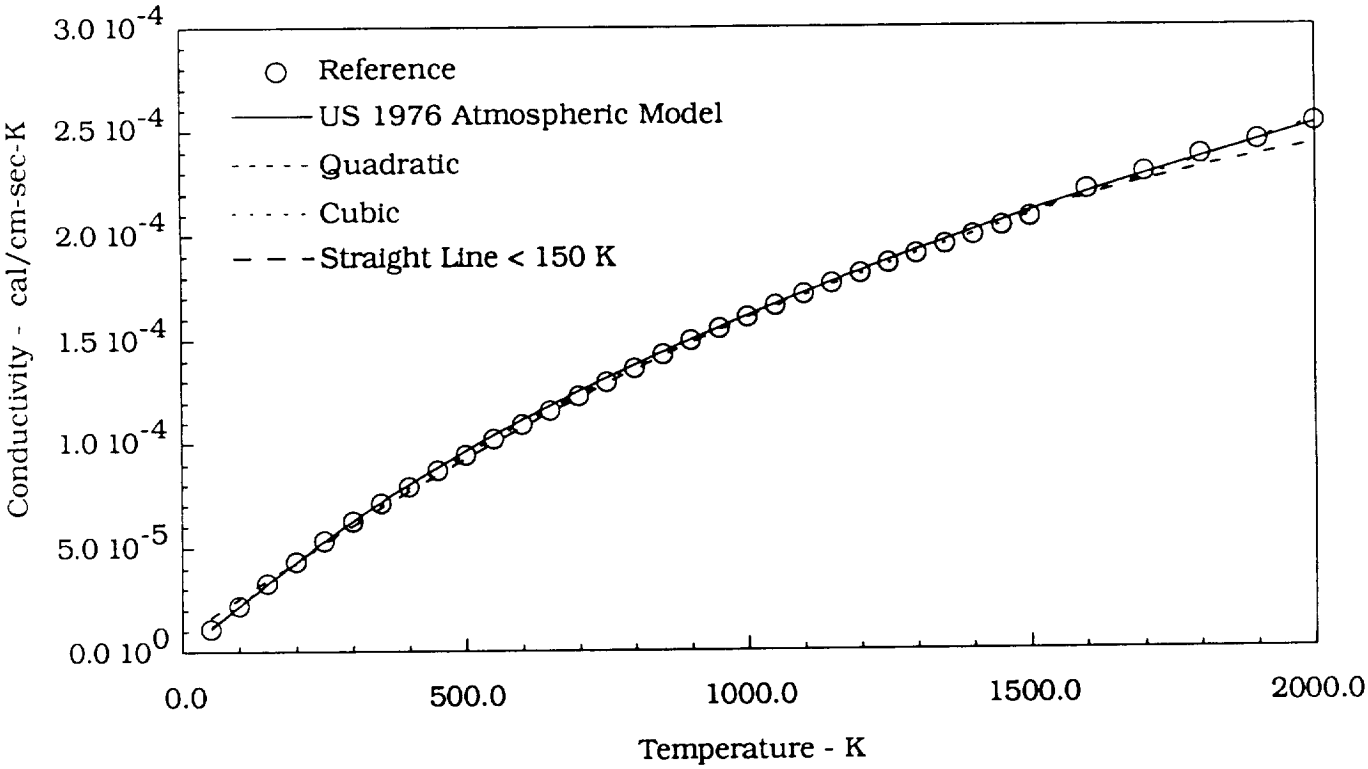

Fig. 3 Air Conductivity - Reference vs. Predicted Methods.

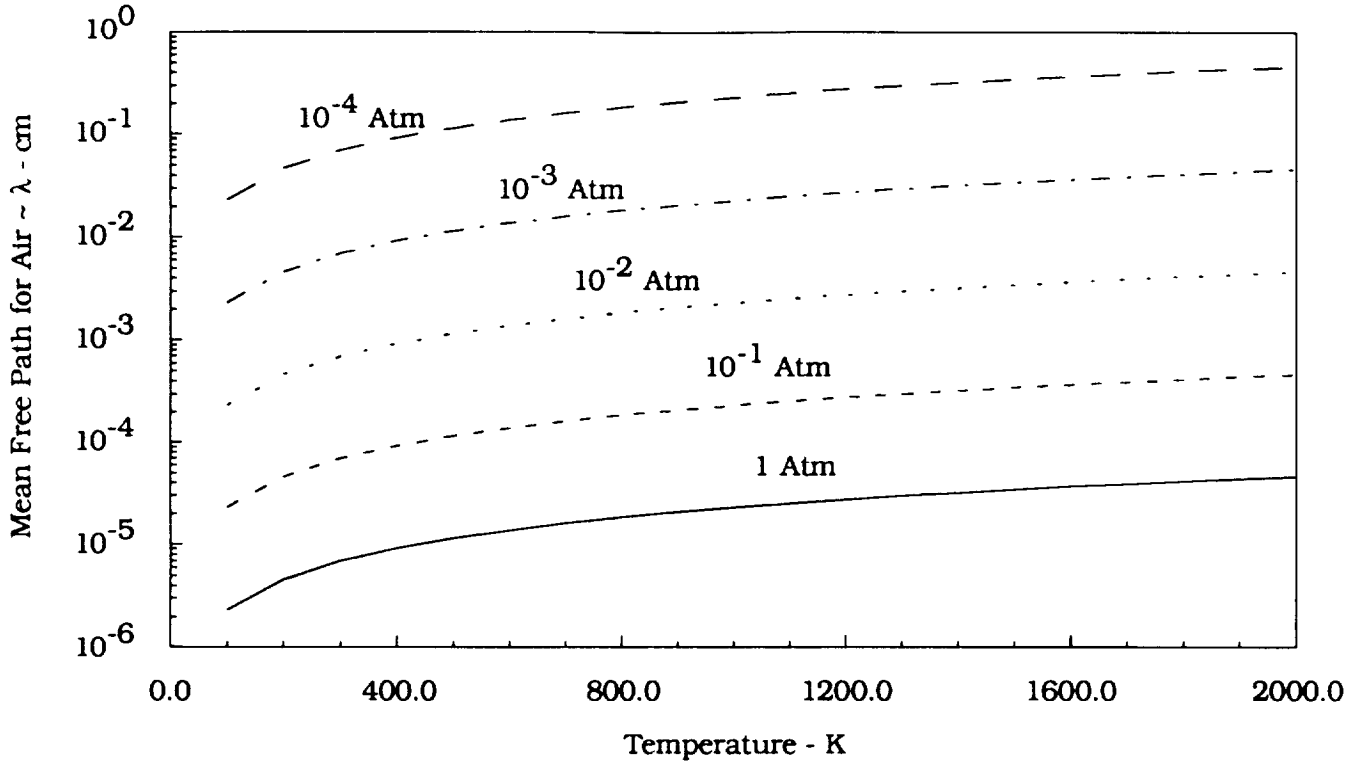

Fig. 4 Mean Free Path for Air as a Function of Temperature and Pressure.

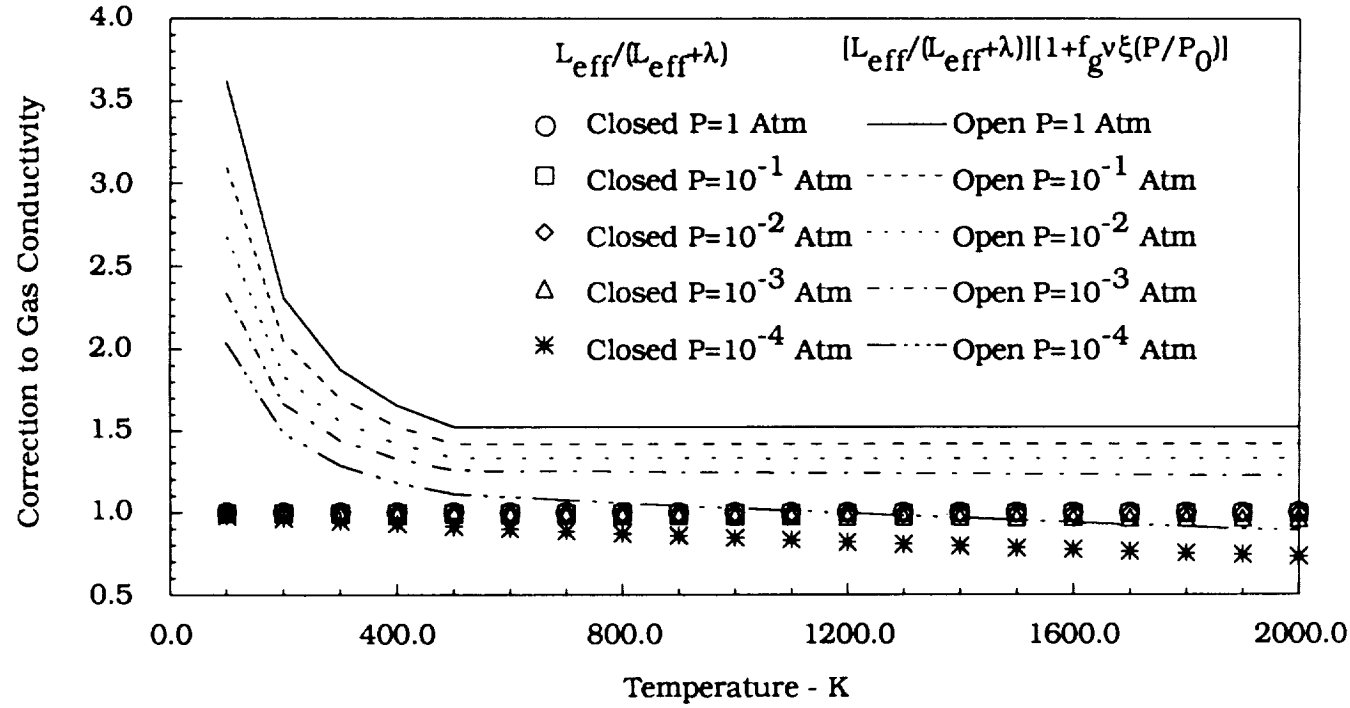

Fig. 5 A Comparison of the Gas Conduction Correction Factor for an Open Cell to a Closed Cell Using L_{eff} for LI-900.

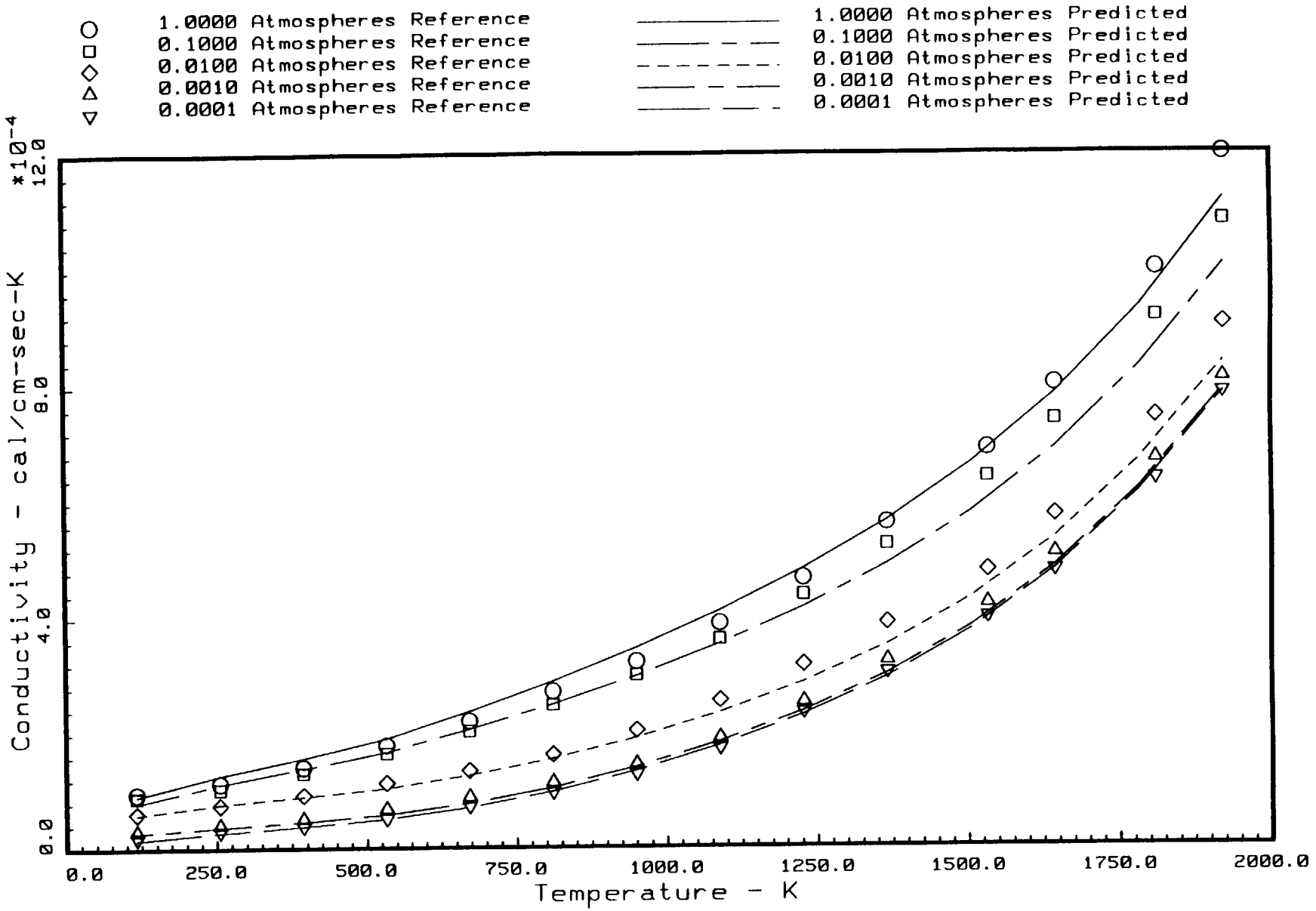

Fig. 6 Predicted LI-900 Conductivity in the Weak Direction vs. Baseline Values.

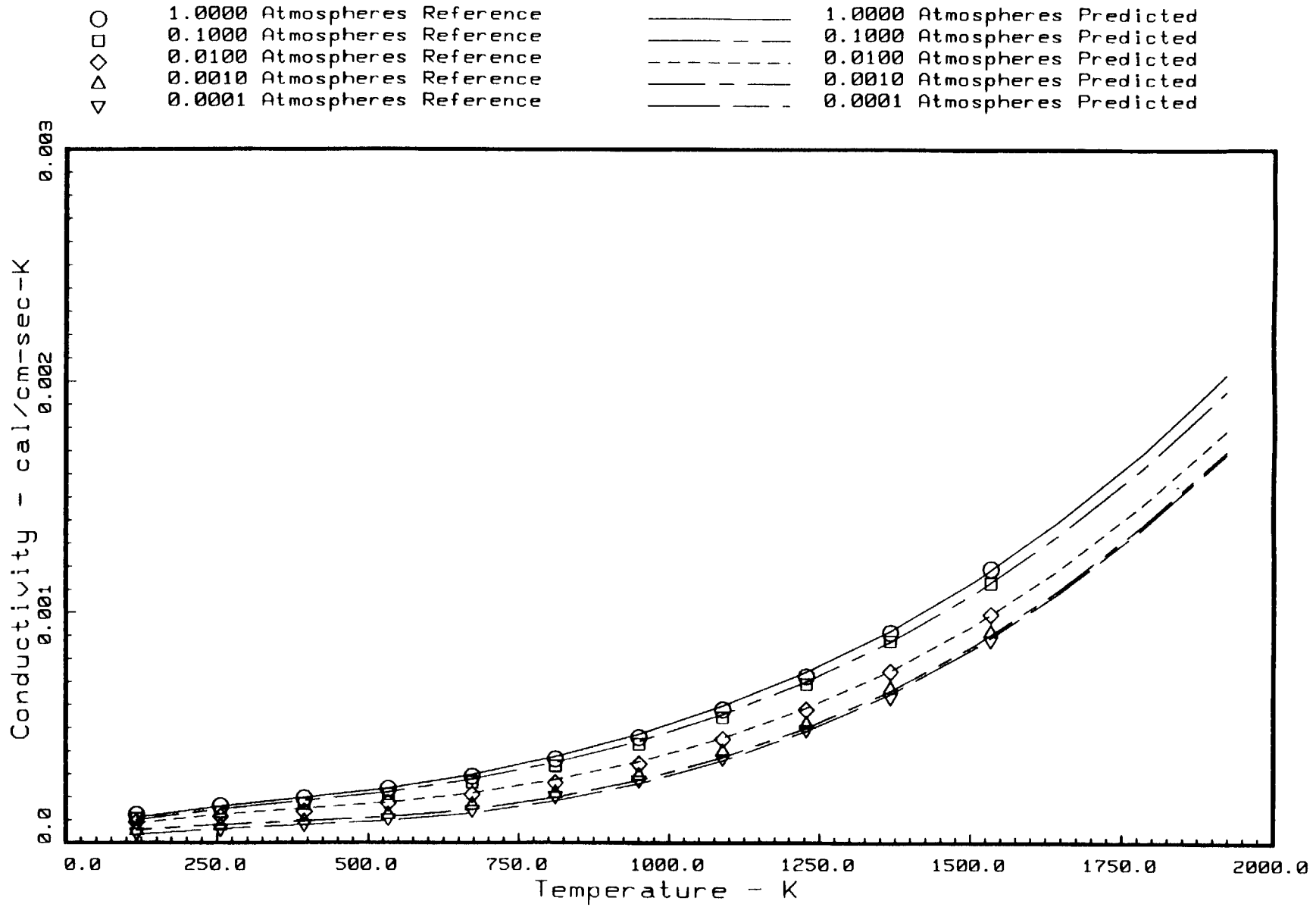

Fig. 7 Predicted LI-900 Conductivity in the Strong Direction vs. Baseline Values.

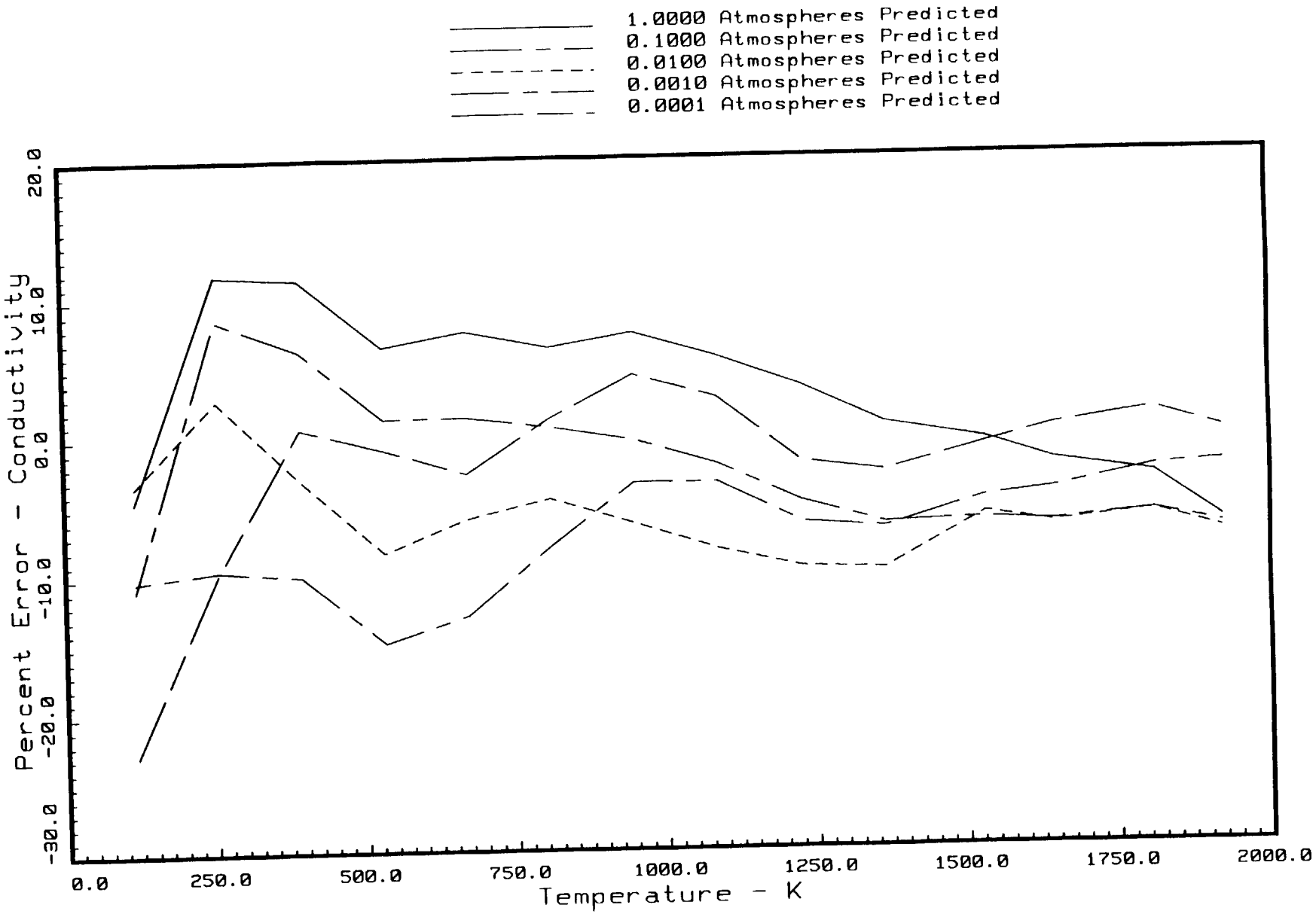

Fig. 8 Percent Error in Predicted LI-900 Conductivity in the Weak Direction Compared to Baseline Data.

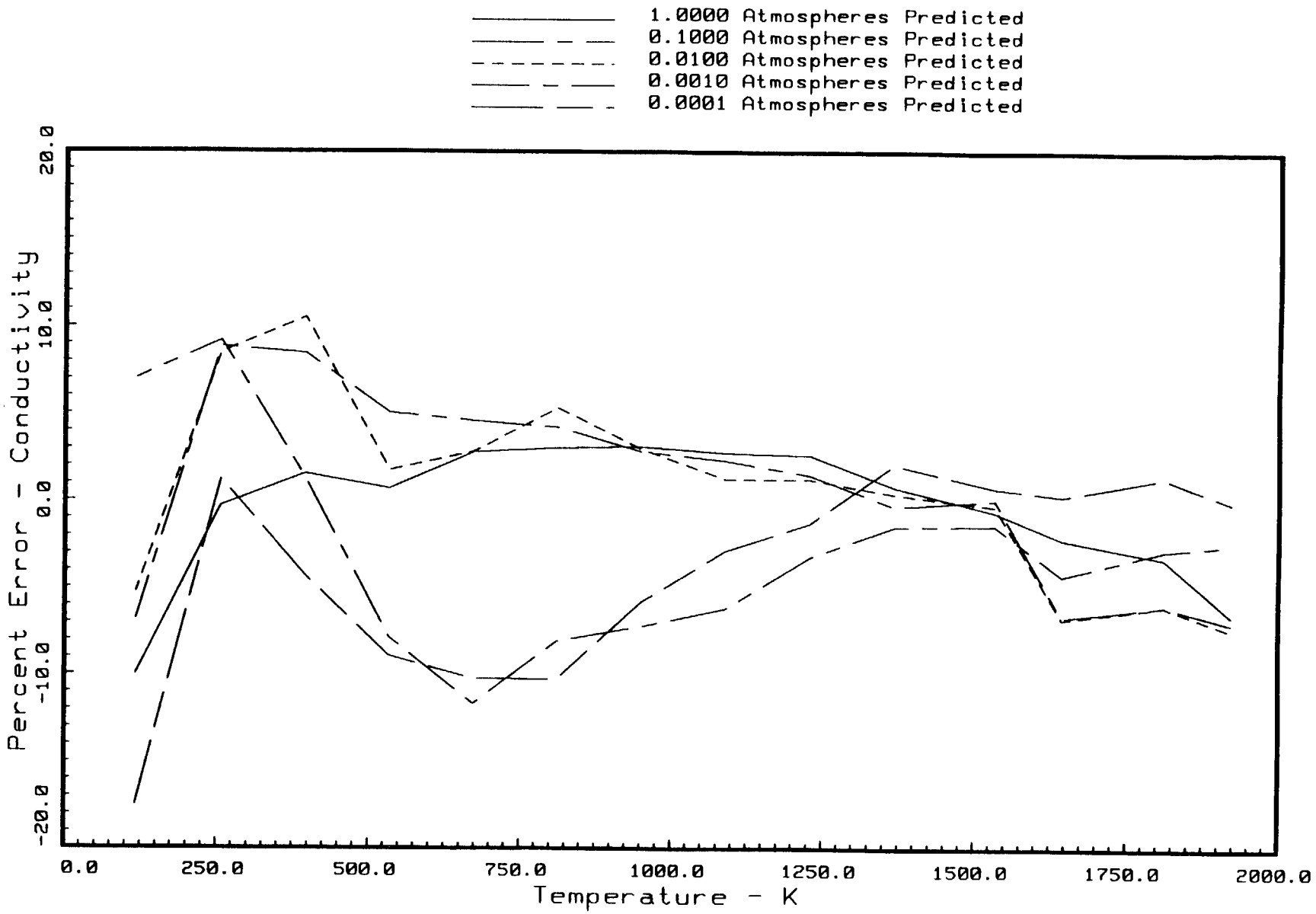

Fig. 9 Percent Error in Predicted LI-900 Conductivity in the Strong Direction Compared to Baseline Data.

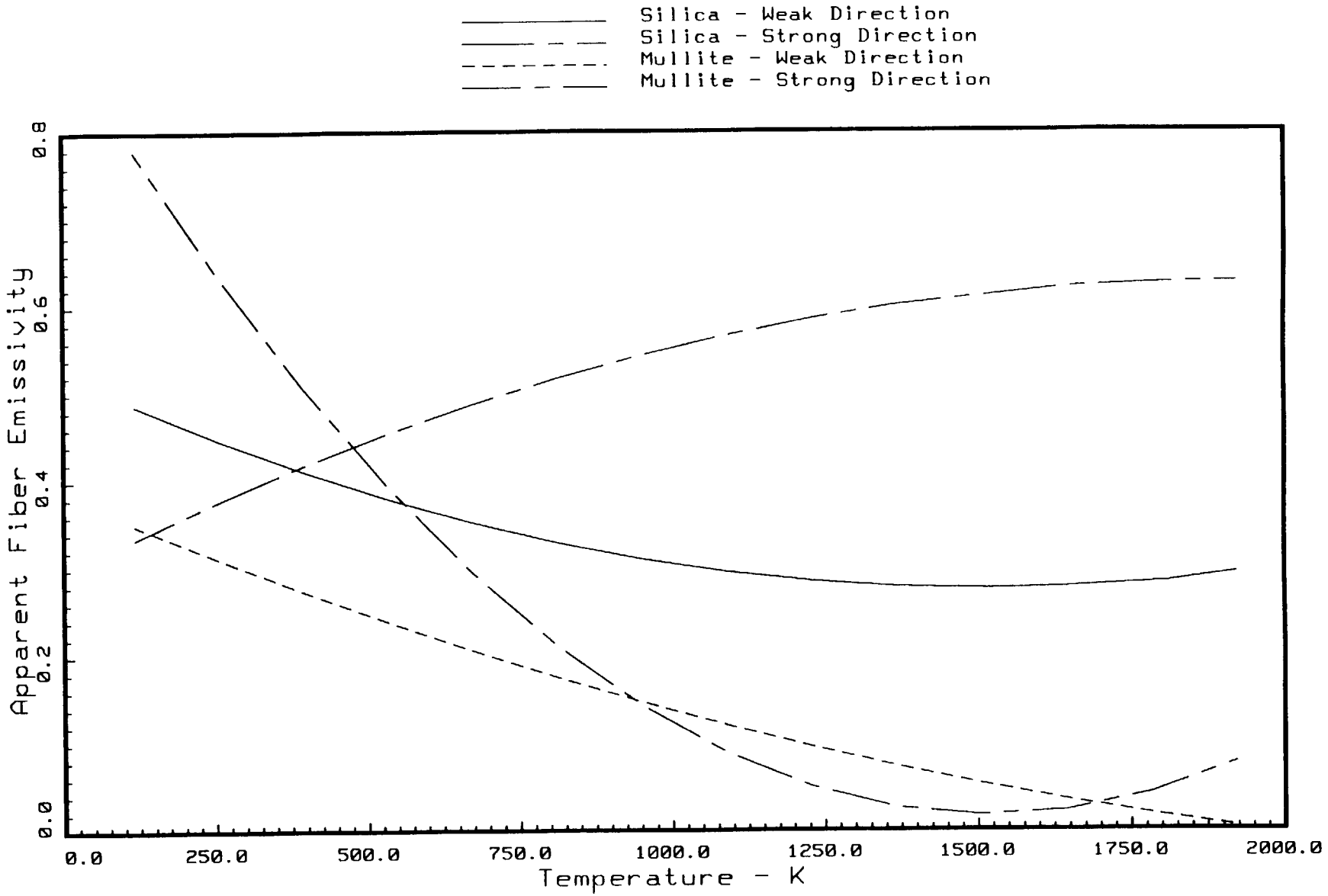

Fig. 10a Predicted Emissivity Values for Silica and Mullite (Nextel) in the Weak and Strong Directions as a Function of Temperature.

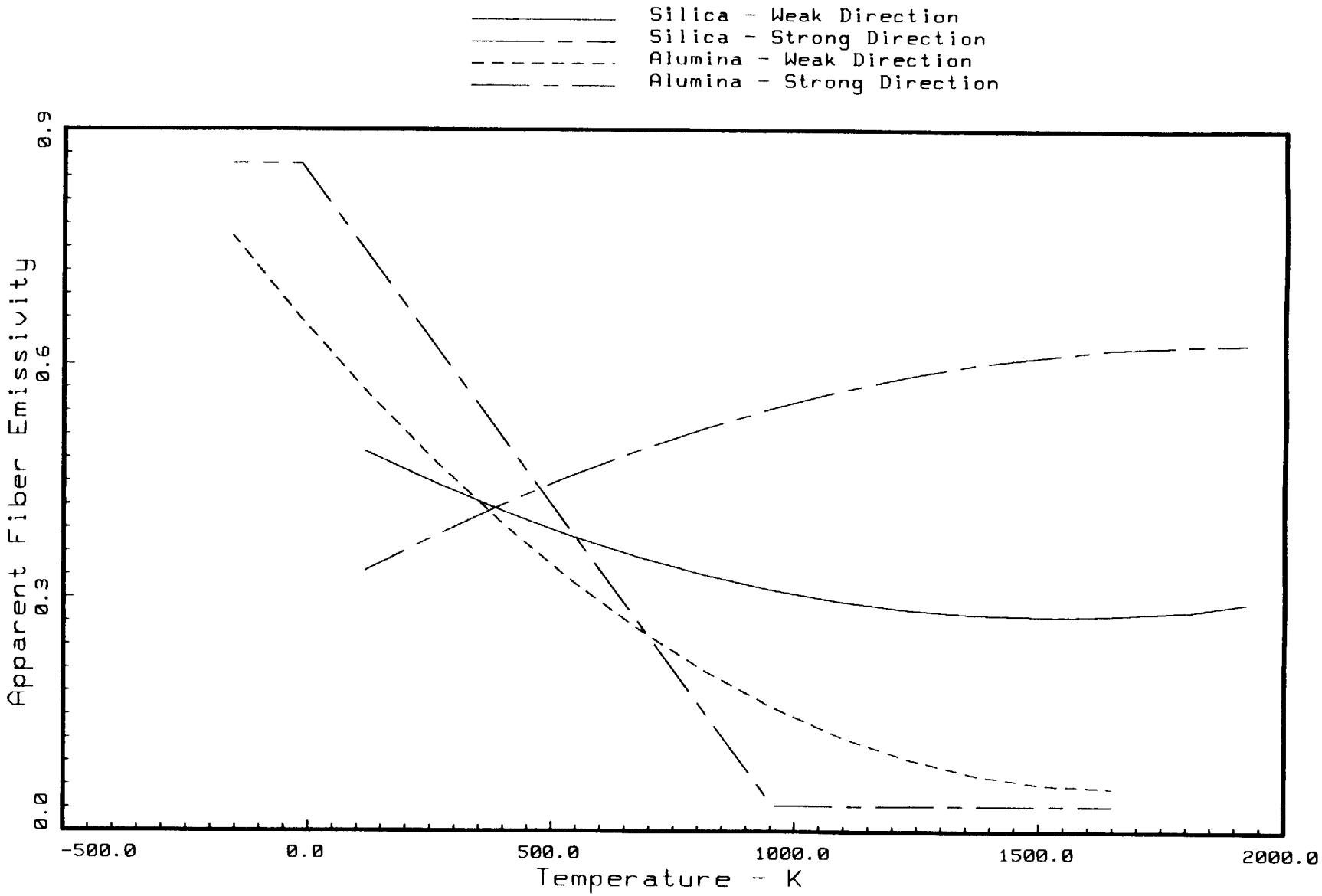

Fig. 10b Predicted Emissivity Values for Silica and Alumina in the Weak and Strong Directions as a Function of Temperature.

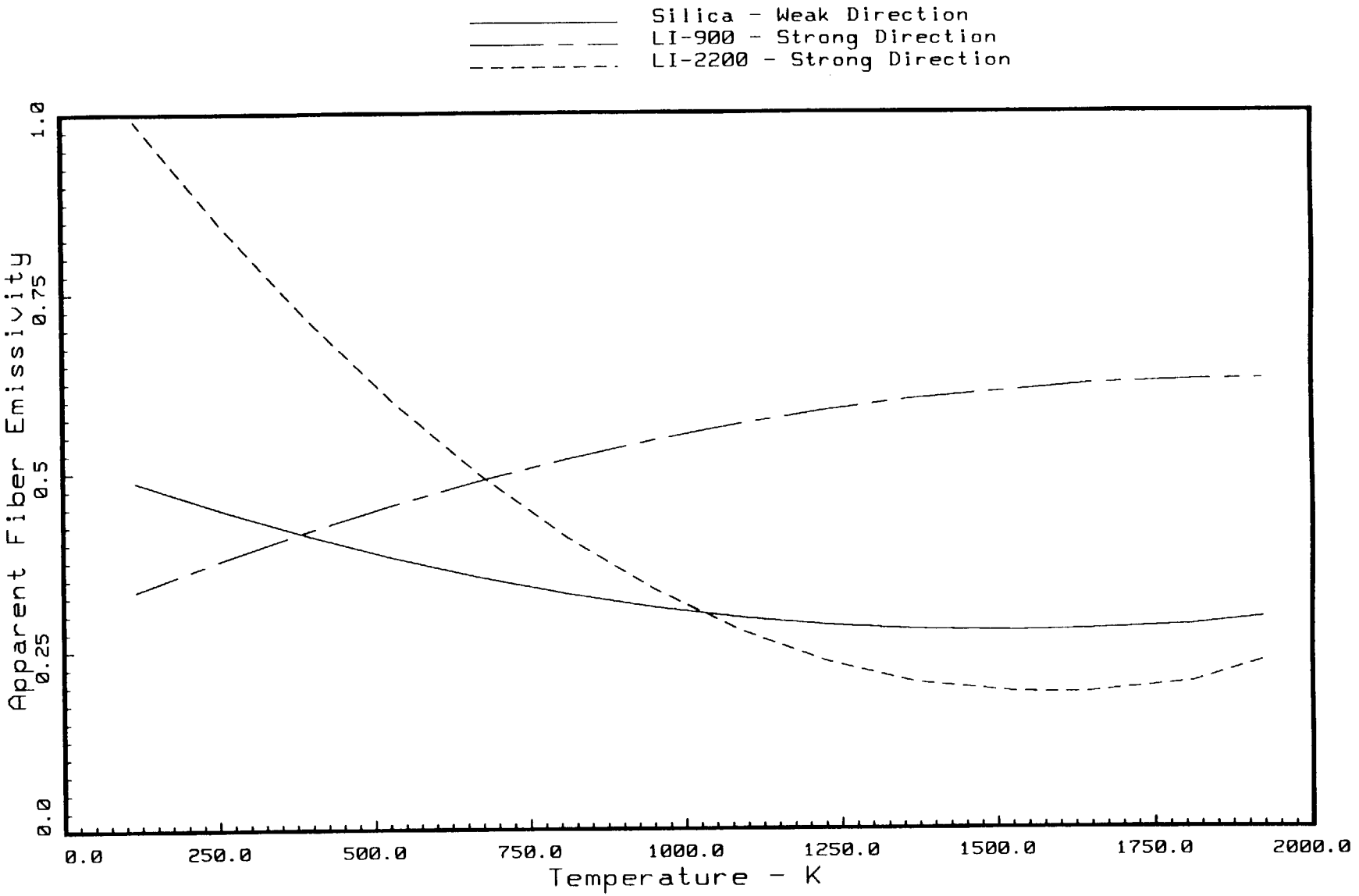

Fig. 10c Predicted Emissivity Values for Silica (LI-900 and LI-2200) in the Weak and Strong Directions as a Function of Temperature.

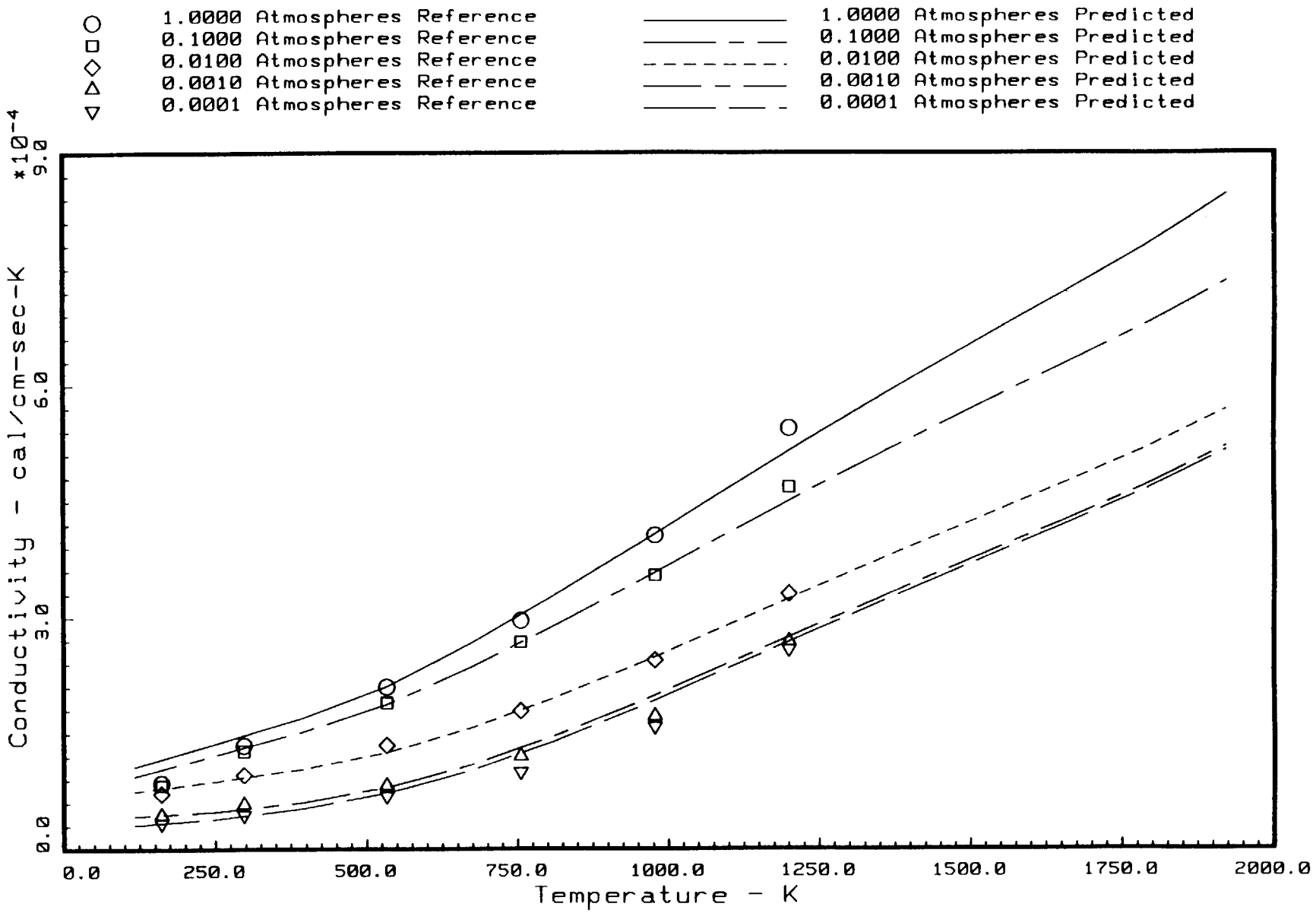

Fig. 11 Predicted FRCI-12 Conductivity in the Weak Direction vs. Baseline Values.

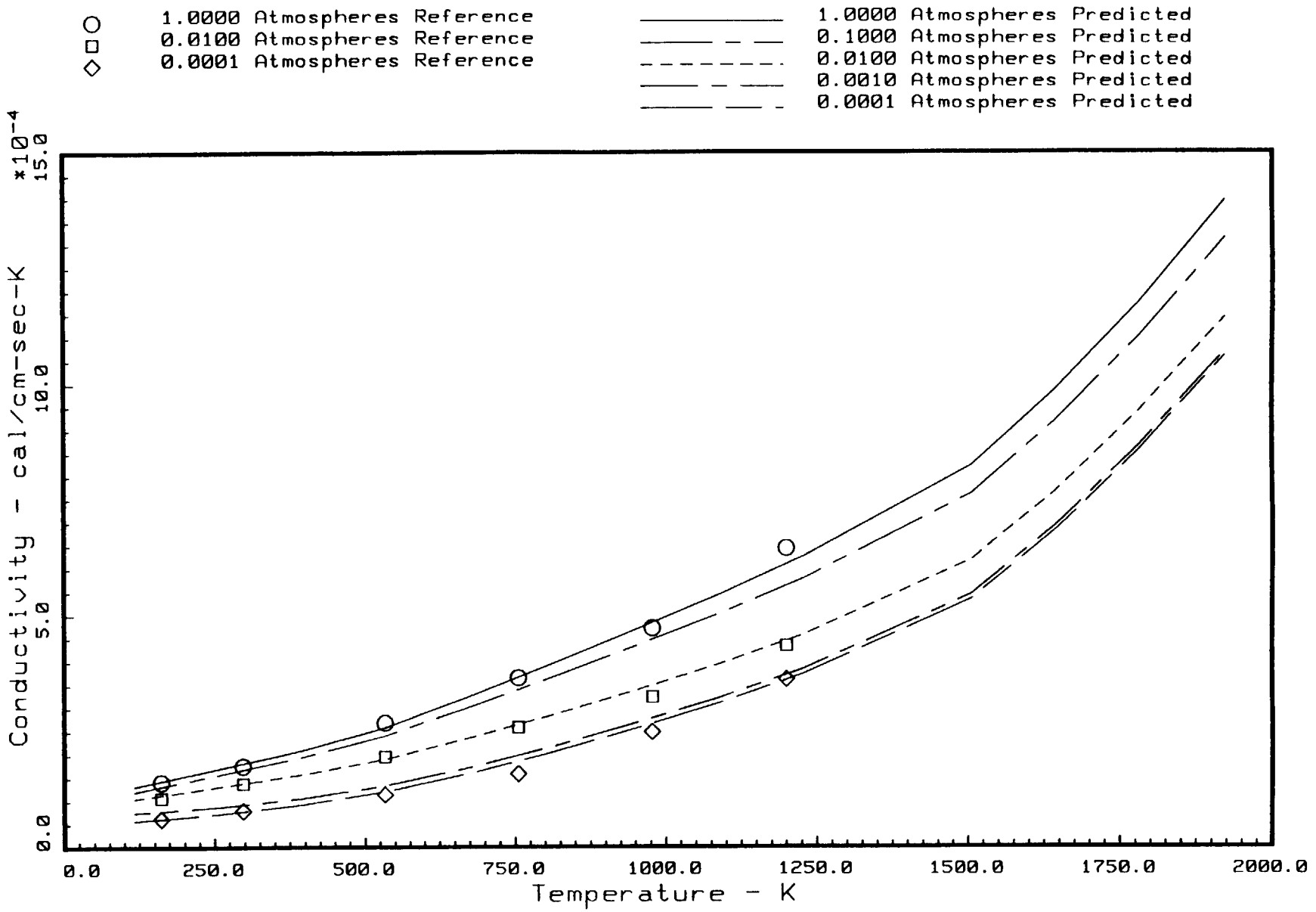

Fig. 12 Predicted FRCI-12 Conductivity in the Strong Direction vs. Baseline Values.

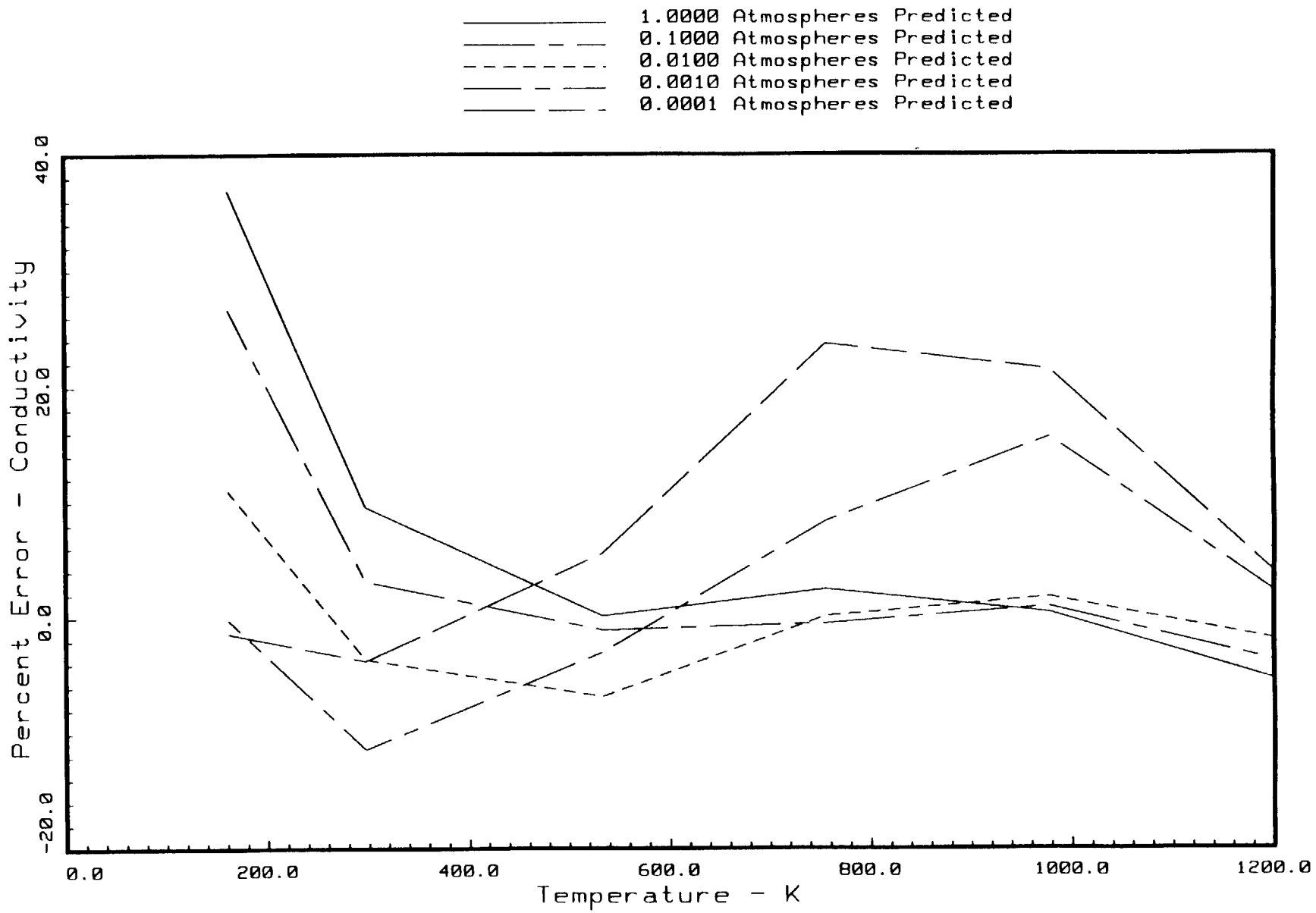

Fig. 13 Percent Error in Predicted FRCI-12 Conductivity in the Weak Direction Compared to Baseline Data.

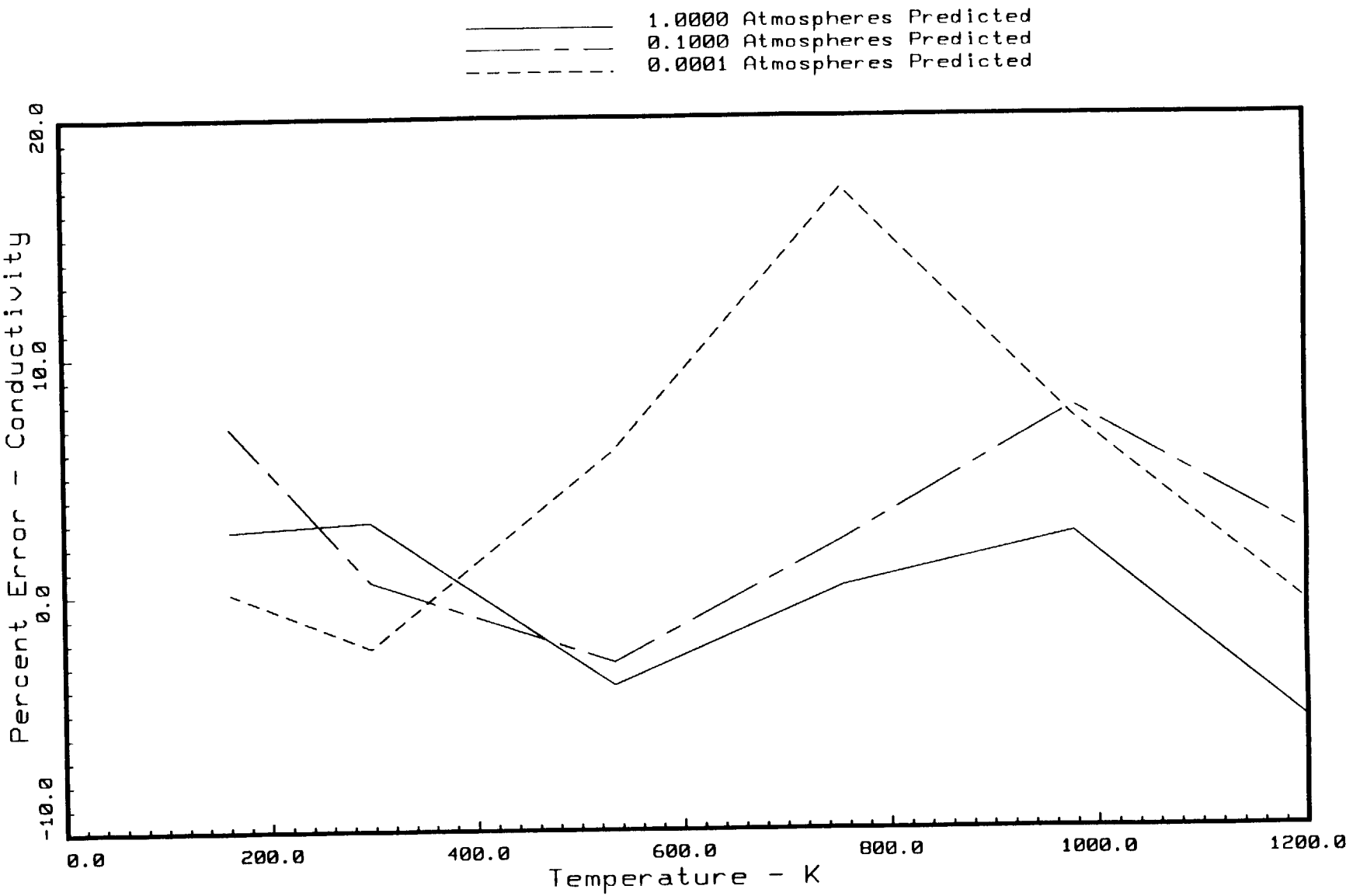

Fig. 14 Percent Error in Predicted FRCI-12 Conductivity in the Strong Direction Compared to Baseline Data.

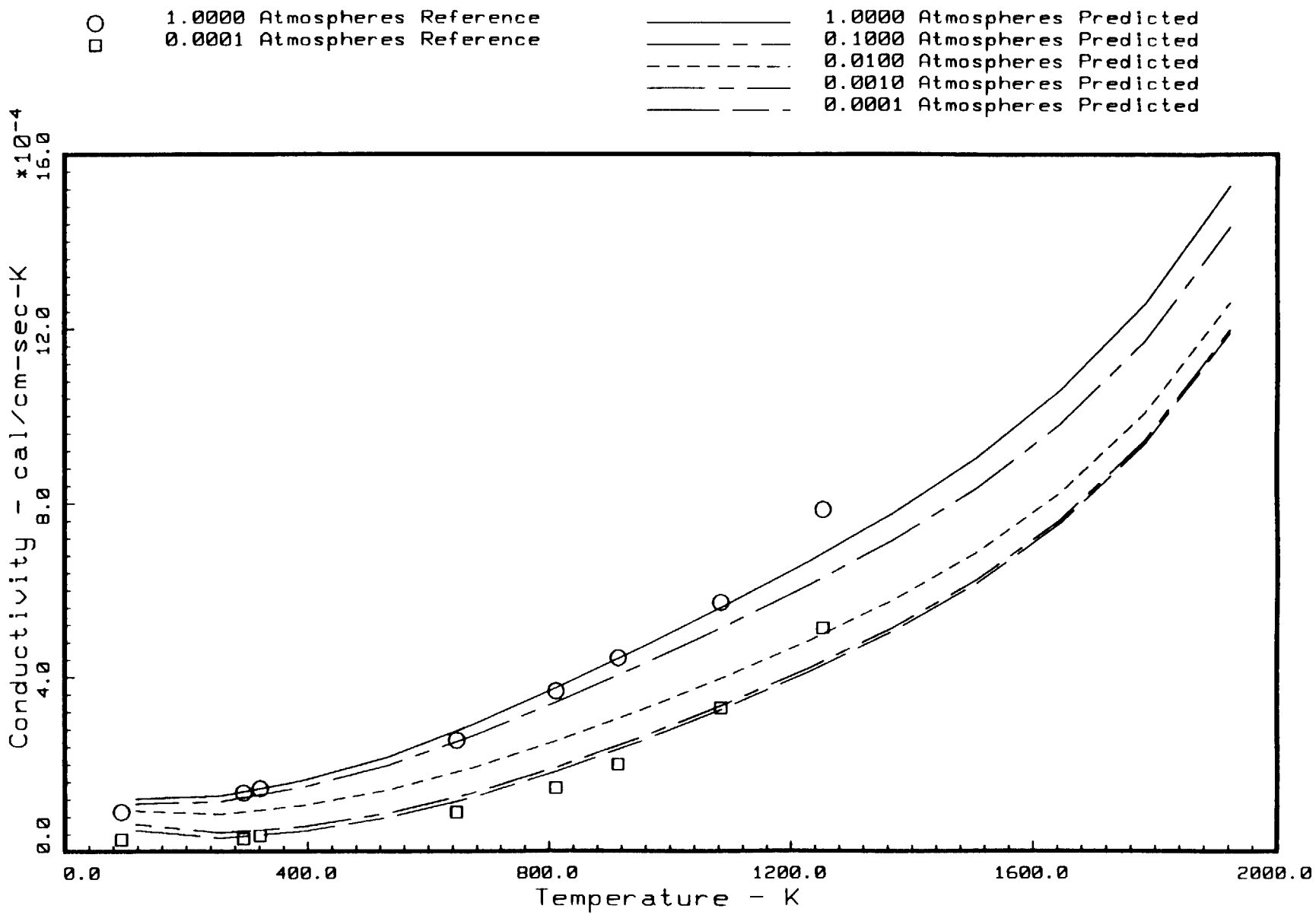

Fig. 15 Predicted HTP-6 Conductivity in the Weak Direction vs. Baseline Values.

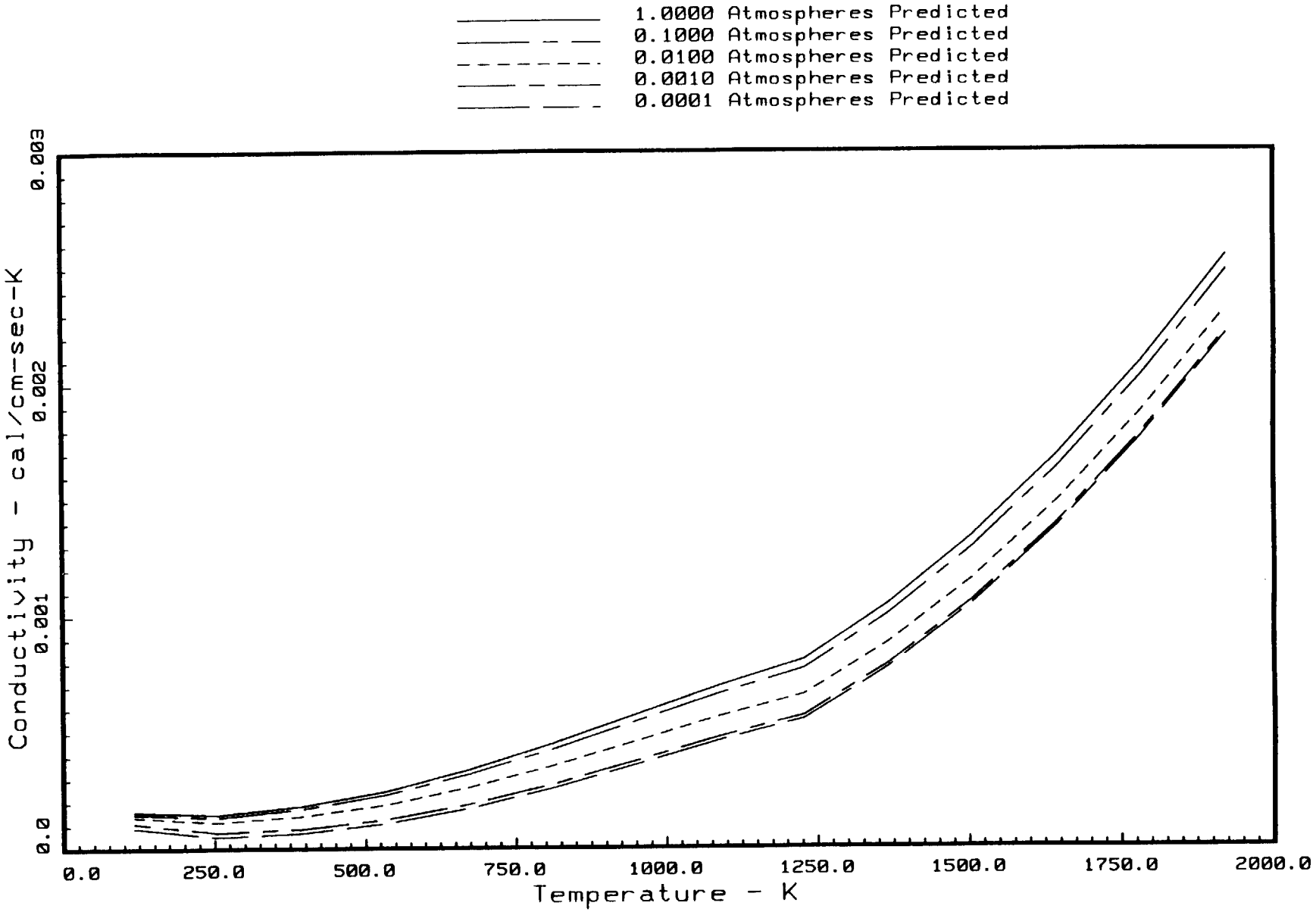

Fig. 16 Predicted HTP-6 Conductivity in the Strong Direction.

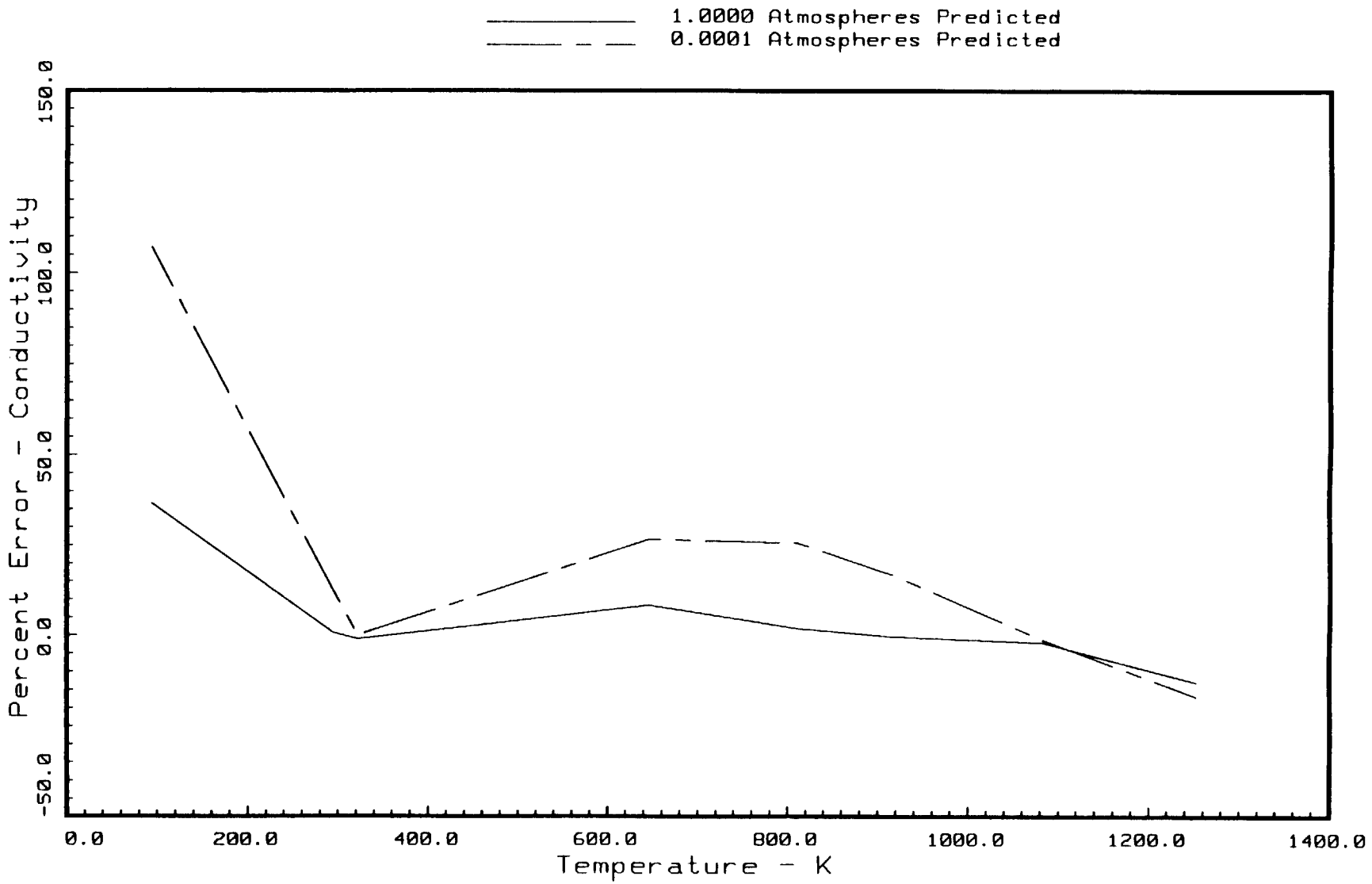

Fig. 17a Percent Error in Predicted HTP-6 Conductivity in the Weak Direction Compared to Baseline Data.

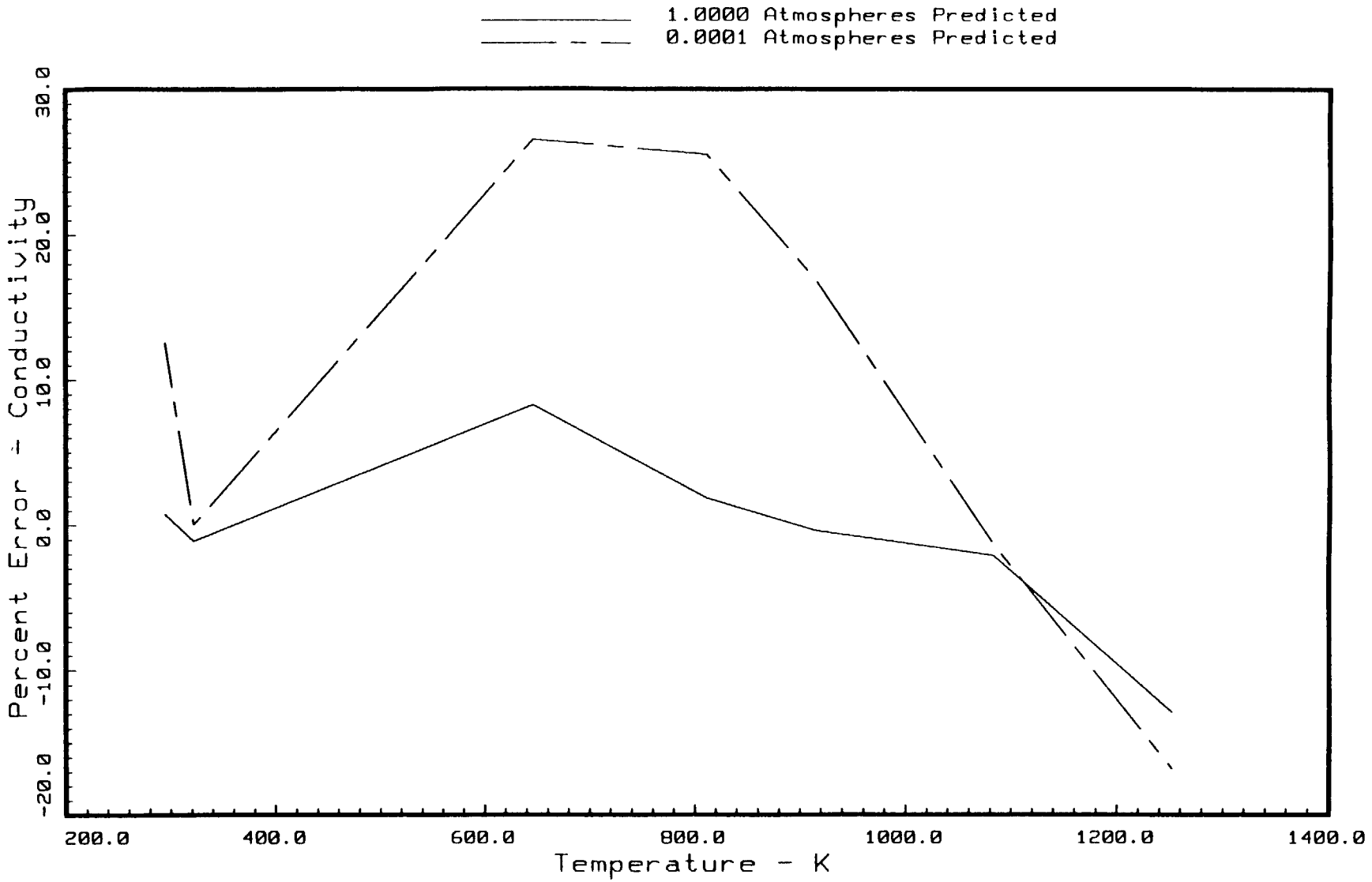

Fig. 17b Percent Error in Predicted HTP-6 Conductivity in the Weak Direction Compared to Baseline Data.

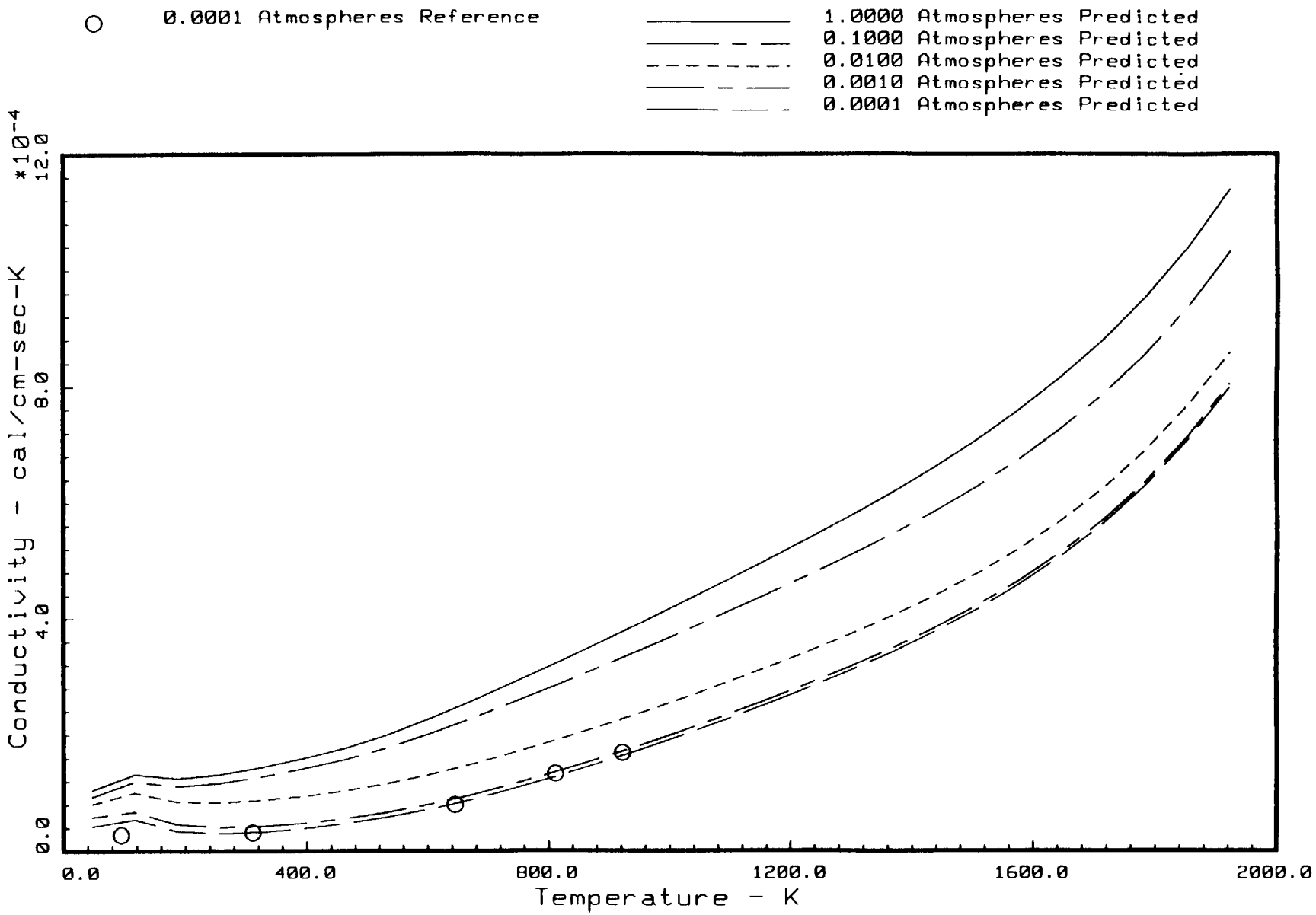

Fig. 18 Predicted HTP-9 Conductivity in the Weak Direction vs. Baseline Values.

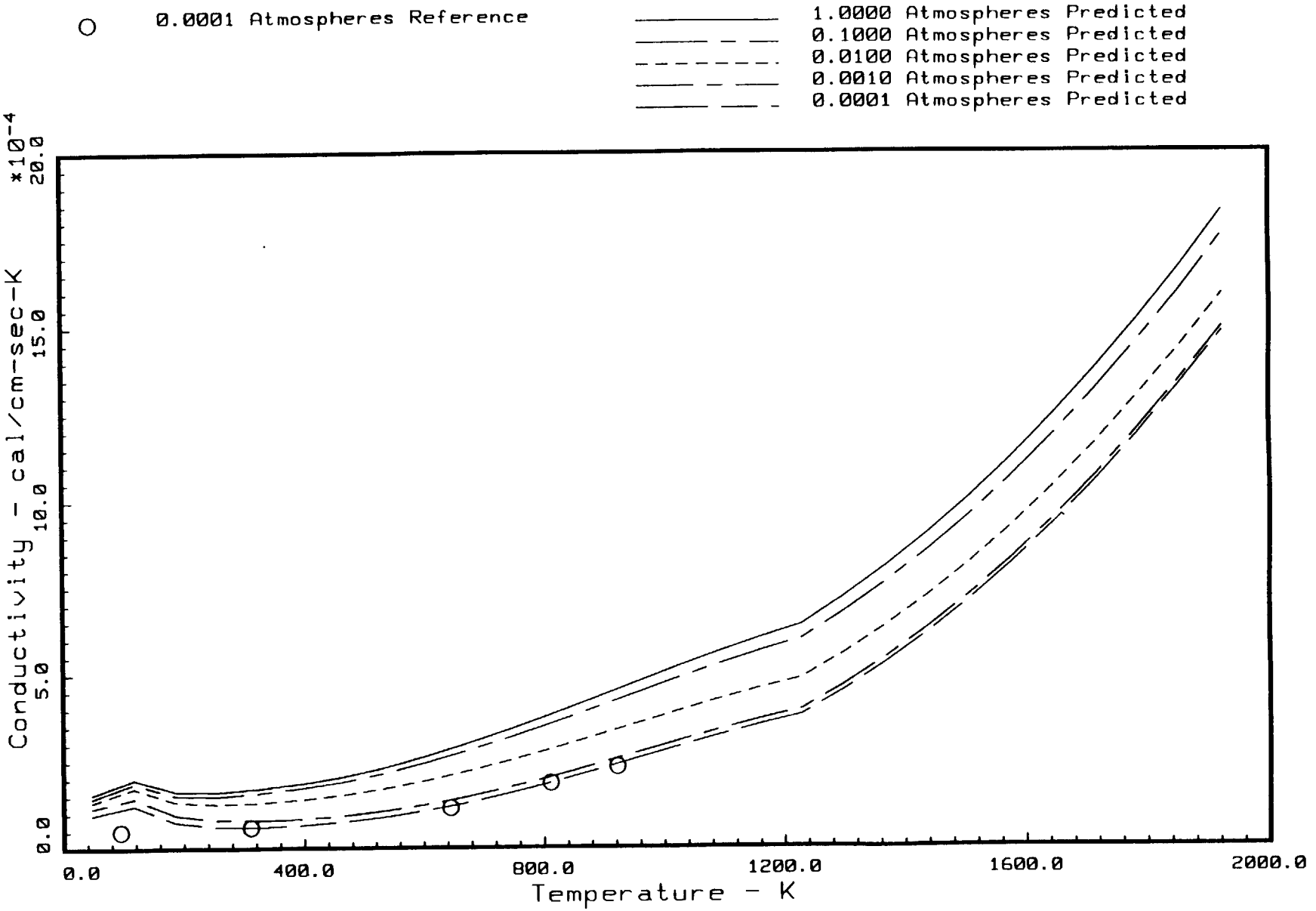

Fig. 19 Predicted HTP-9 Conductivity in the Strong Direction vs. Baseline Values.

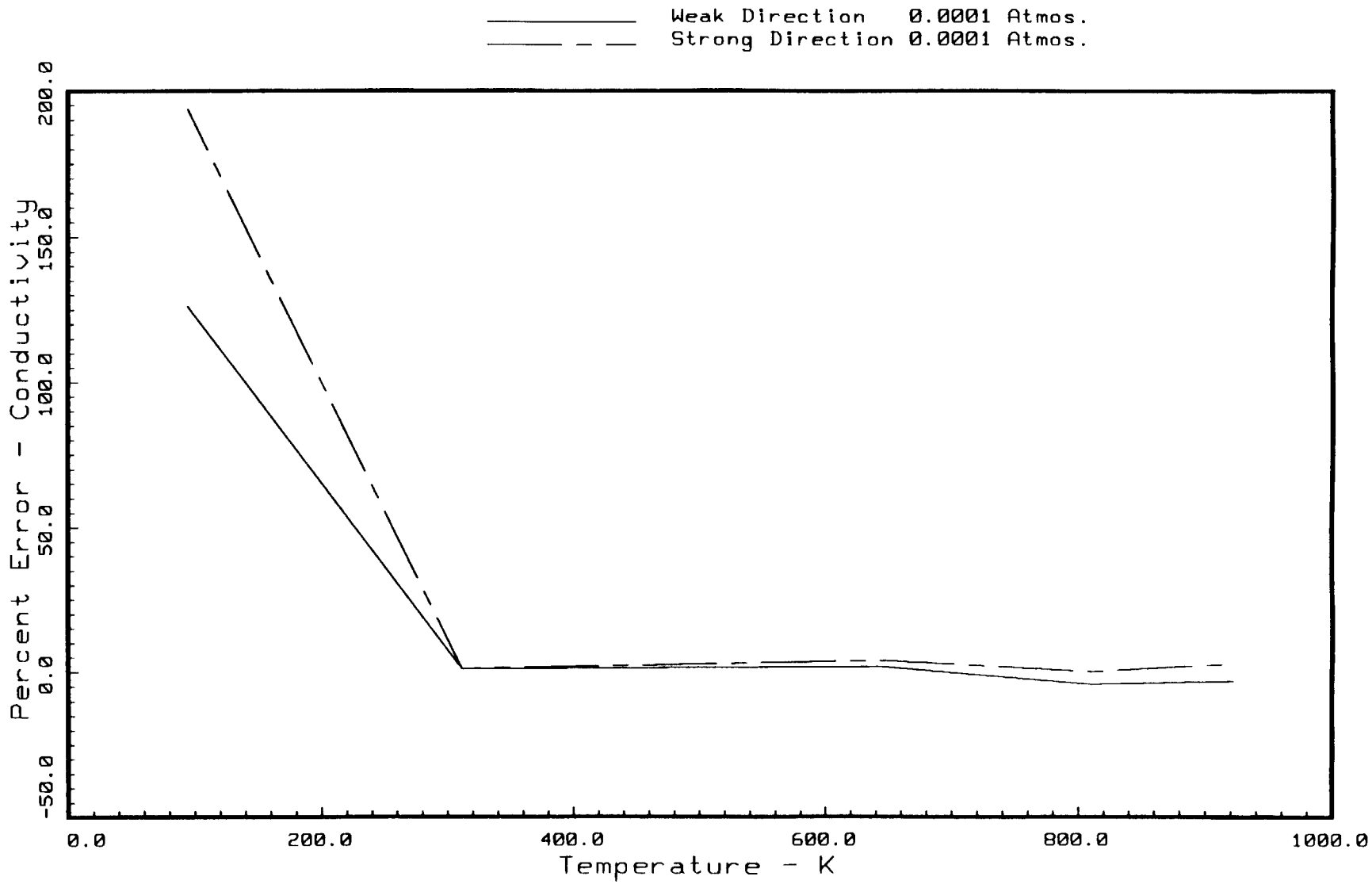

Fig. 20a Percent Error in Predicted HTP-9 Conductivity in the Weak and Strong Directions Compared to Baseline Data.

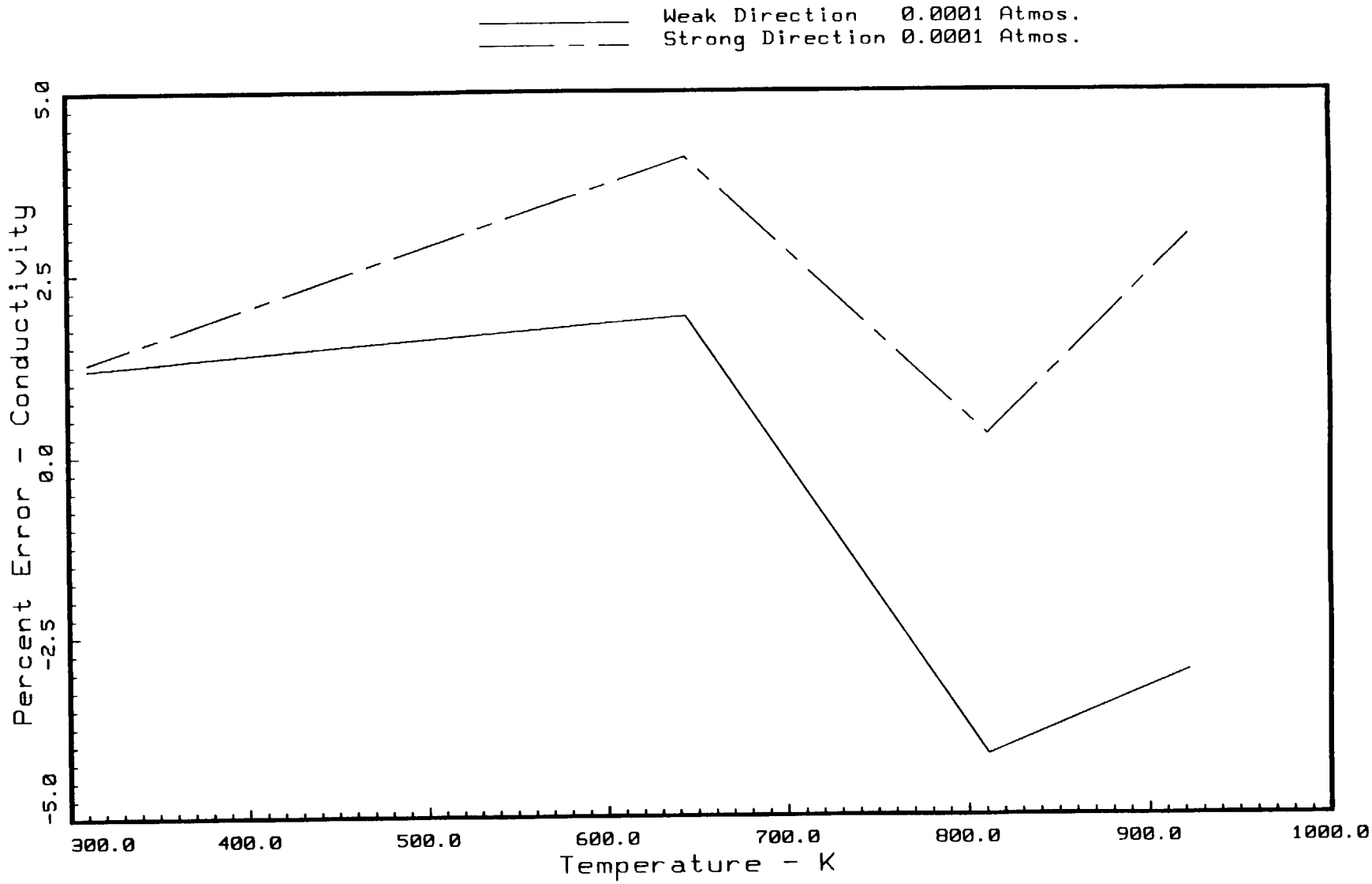

Fig. 20b Percent Error in Predicted HTP-9 Conductivity in the Weak and Strong Directions Compared to Baseline Data.

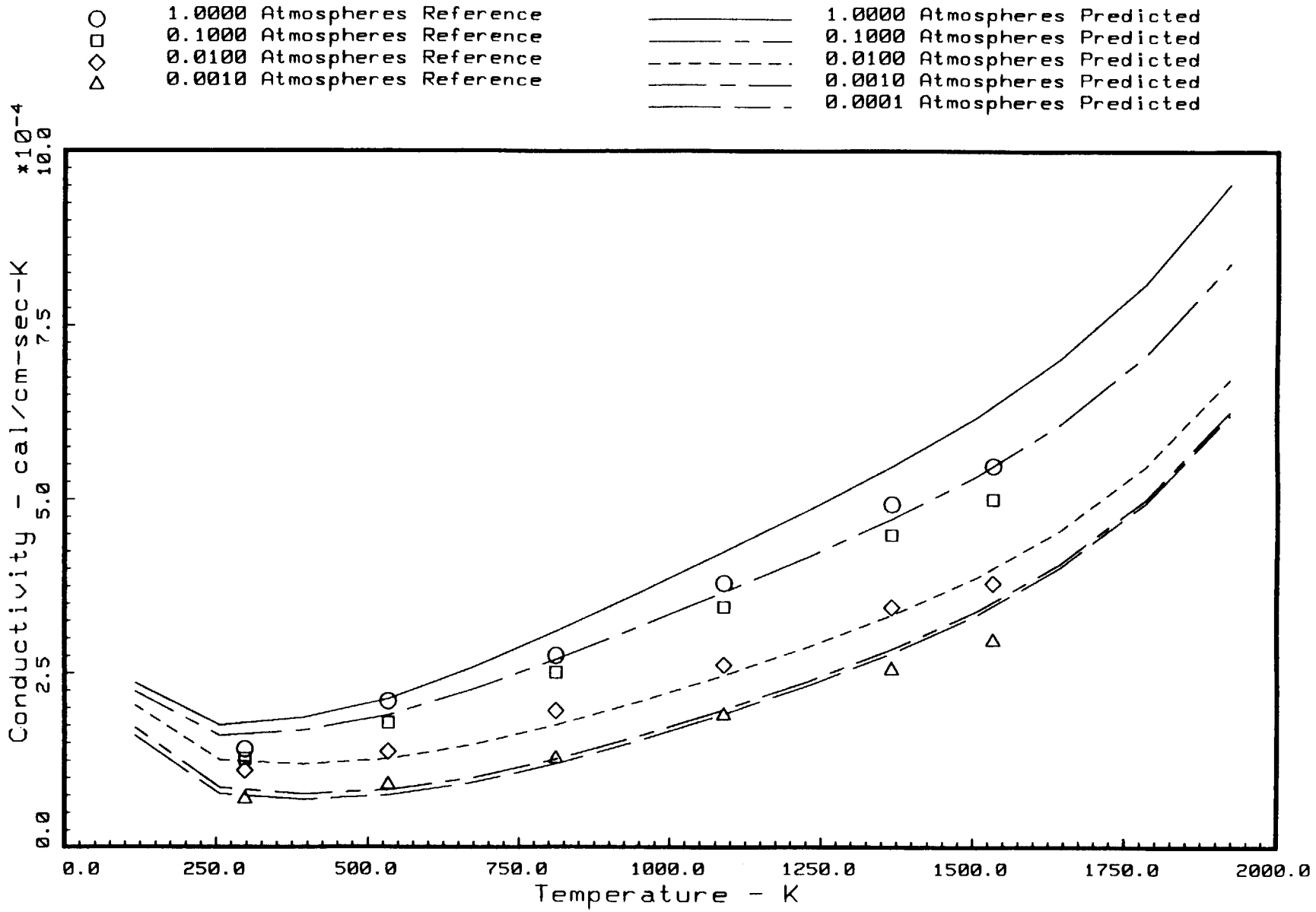

Fig. 21 Predicted HTP-12 Conductivity in the Weak Direction vs. Baseline Values.

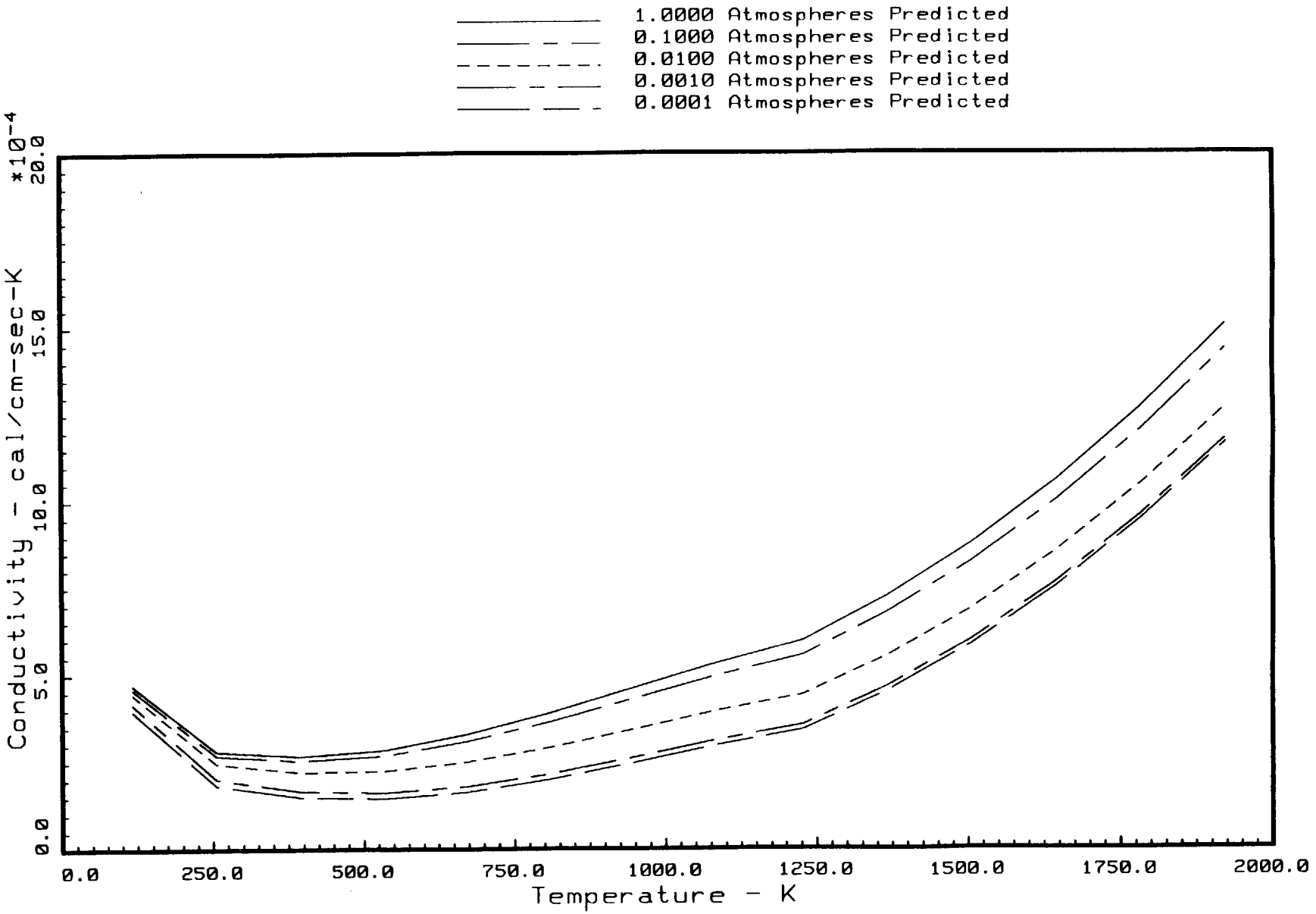

Fig. 22 Predicted HTP-12 Conductivity in the Strong Direction.

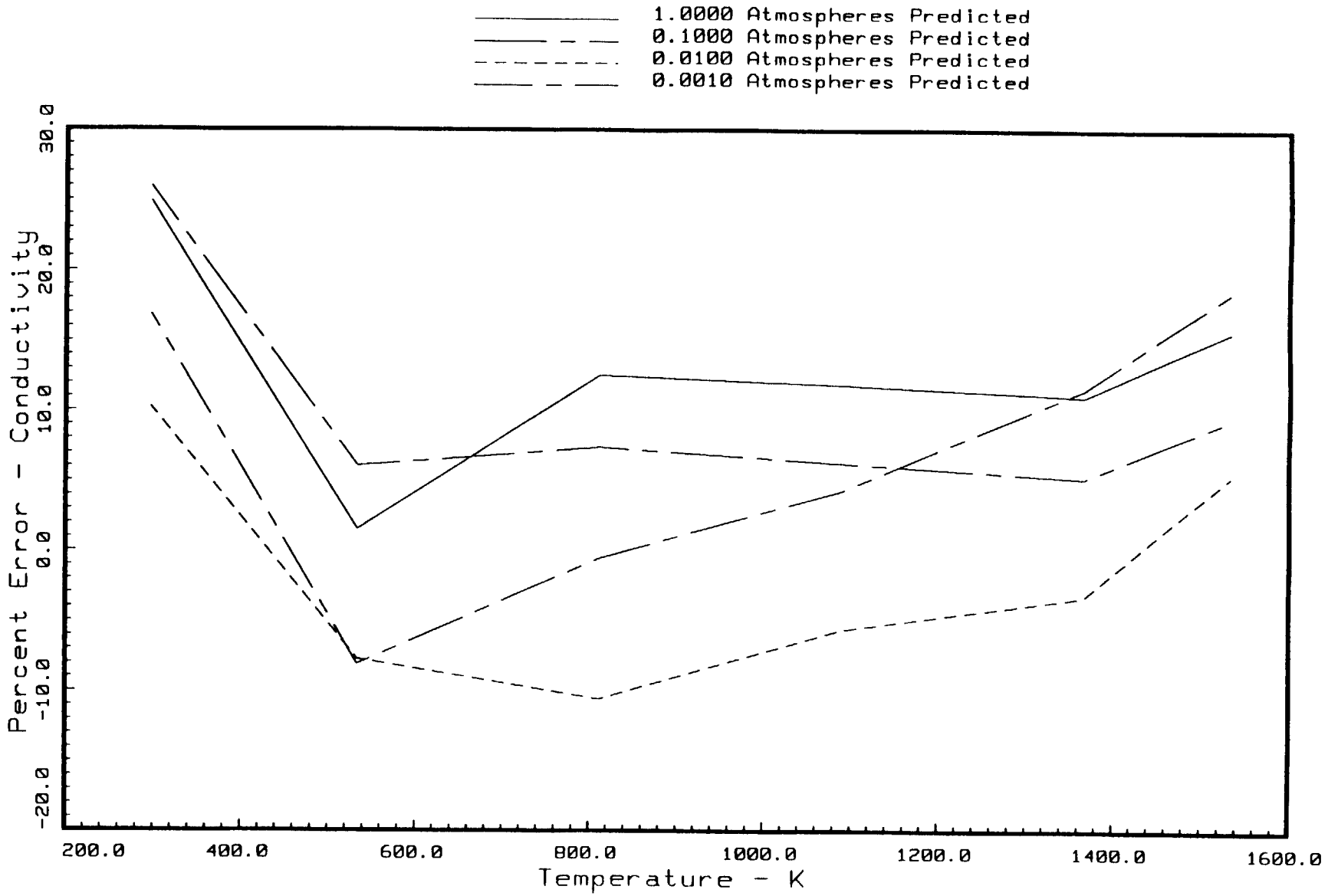

Fig. 23 Percent Error in Predicted HTP-12 Conductivity in the Weak Direction Compared to Baseline Data.

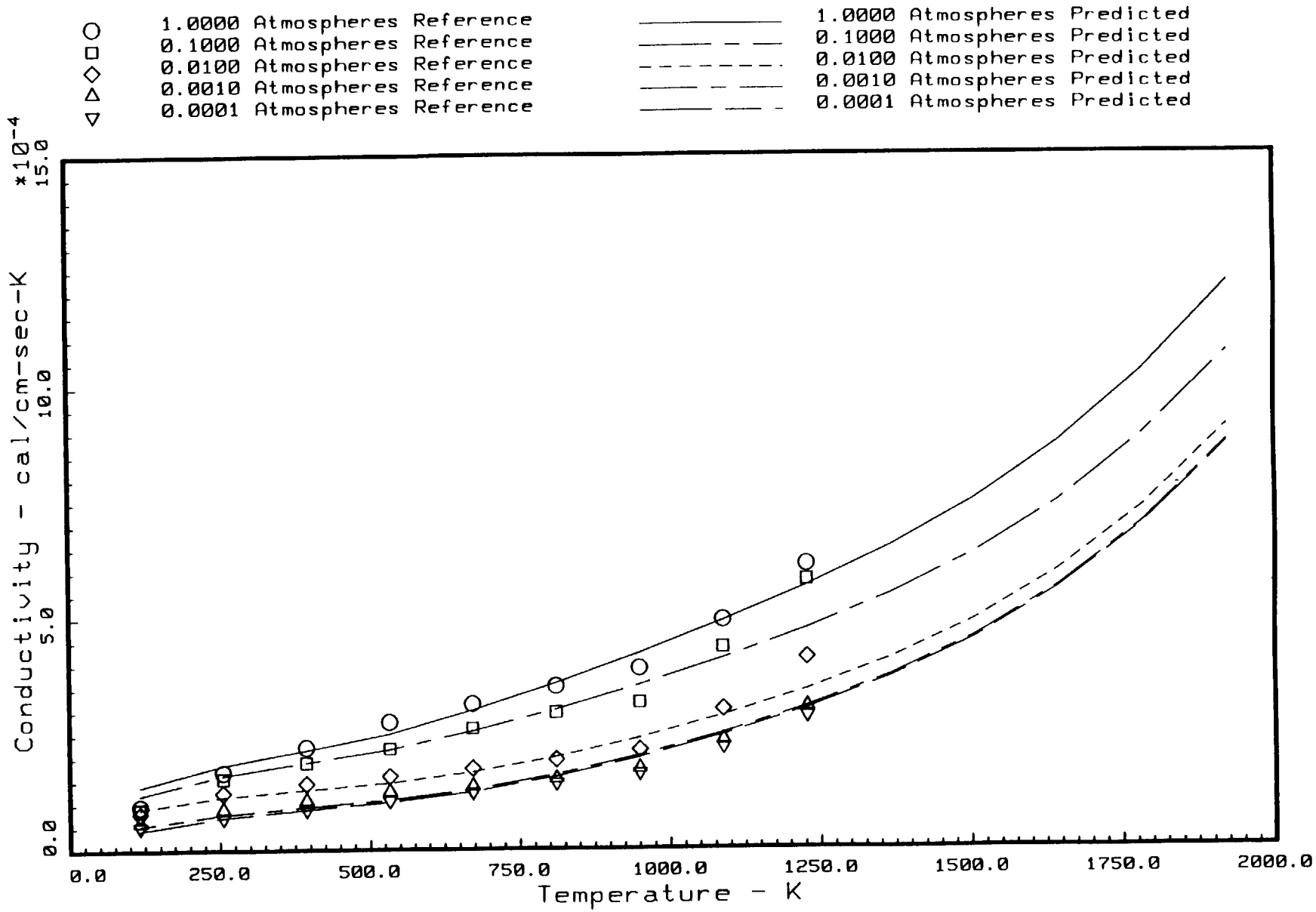

Fig. 24 Predicted LI-2200 Conductivity in the Weak Direction vs. Baseline Values.

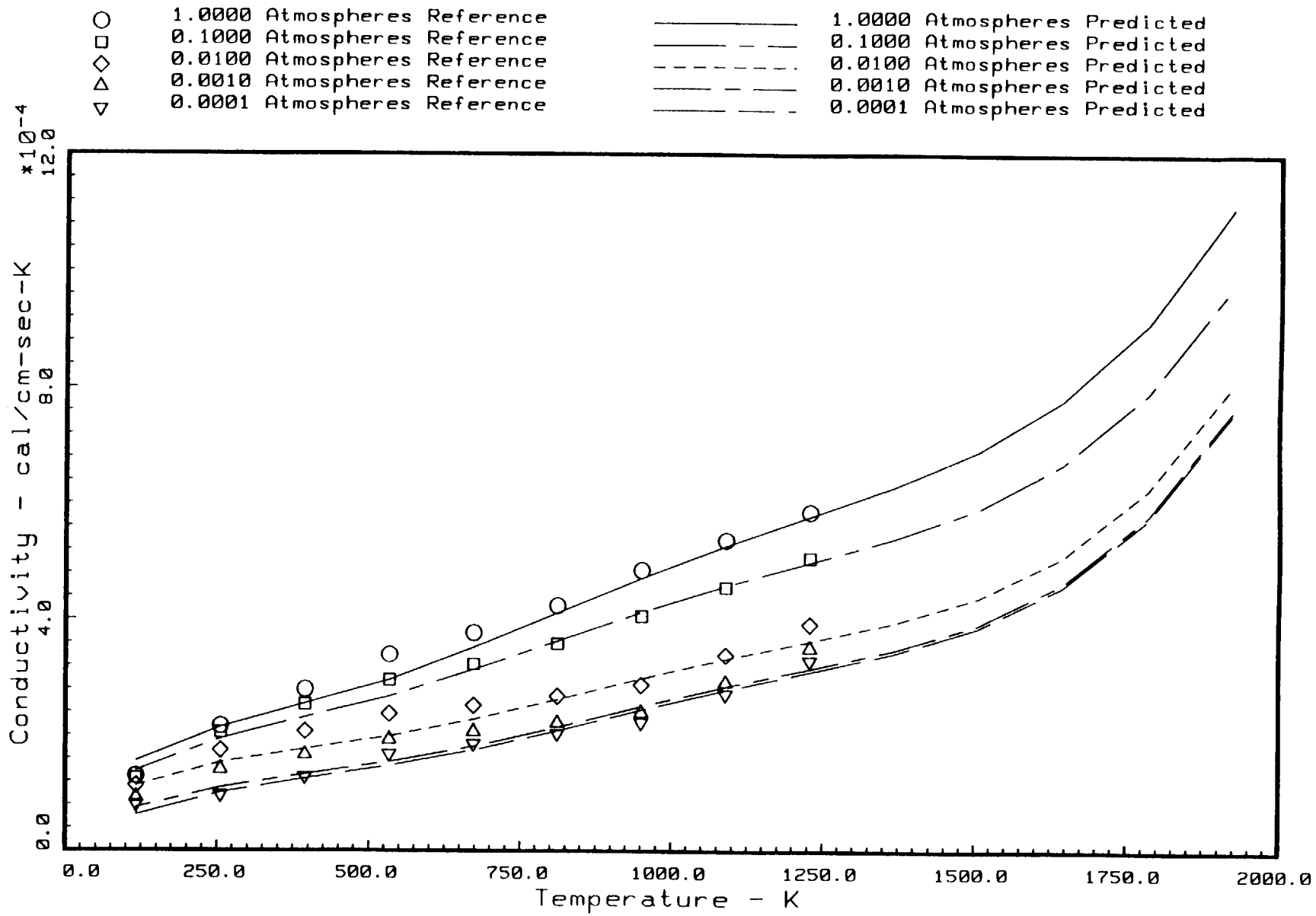

Fig. 25 Predicted LI-2200 Conductivity in the Strong vs. Baseline Values.

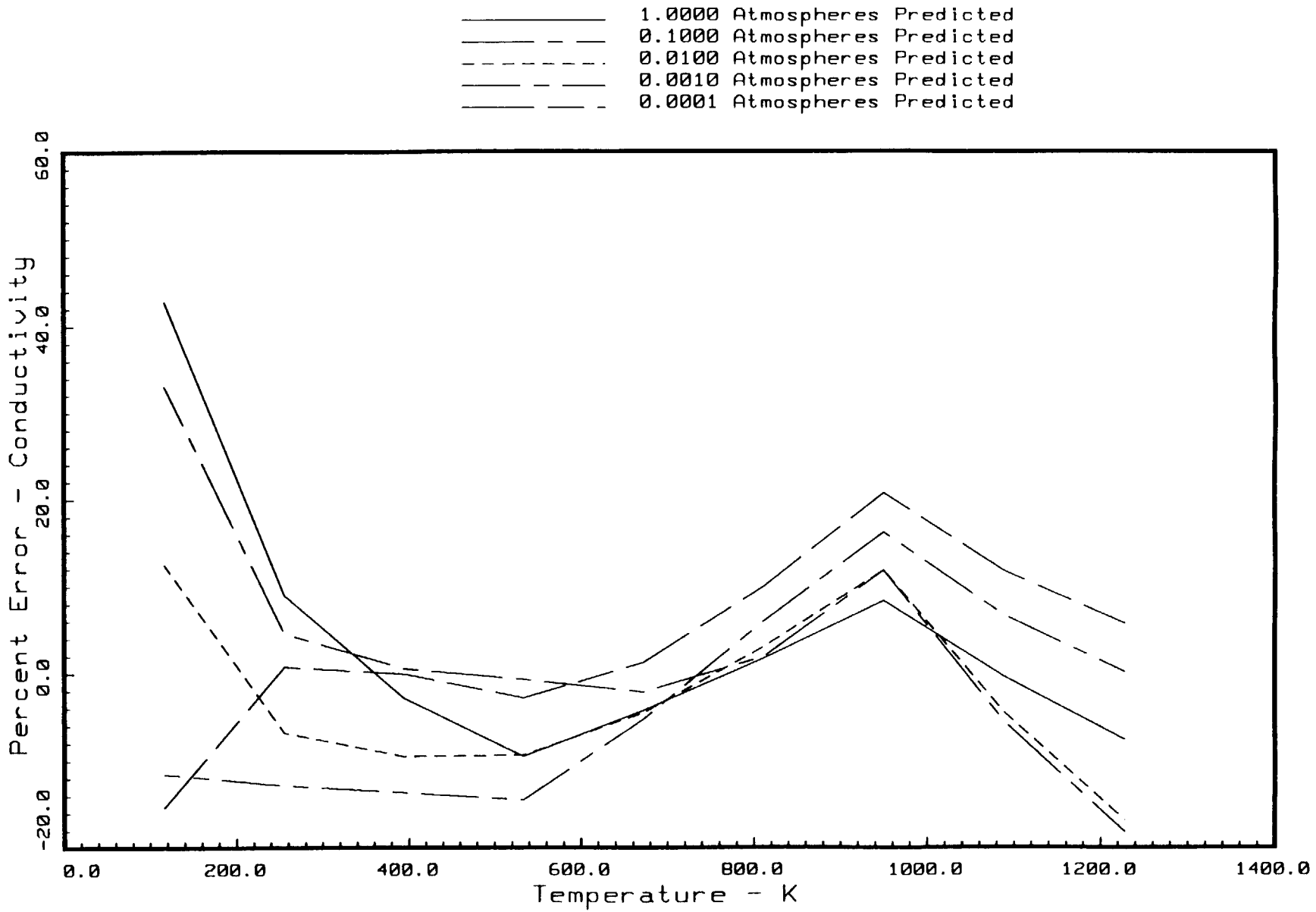

Fig. 26 Percent Error in Predicted LI-2200 Conductivity in the Weak Direction Compared to Baseline Data.

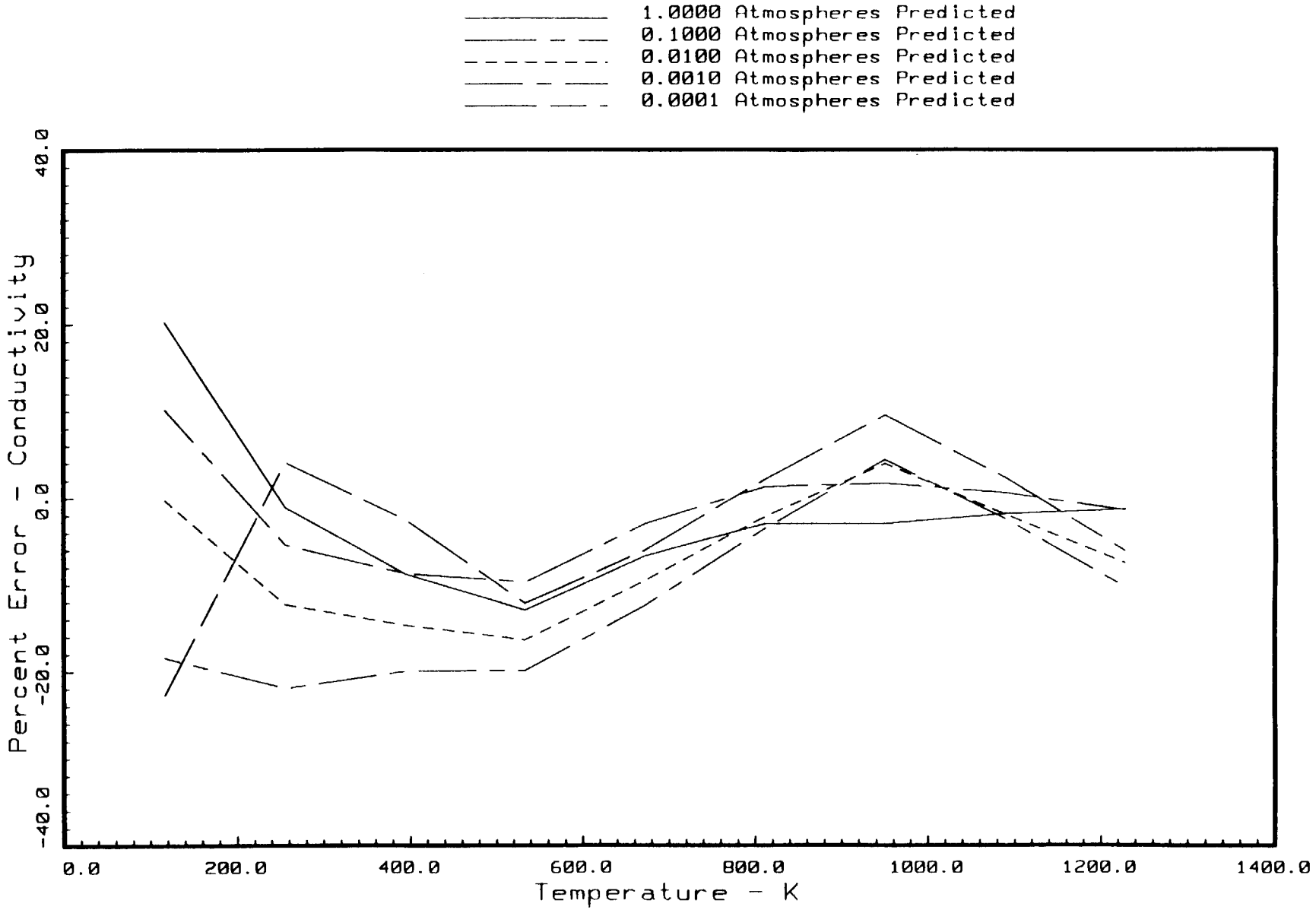

Fig. 27 Percent Error in Predicted LI-2200 Conductivity in the Strong Direction Compared to Baseline Data.

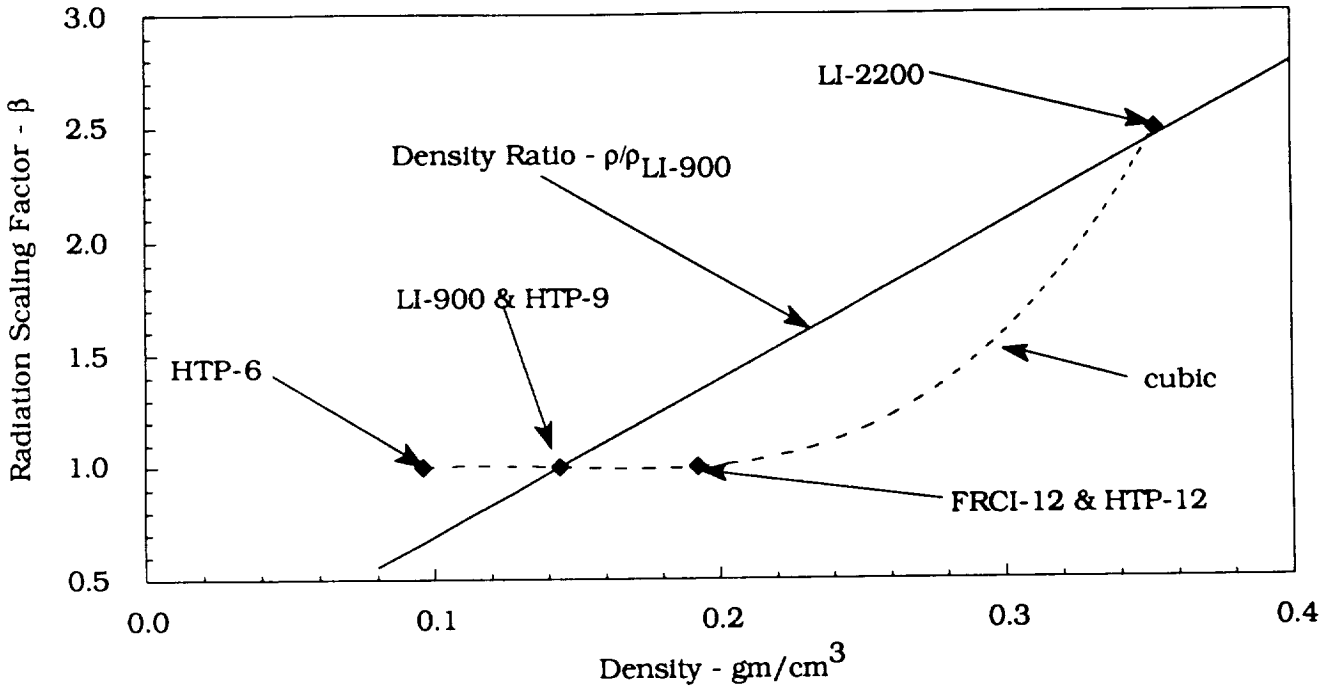

Fig. 28 Radiation Scaling Factor, β, as a Function of Density.

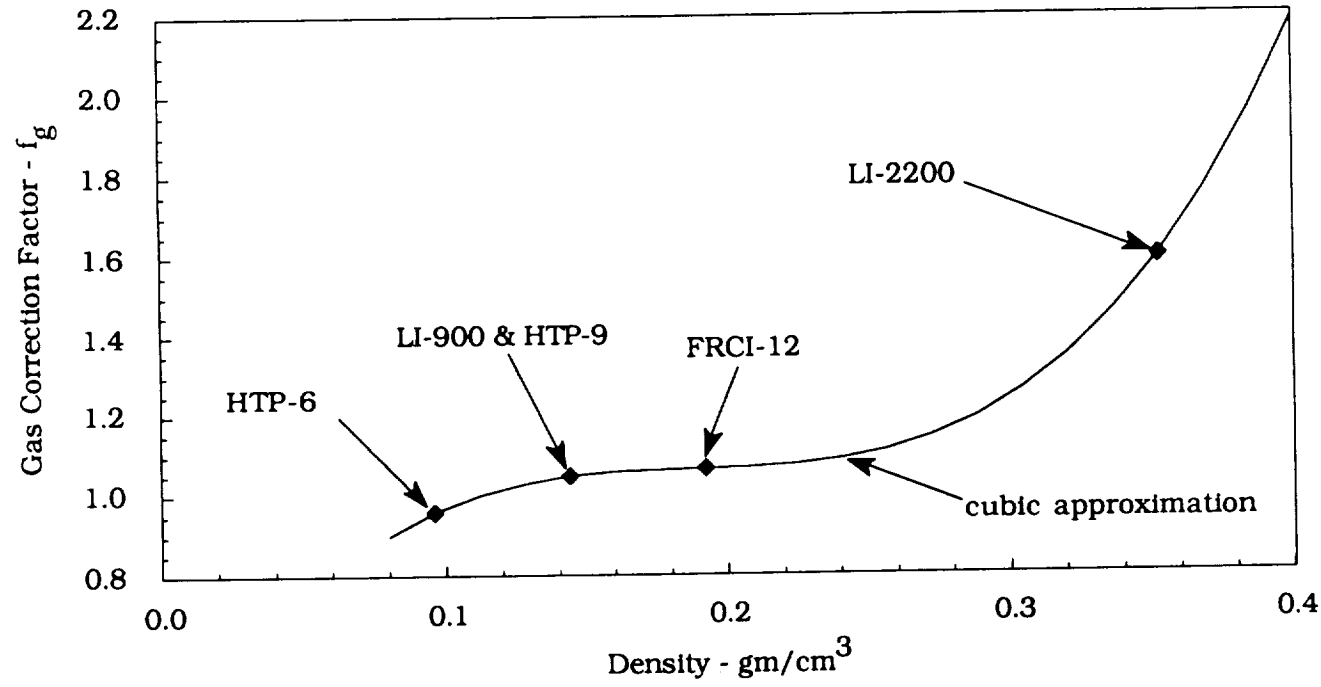

Fig. 29 Gas Correction Factor, f_g, as a Function of Density.

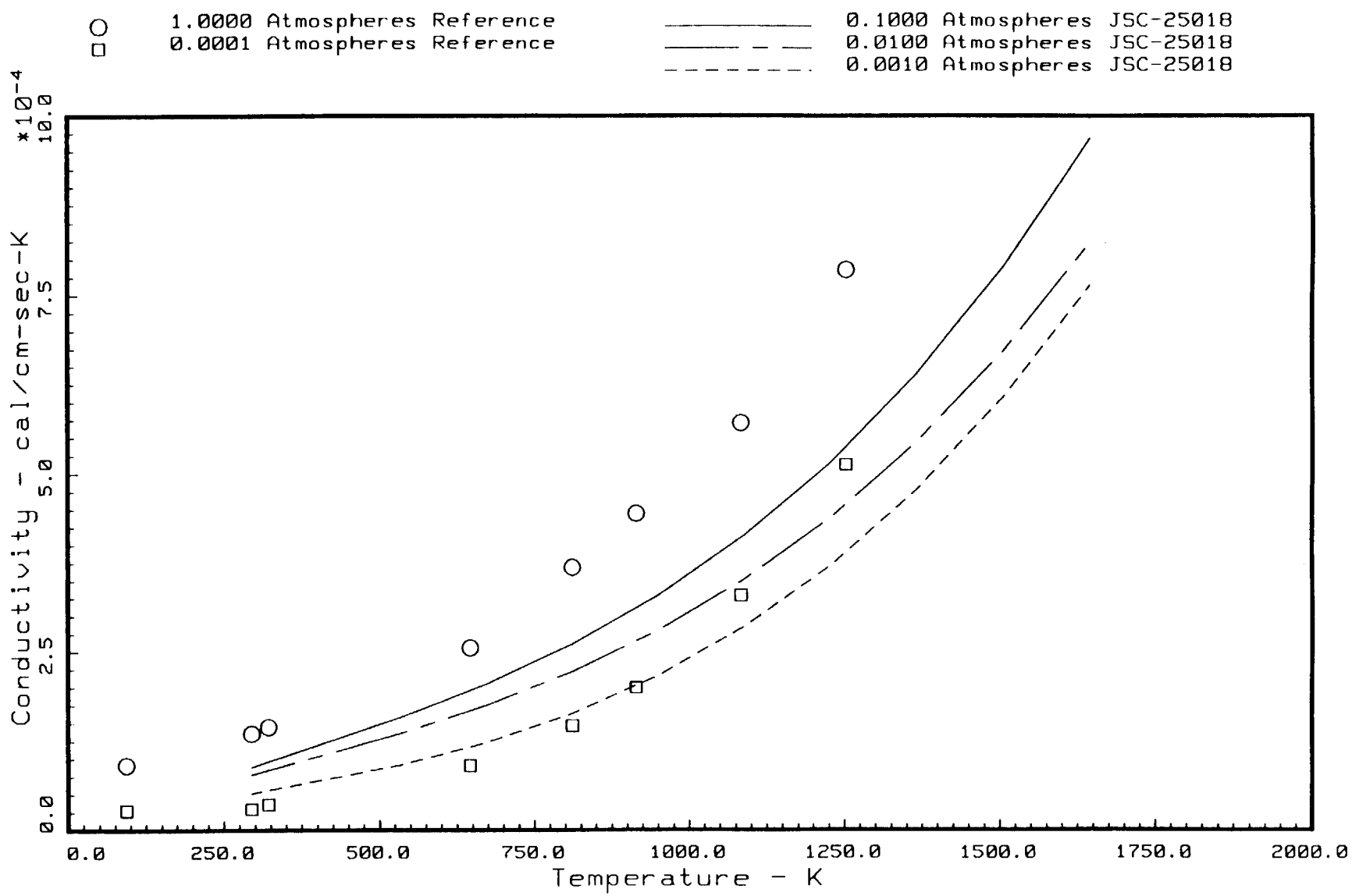

Fig. 30 HTP-6 Calculated Conductivity (JSC-25018) in the Weak Direction vs. Baseline Values.

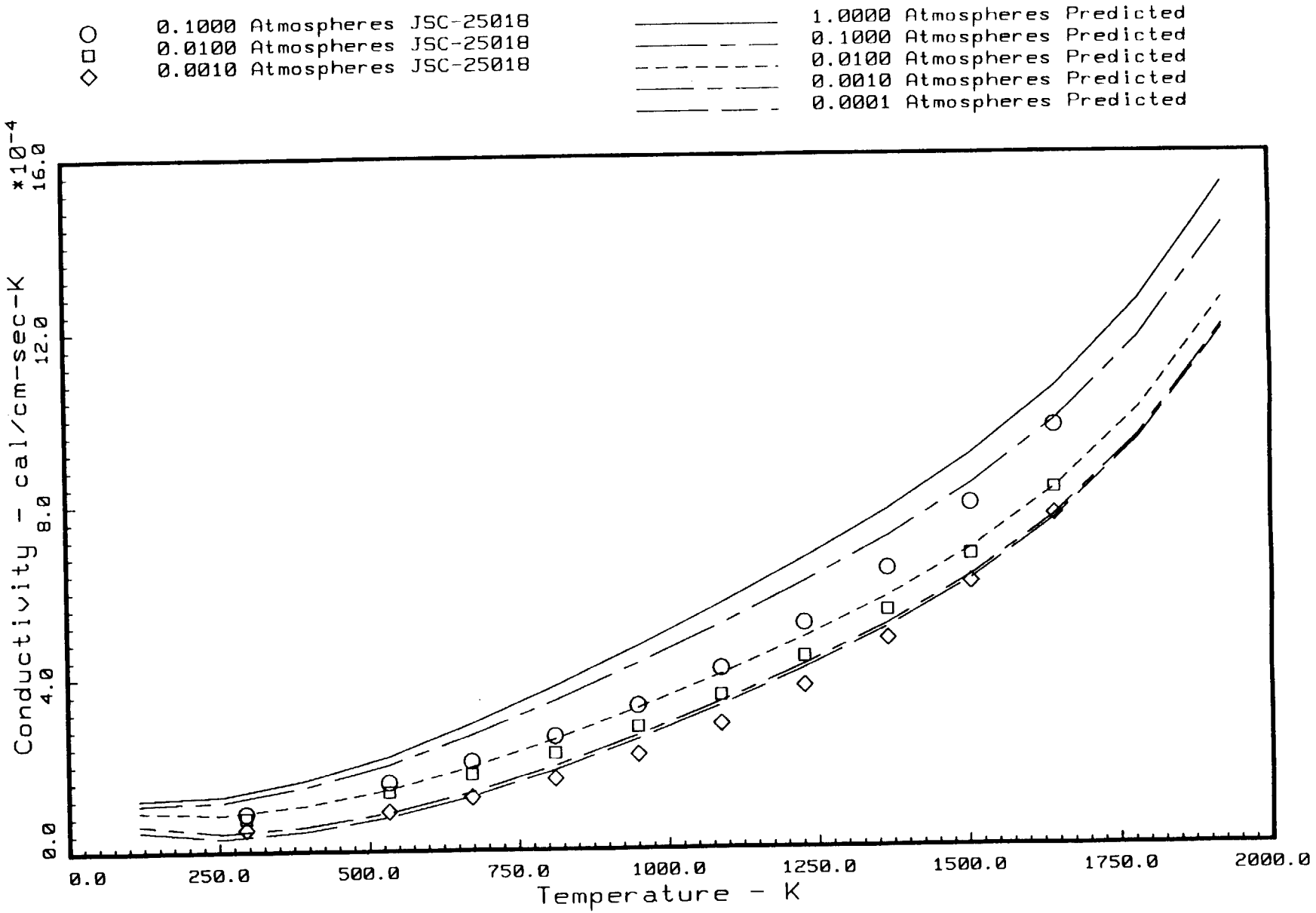

Fig. 31 Predicted HTP-6 Conductivity in the Weak Direction vs. JSC-25018 Calculated Conductivity Data.

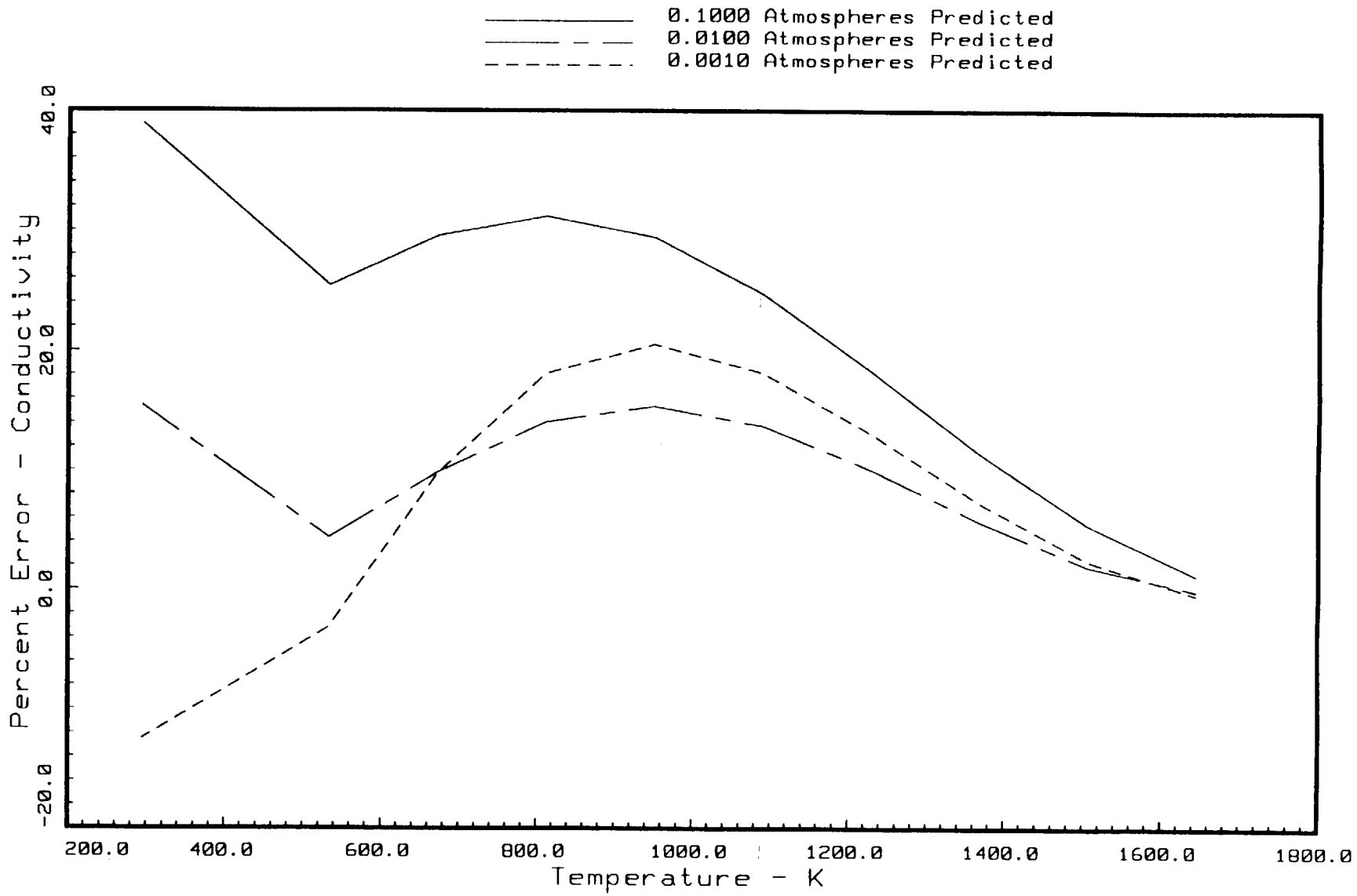

Fig. 32 Percent Error in Predicted HTP-6 Conductivity in the Weak Direction Compared to JSC-25018 Calculated Conductivity Data.

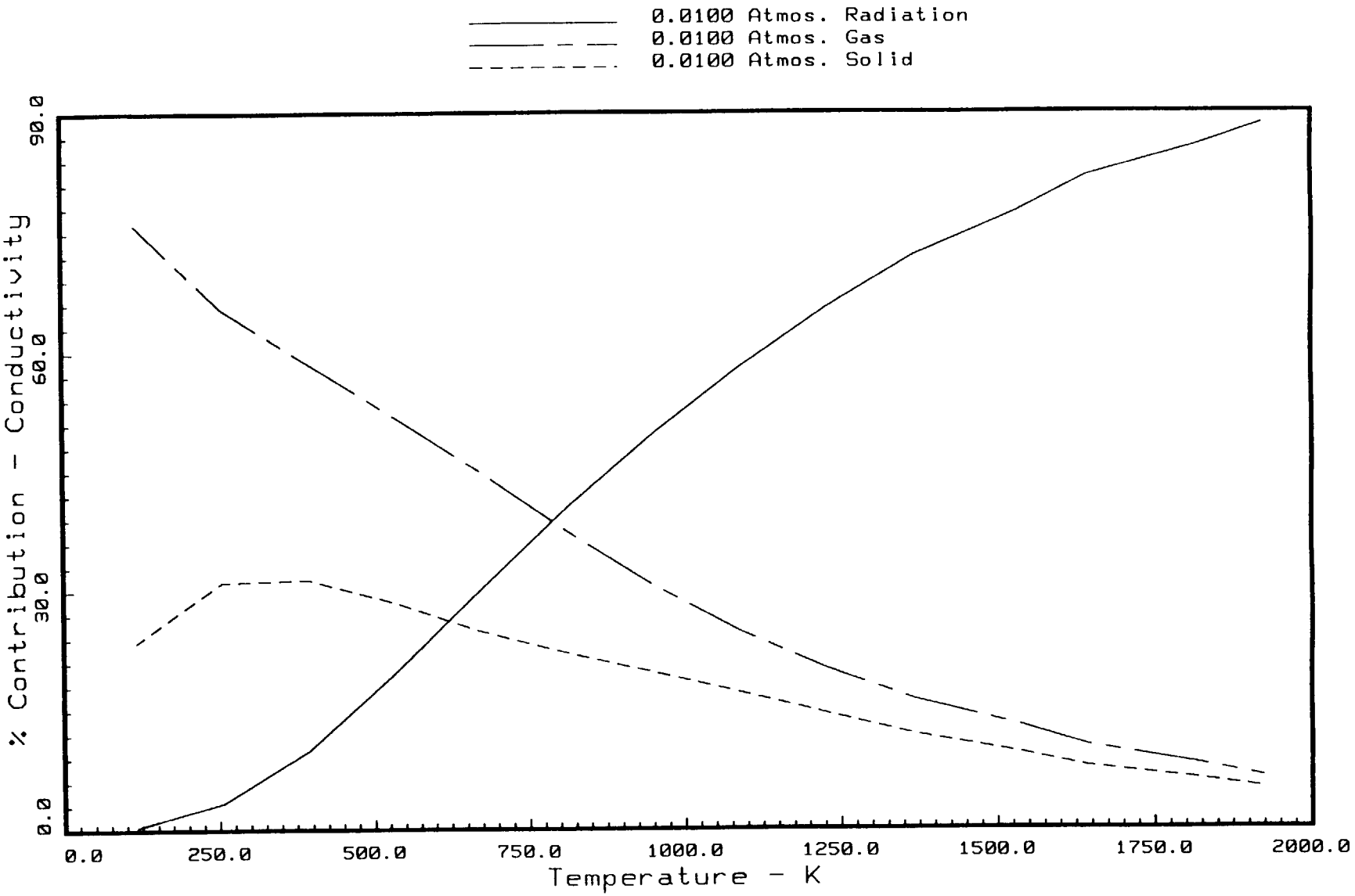

Fig. 33 Percent Contribution of the Solid, Gas, and Radiation for LI-900 in the Weak Direction at a Pressure of 0.01 Atmospheres.

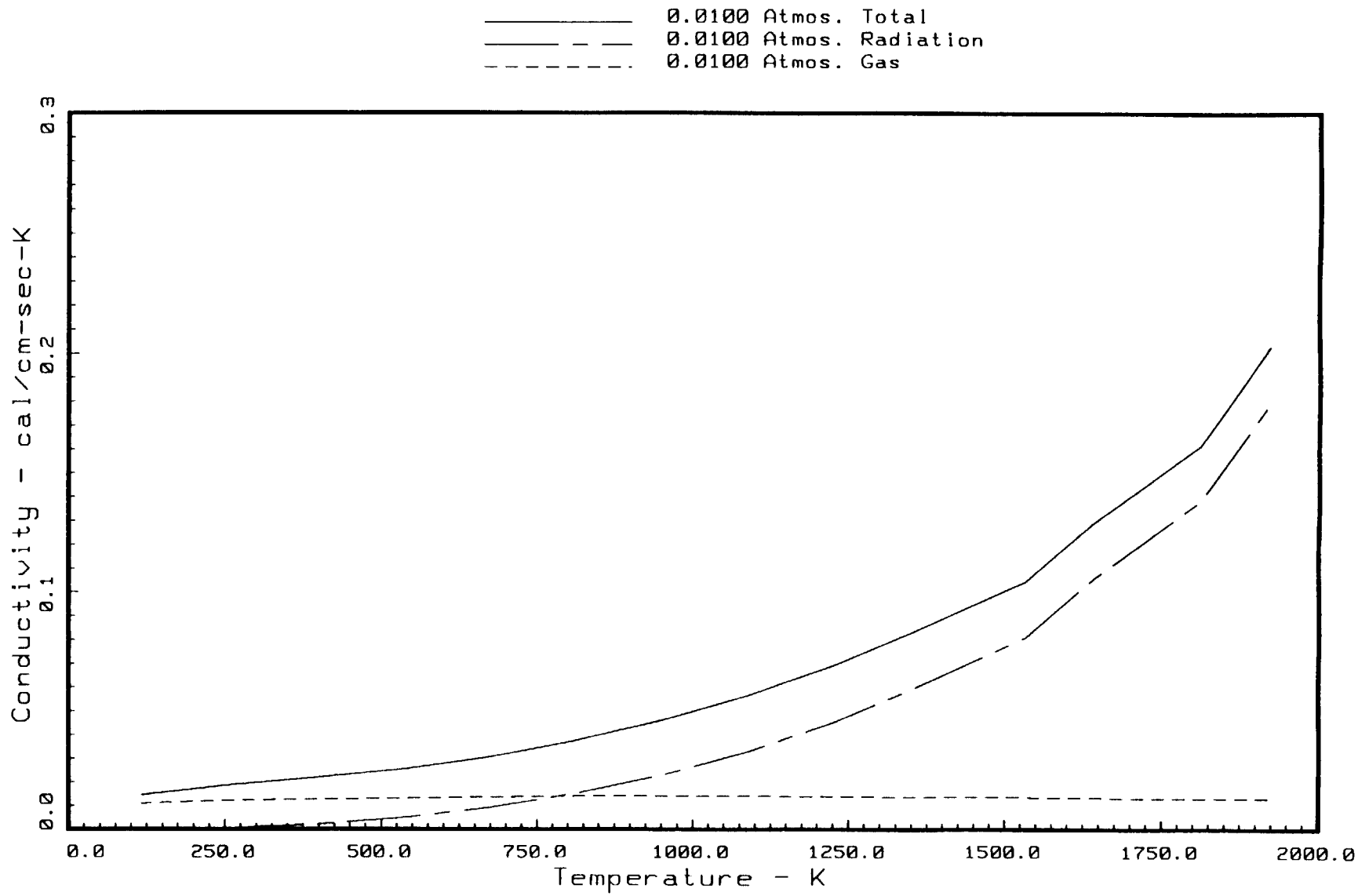

Fig. 34 Predicted Conductivity of Solid, Gas, and Radiation Contribution for LI-900 in the Weak Direction at a Pressure of 0.01 Atmospheres.

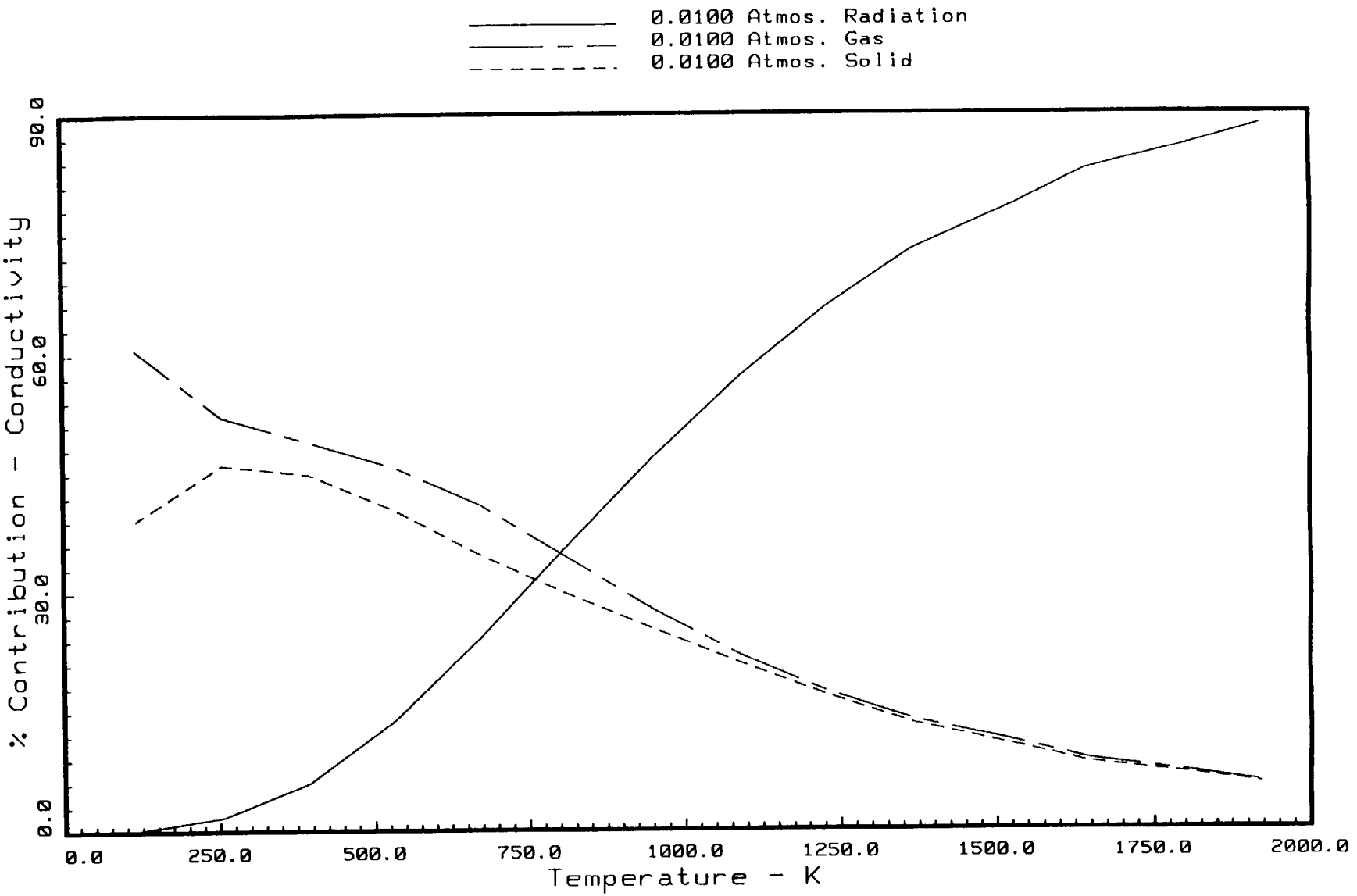

Fig. 35 Percent Contribution of the Solid, Gas, and Radiation for LI-900 in the Strong Direction at a Pressure of 0.01 Atmospheres.

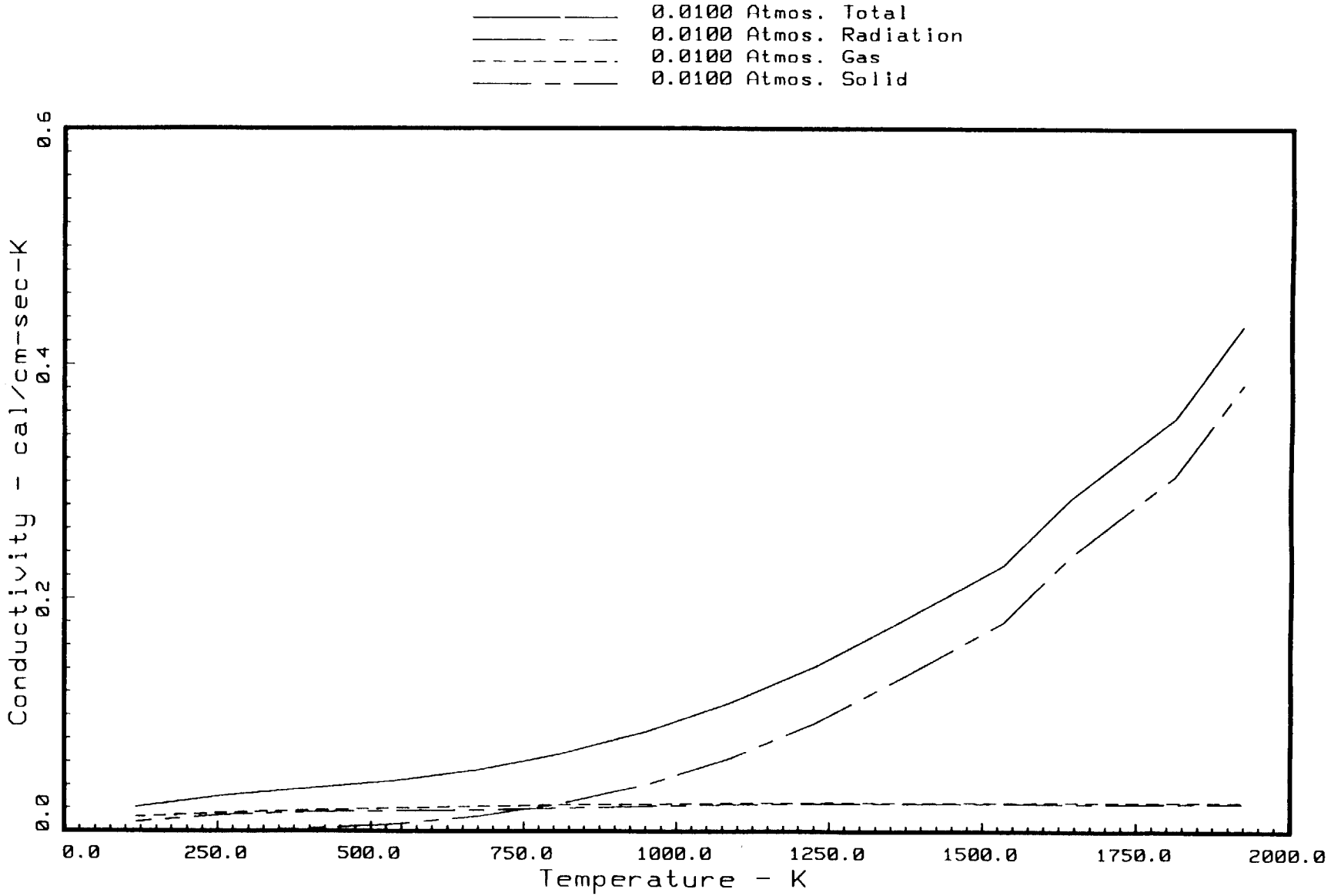

Fig. 36 Predicted Conductivity of Solid, Gas, and Radiation Contribution for LI-900 in the Strong Direction at a Pressure of 0.01 Atmospheres.

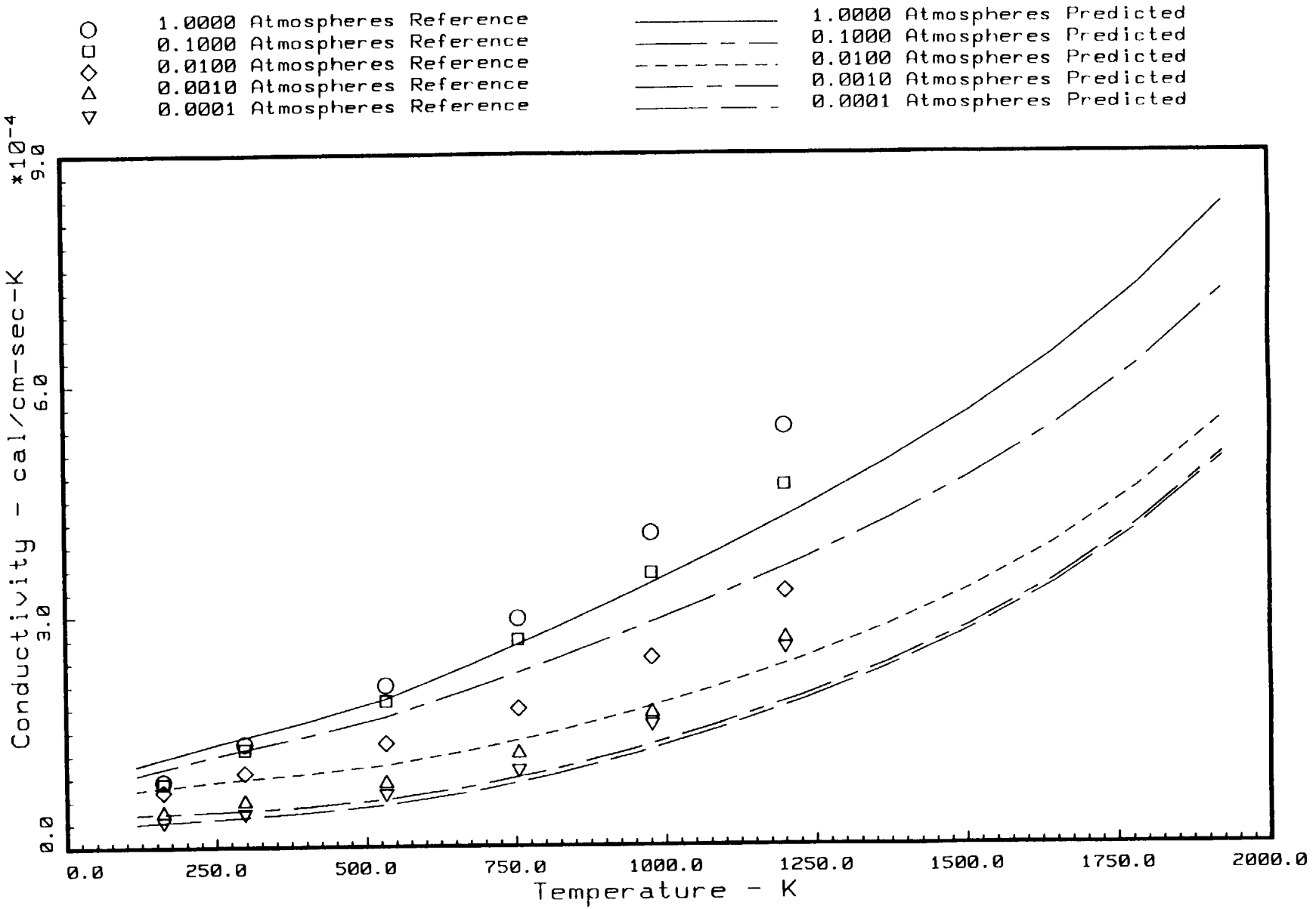

Fig. 37 Predicted FRCI-12 Conductivity in the Weak Direction Using 3 Micron Diameter Nextel Fibers vs. Baseline Values.

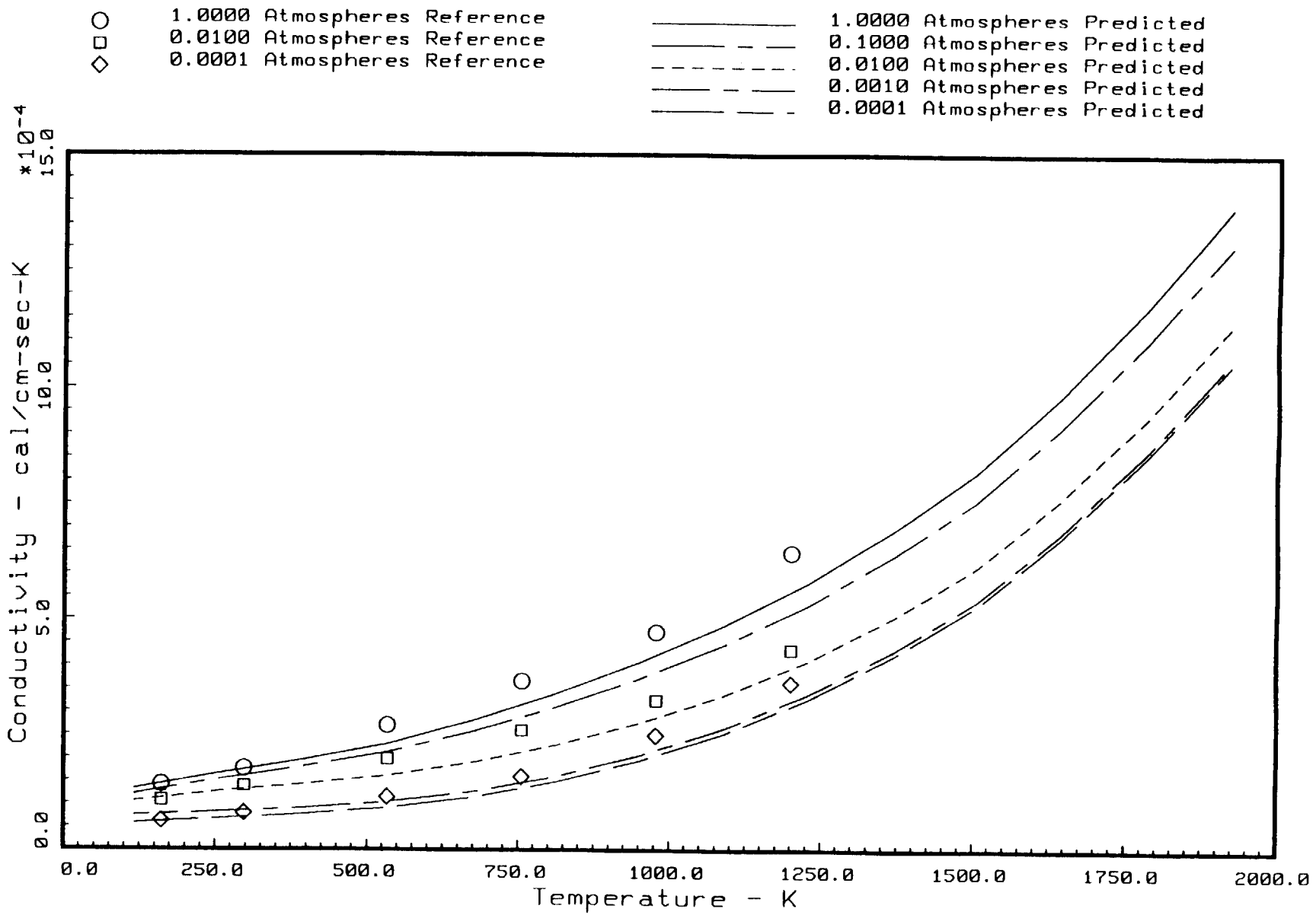

Fig. 38 Predicted FRCI-12 Conductivity in the Strong Direction Using 3 Micron Diameter Nextel Fibers vs. Baseline Values.

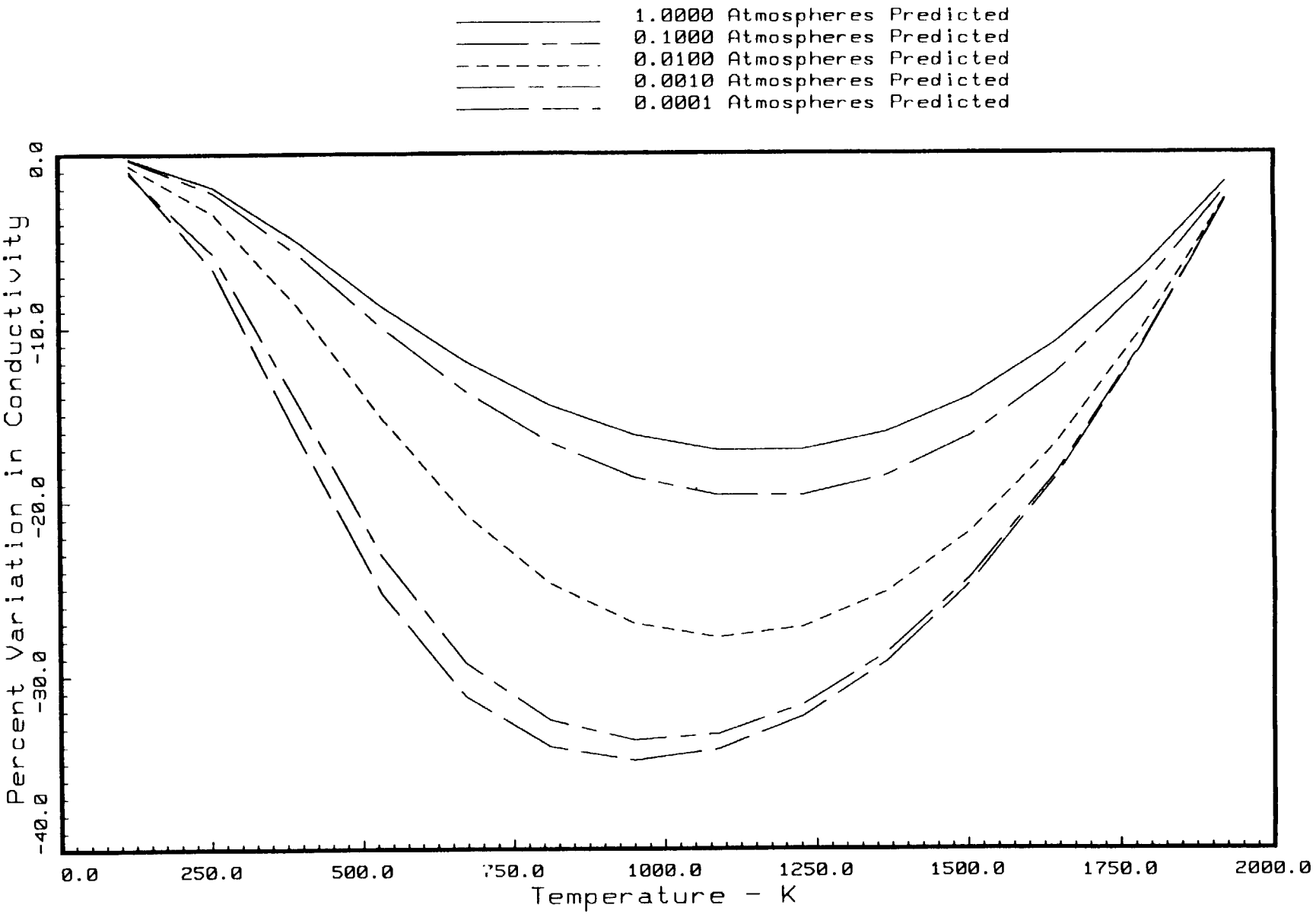

Fig. 39 Percent Variation in FRCI-12 Predicted Conductivity in the Weak Direction Using 3 Micron Diameter Nextel Fibers Compared to 11 Micron Predicted Values.

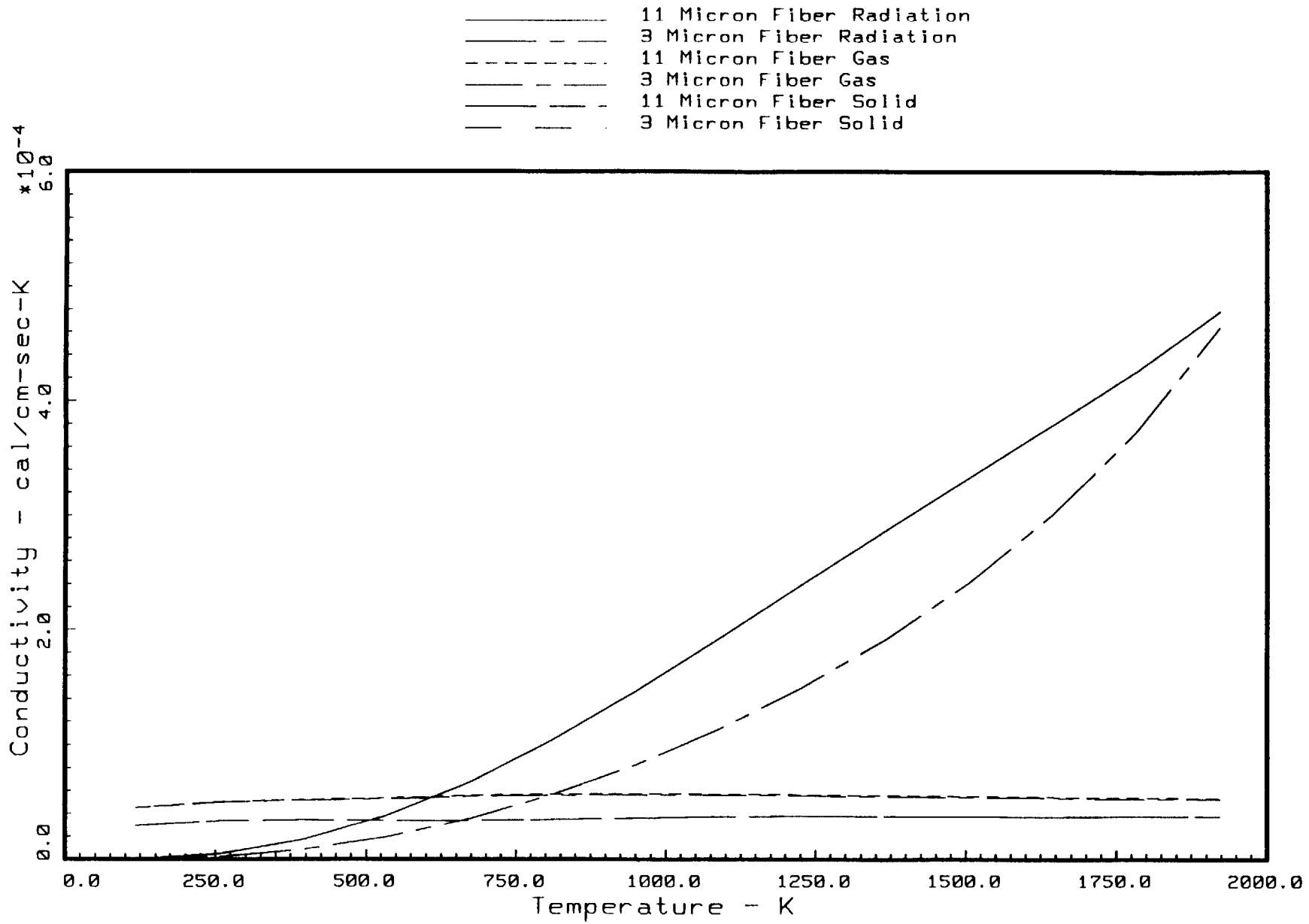

Fig. 40 Predicted Conductivity of Solid, Gas, and Radiation Contribution for 11 and 3 Micron Nextel Fiber Diameters at a Pressure of 0.01 Atmospheres for FRCI-12 in the Weak Direction.

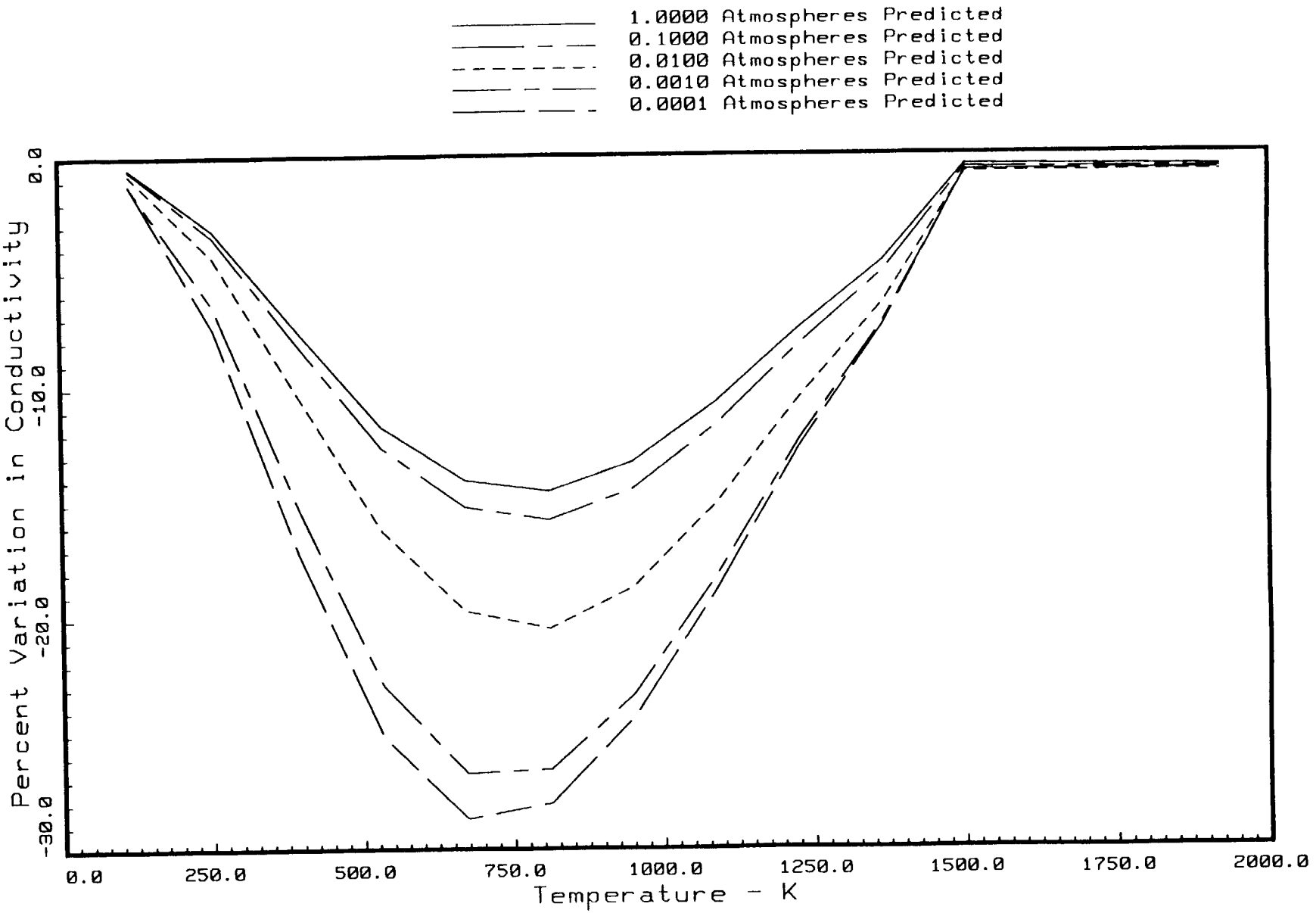

Fig. 41 Percent Variation in FRCI-12 Predicted Conductivity in the Strong Direction Using 3 Micron Diameter Nextel Fibers Compared 11 Micron Predicted Values.

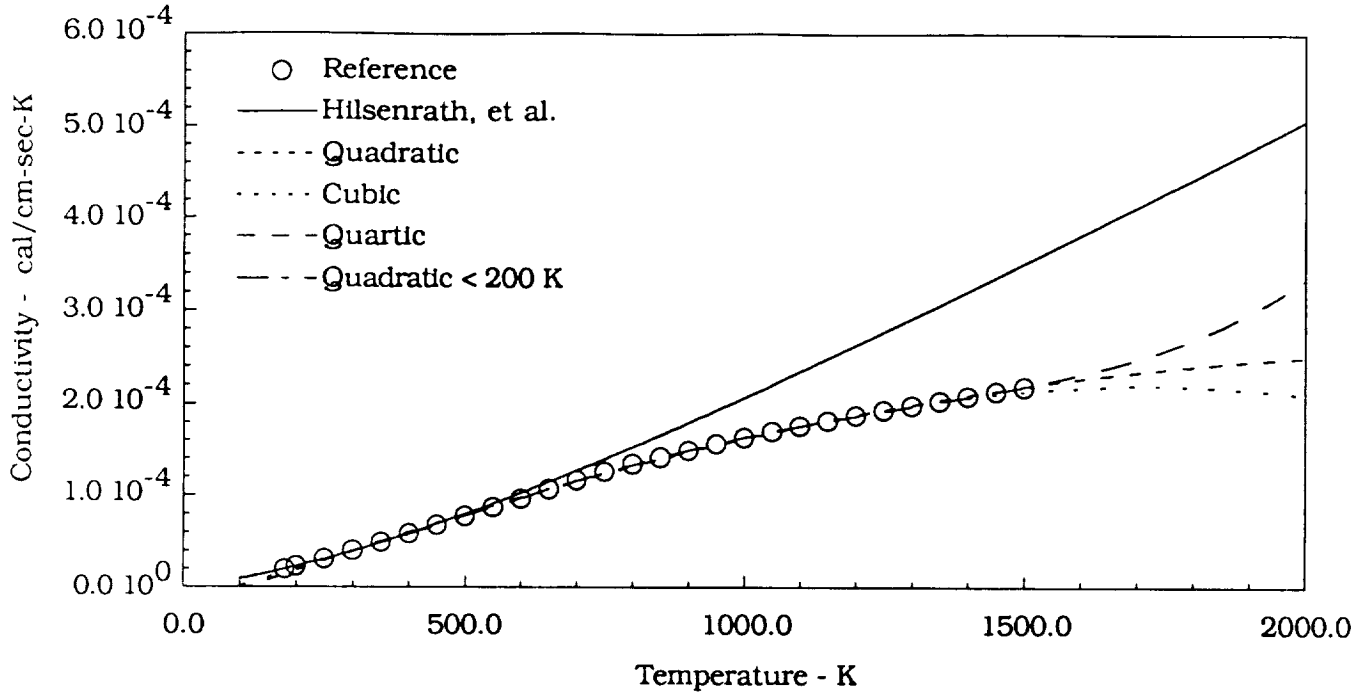

Fig. 42 Carbon Dioxide Conductivity - Reference vs. Predicted Methods.

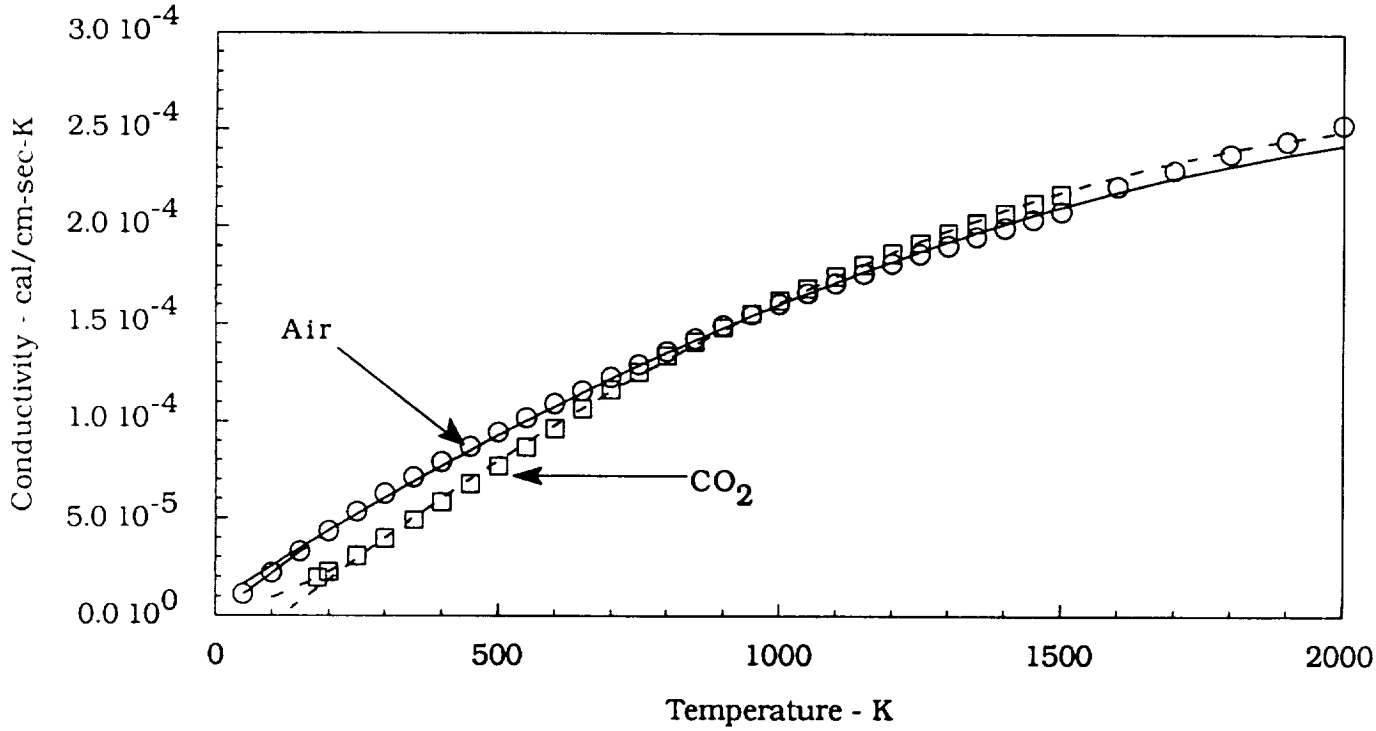

Fig. 43 Comparison of Air and Carbon Dioxide Conductivity.

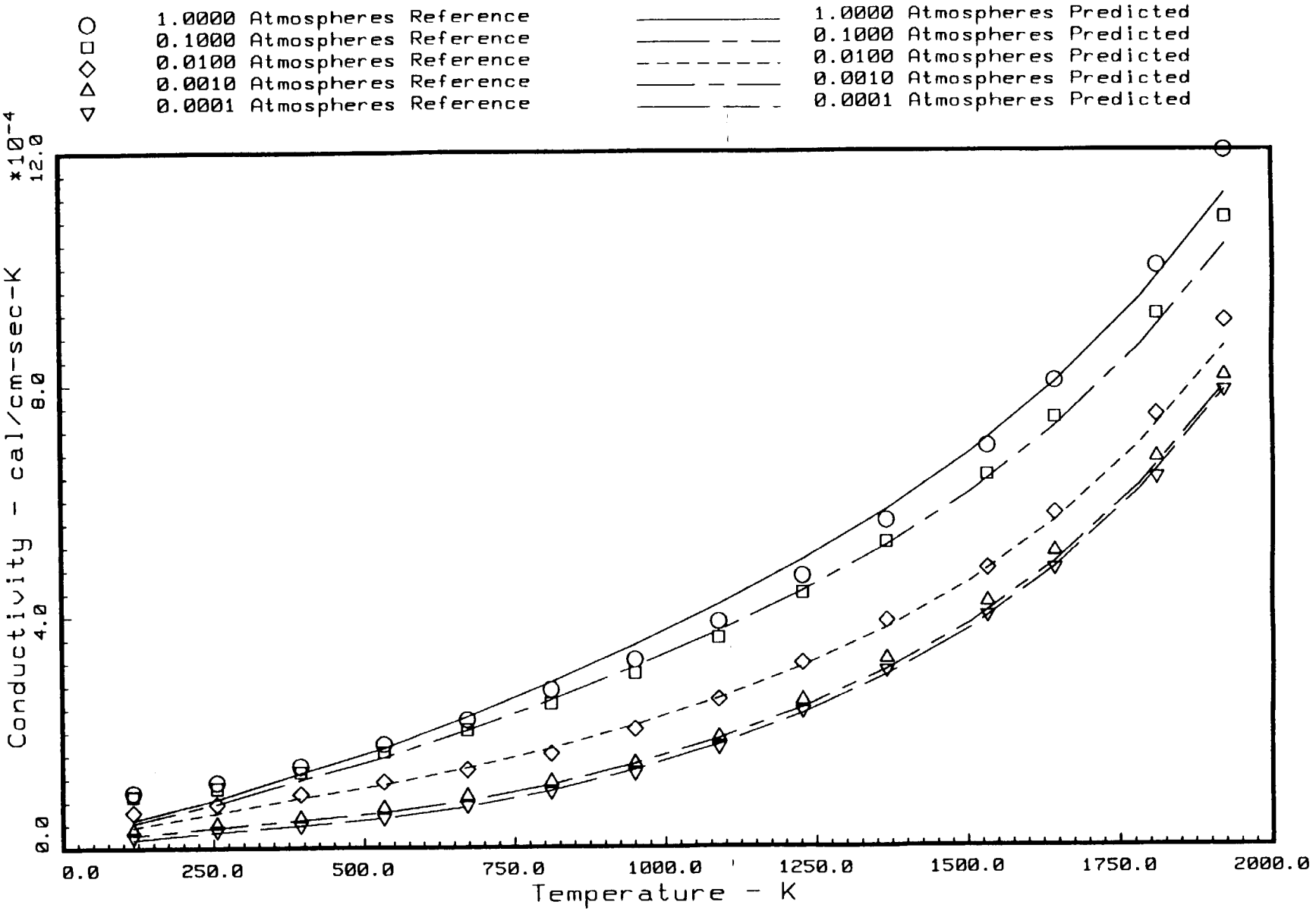

Fig. 44 Predicted LI-900 Conductivity in the Weak Direction in a CO2 Atmosphere vs. Baseline Values in Air.

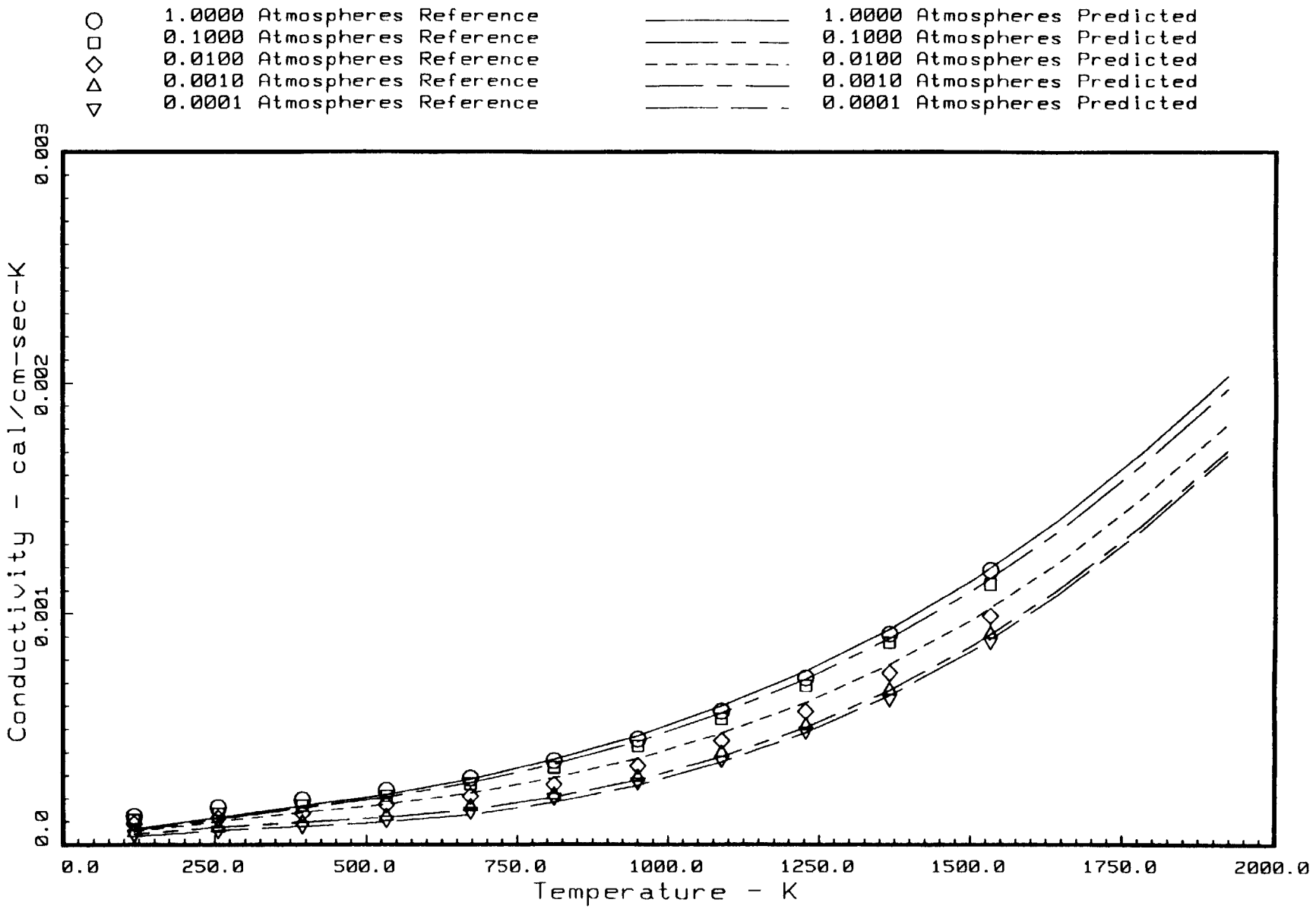

Fig. 45 Predicted LI-900 Conductivity in the Strong Direction in a C02 Atmosphere Vs. Baseline Values in Air.

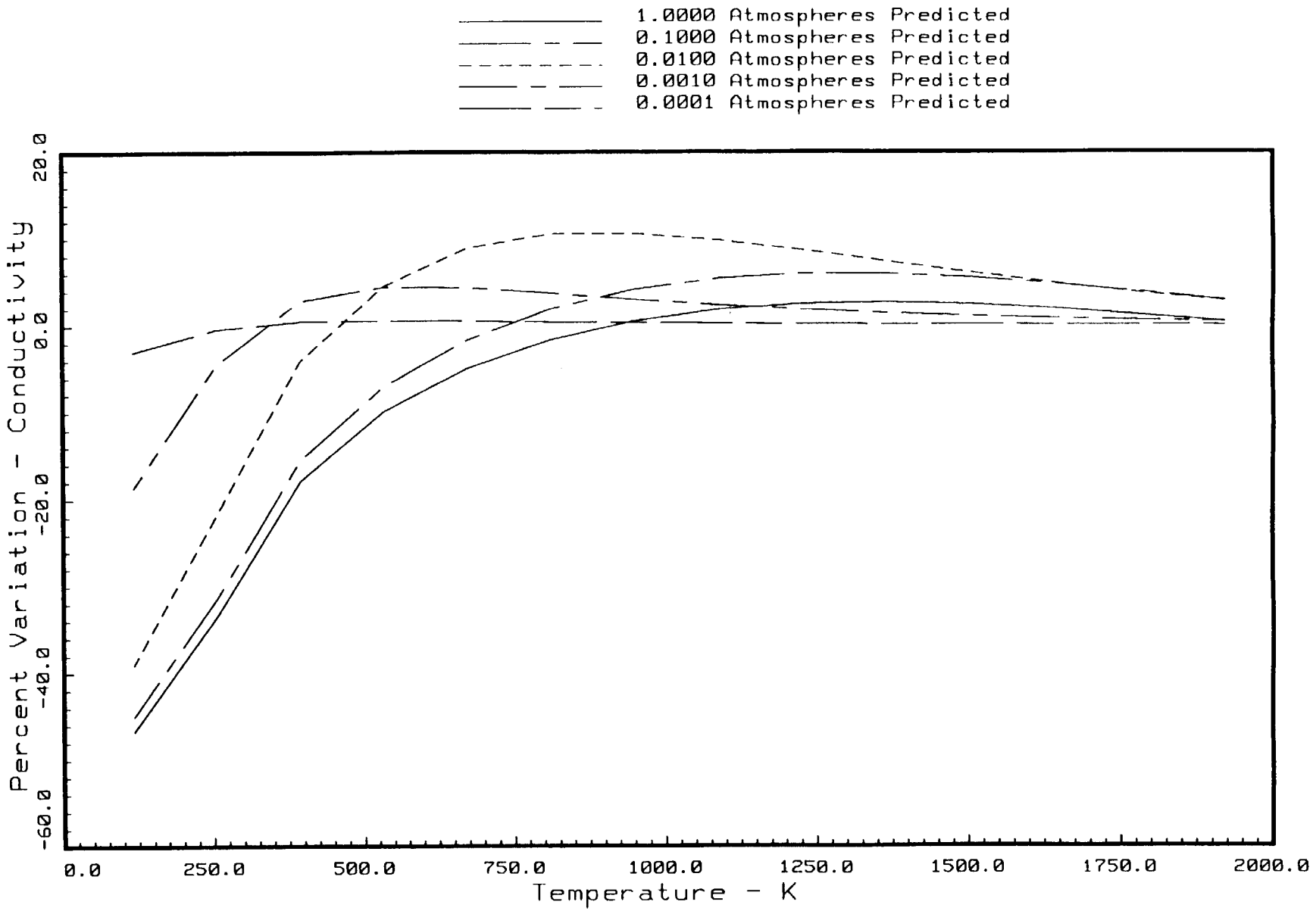

Fig. 46 Percent Variation in Predicted LI-900 Conductivity in the Weak Direction in a C02 Atmosphere vs. Predicted Values in Air.

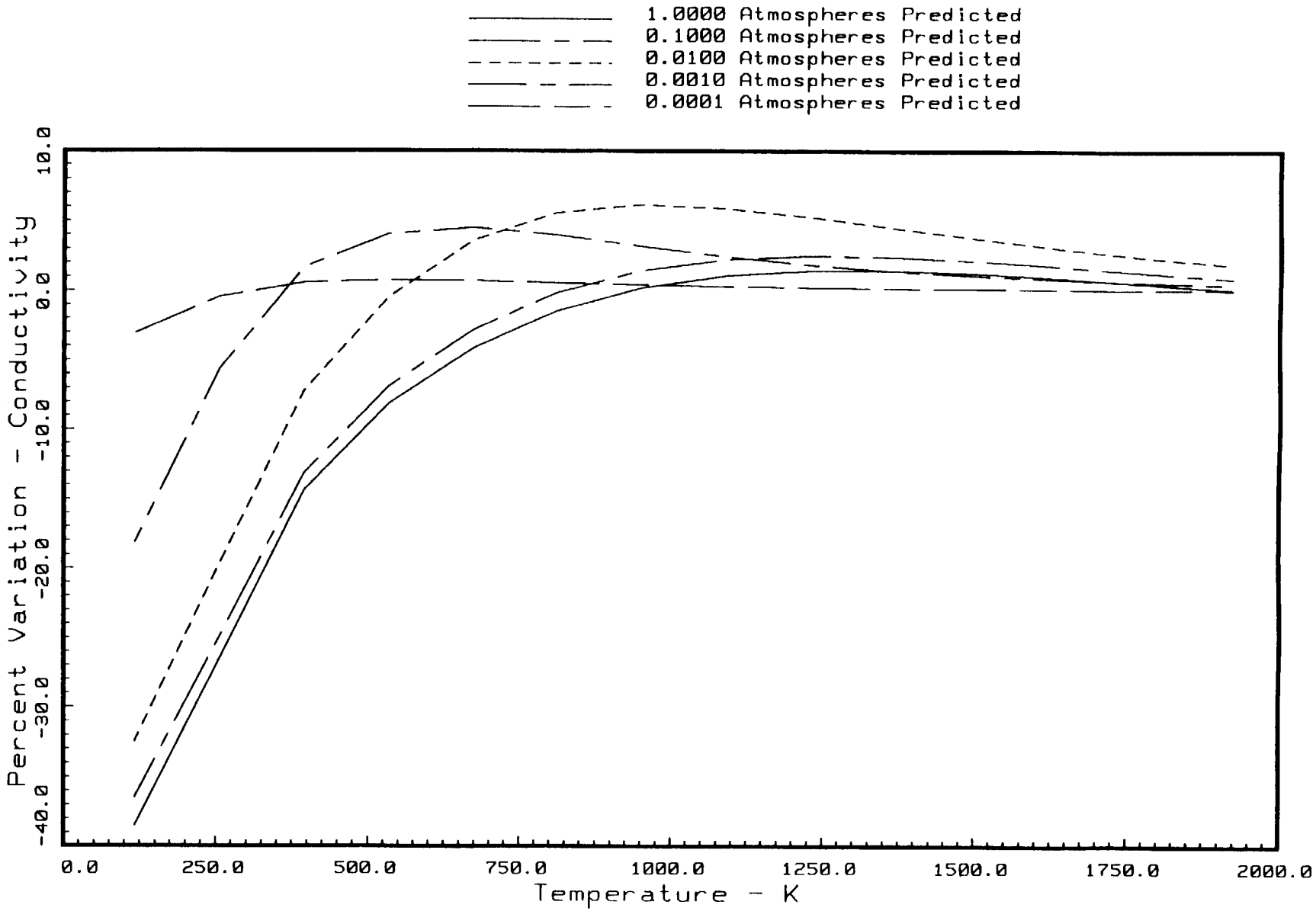

Fig. 47 Percent Variation in Predicted LI-900 Conductivity in the Strong Direction in a C02 Atmosphere vs. Predicted Values in Air.

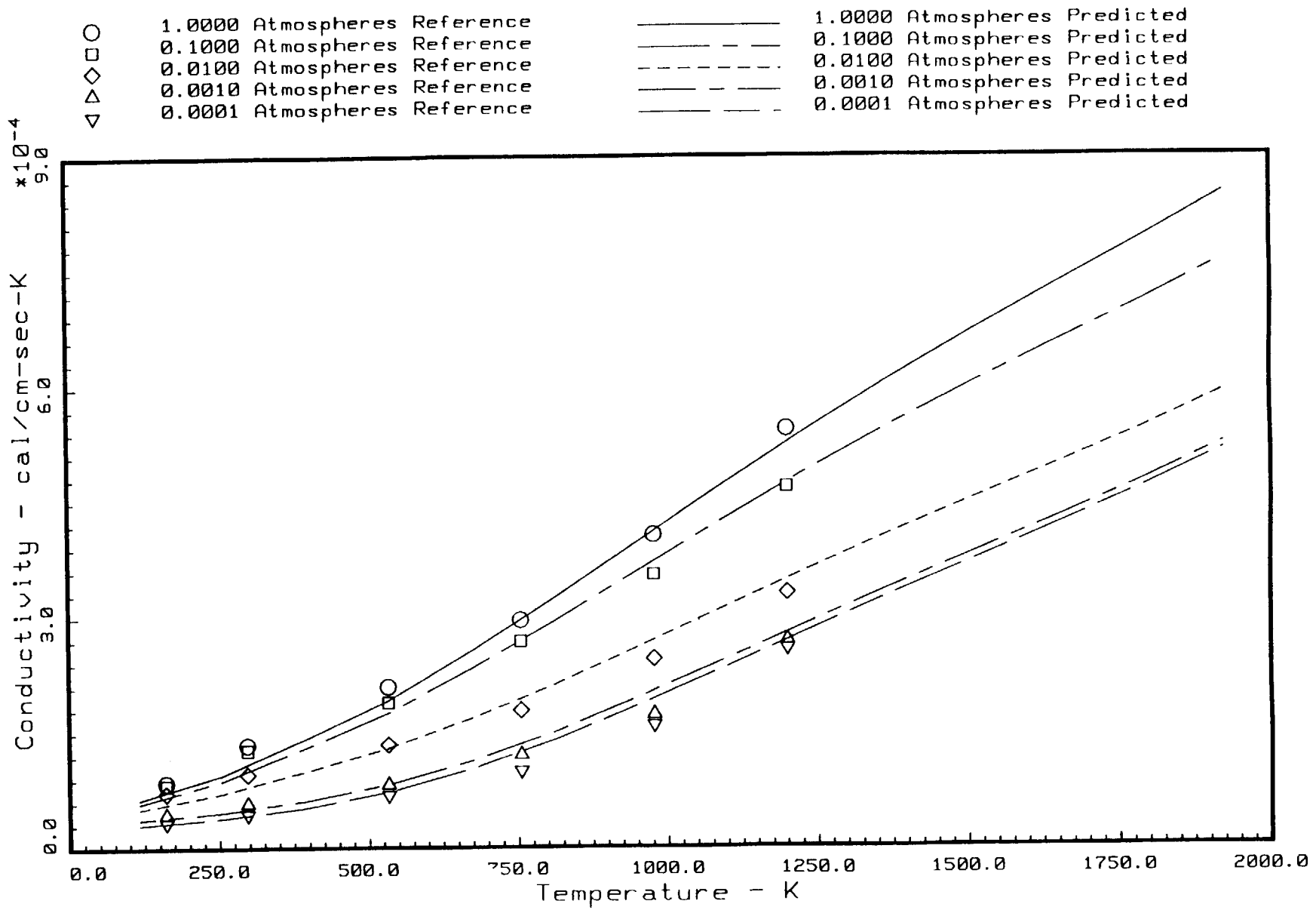

Fig. 48 Predicted FRCI-12 Conductivity in the Weak Direction in a C02 Atmosphere vs. Bas :line Values in Air.

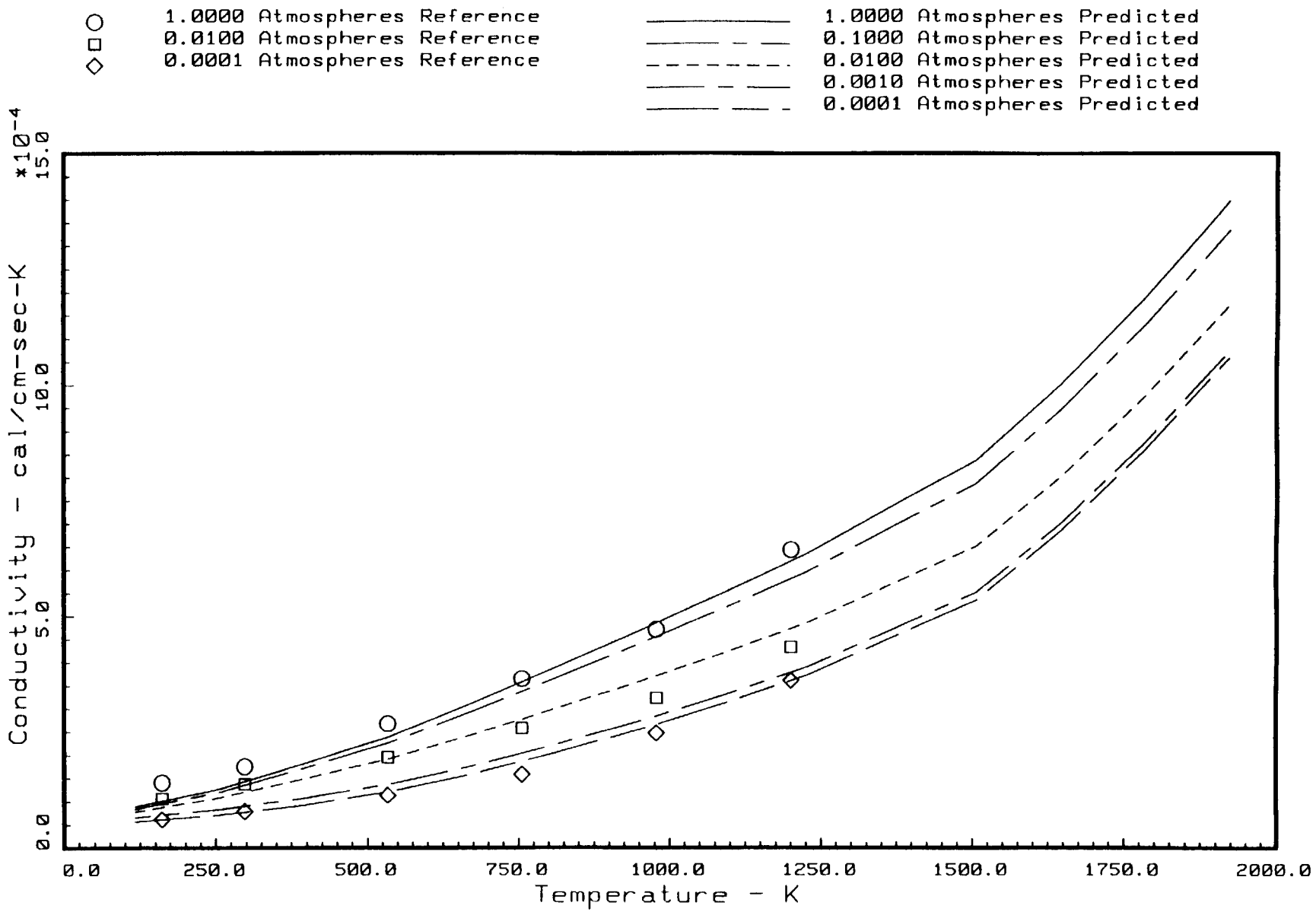

Fig. 49 Predicted FRCI-12 Conductivity in the Strong Direction in a C02 Atmosphere vs. Baseline Values in Air.

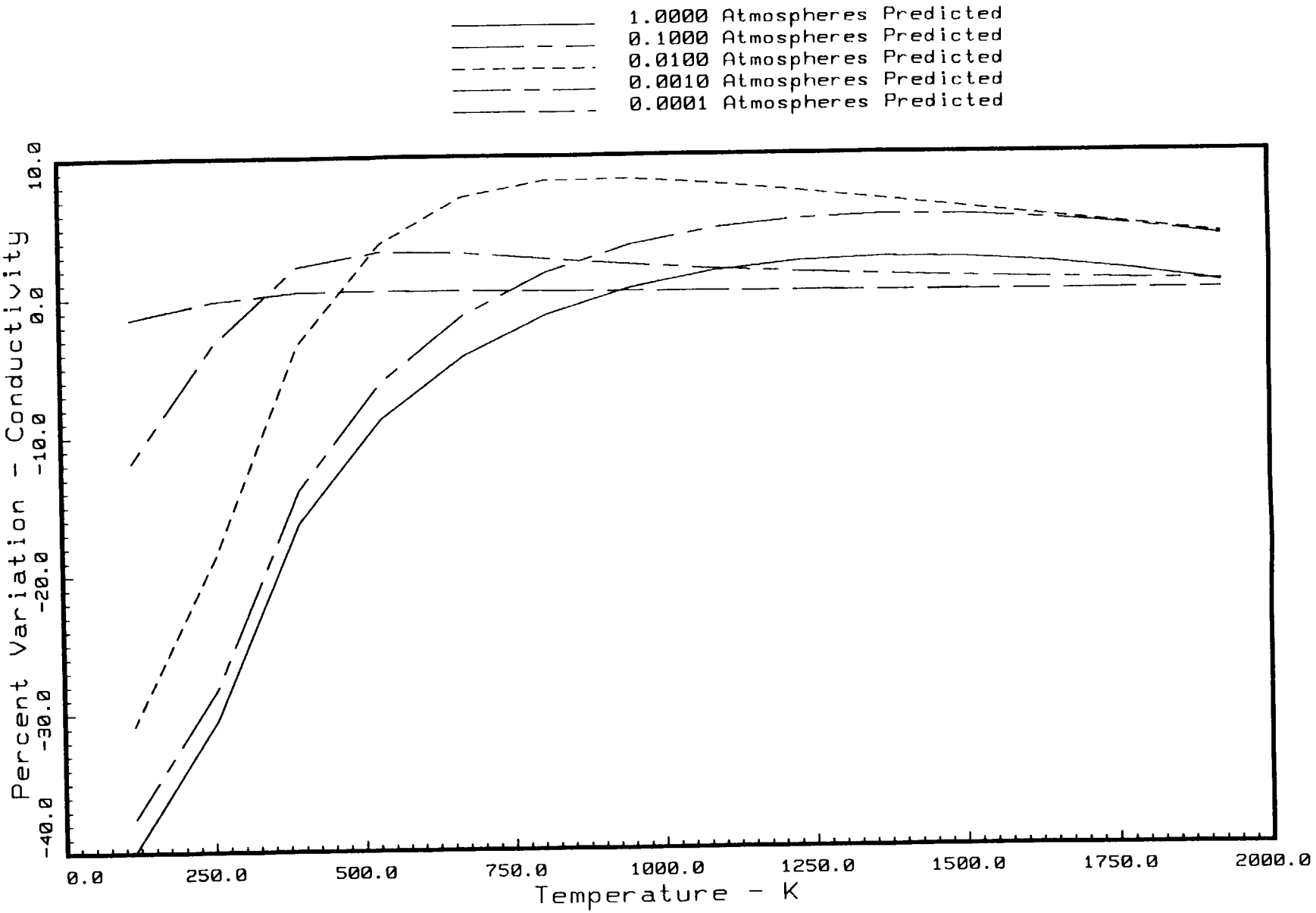

Fig. 50 Percent Variation in Predicted FRCI-12 Conductivity in the Weak Direction in a C02 Atmosphere vs. Predicted Values in Air.

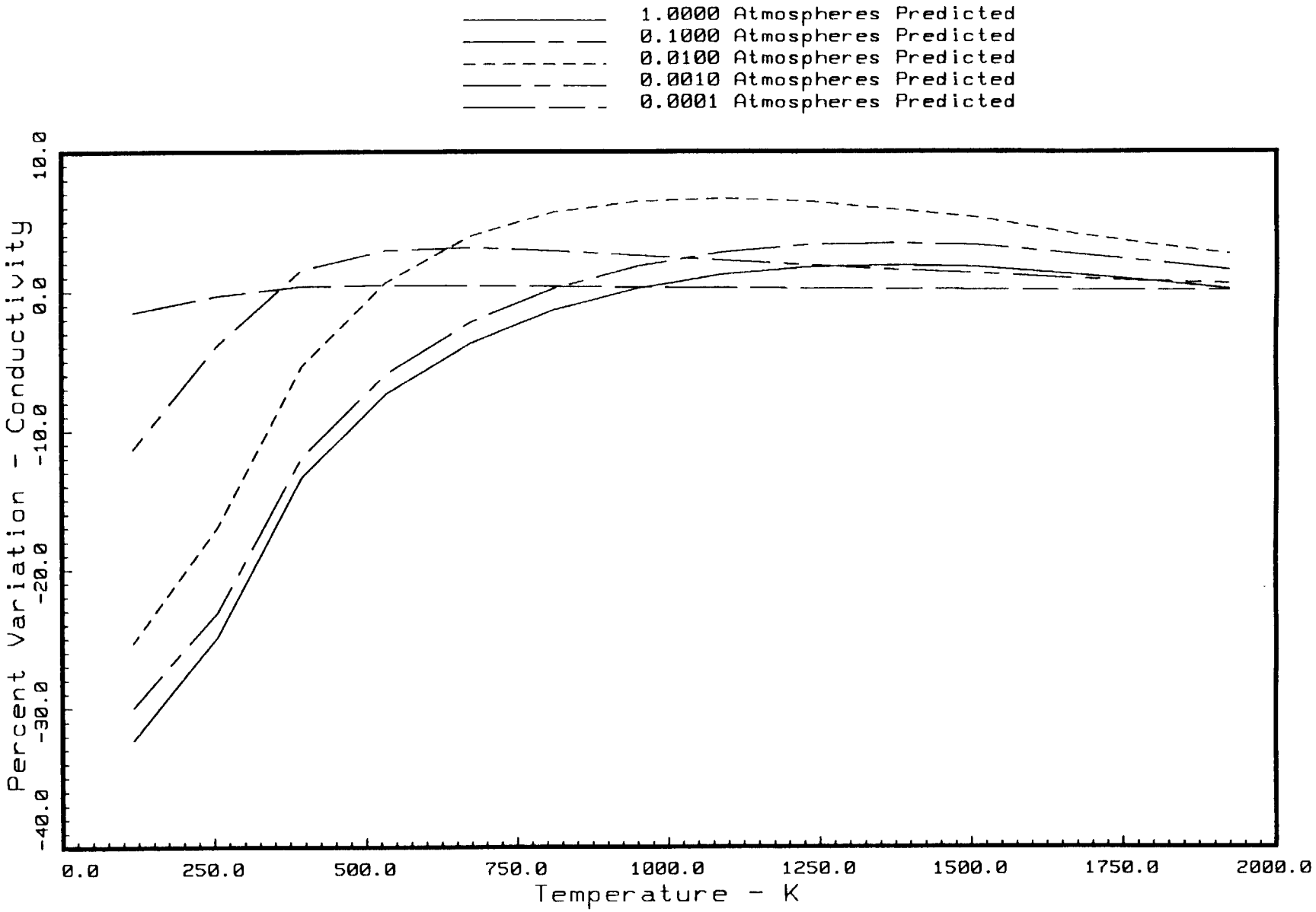

Fig. 51 Percent Variation in Predicted FRCI-12 Conductivity in the Strong Direction in a C02 Atmosphere vs. Predicted Values in Air.

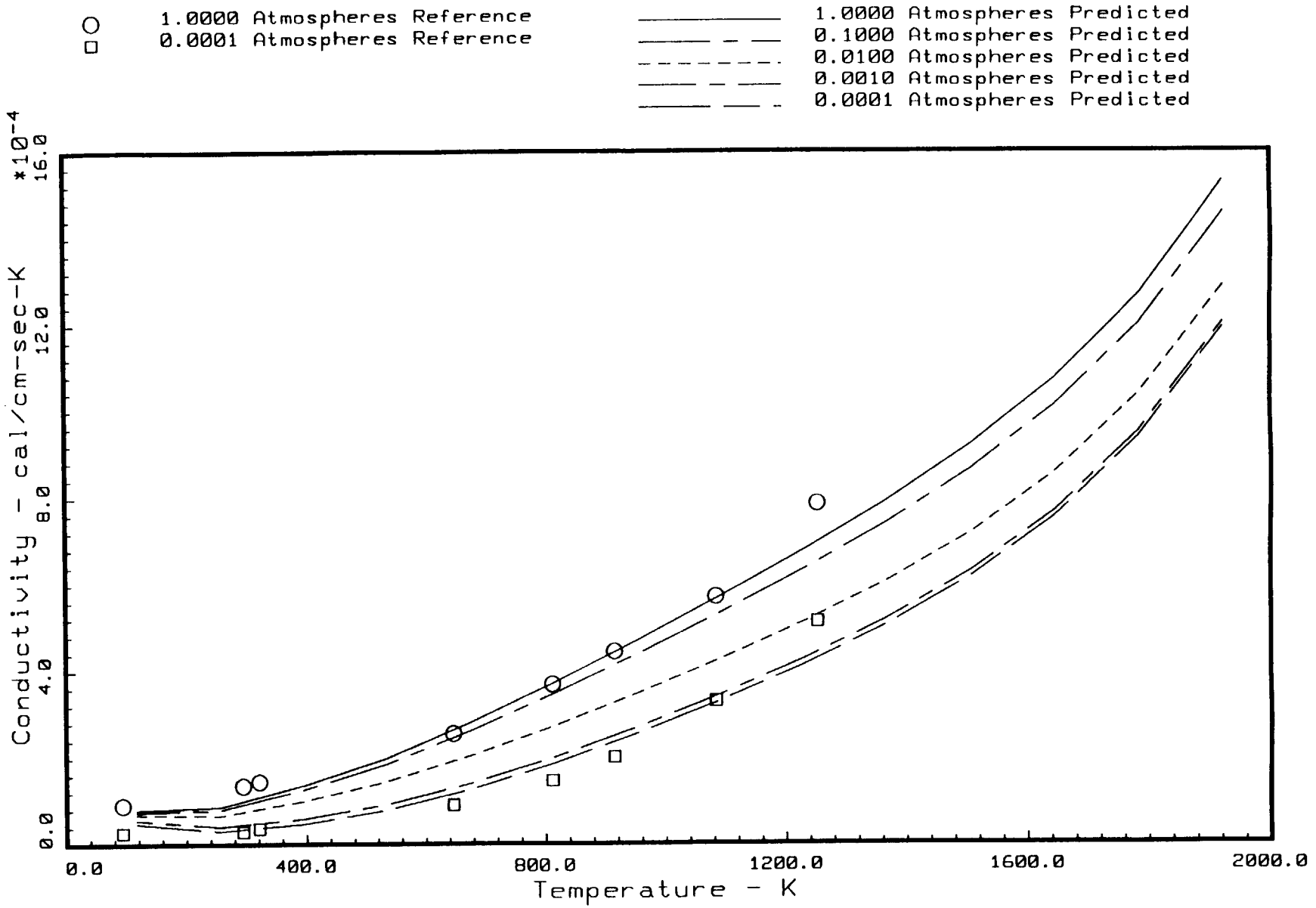

Fig. 52 Predicted HTP-6 Conductivity in the Weak Direction in a C02 Atmosphere vs. Baseline Values in Air.

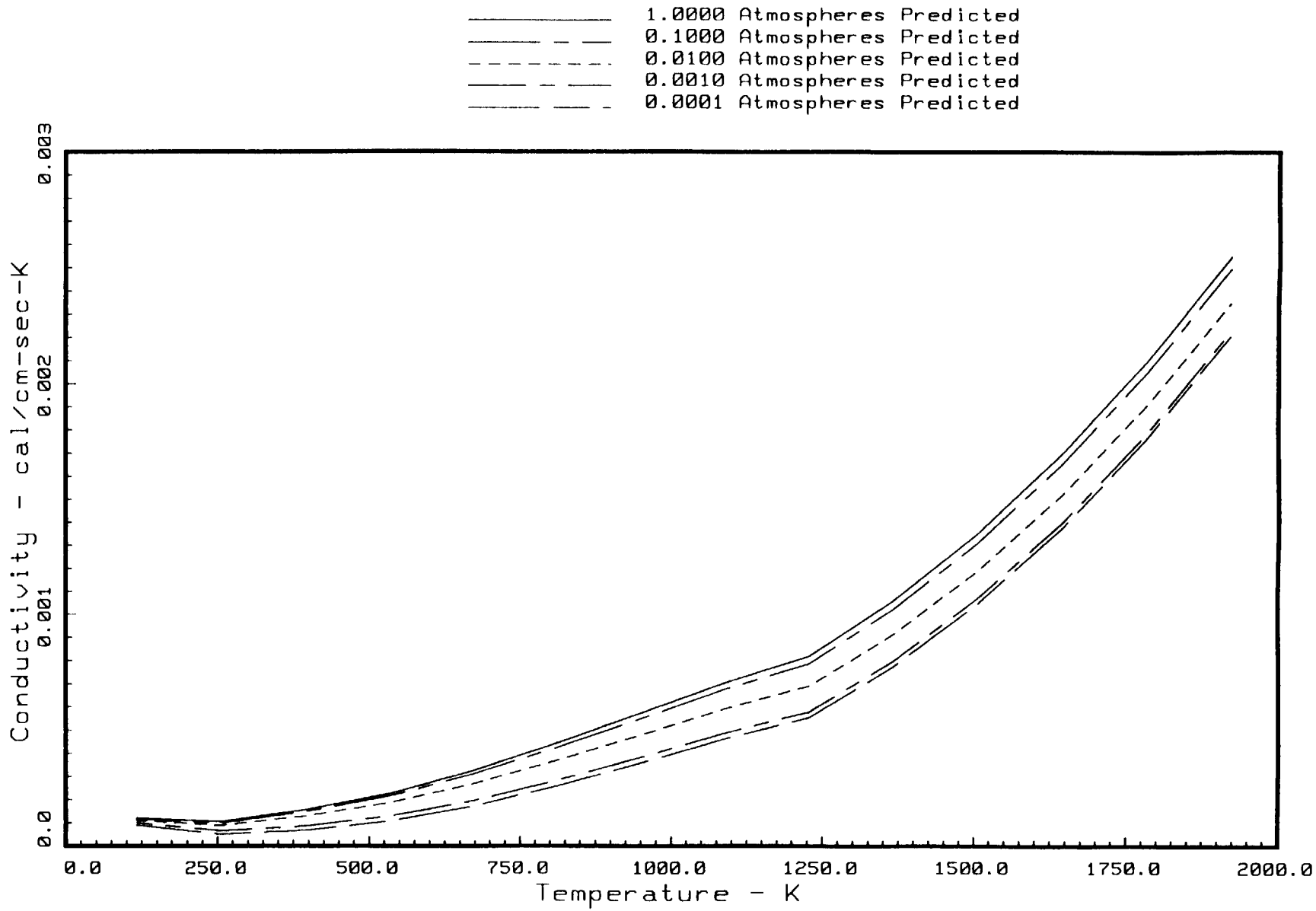

Fig. 53 Predicted HTP-6 Conductivity in the Strong Direction in a C02 Atmosphere.

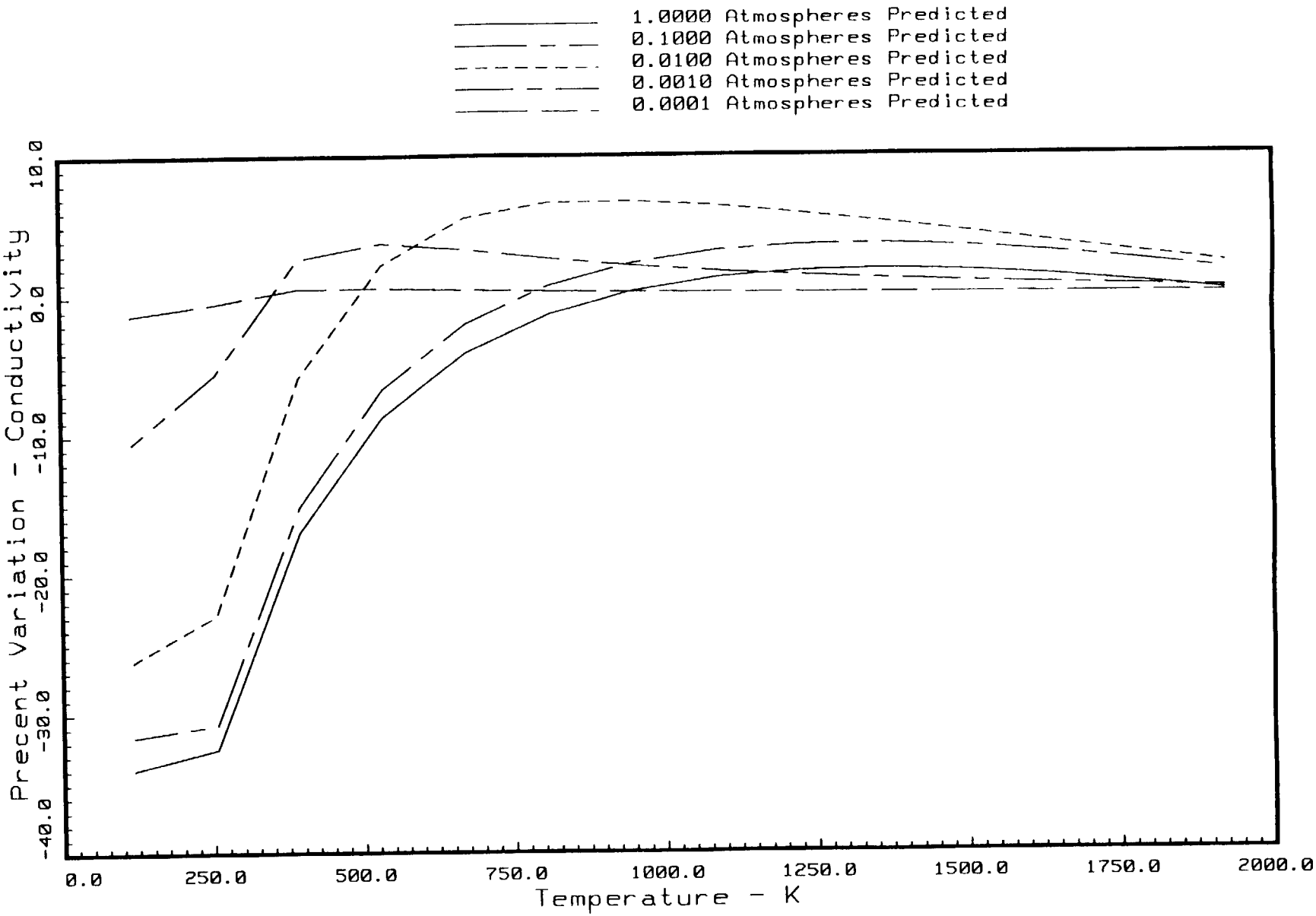

Fig. 54 Percent Variation in Predicted HTP-6 Conductivity in the Weak Direction in a C02 Atmosphere vs. Predicted Values in Air.

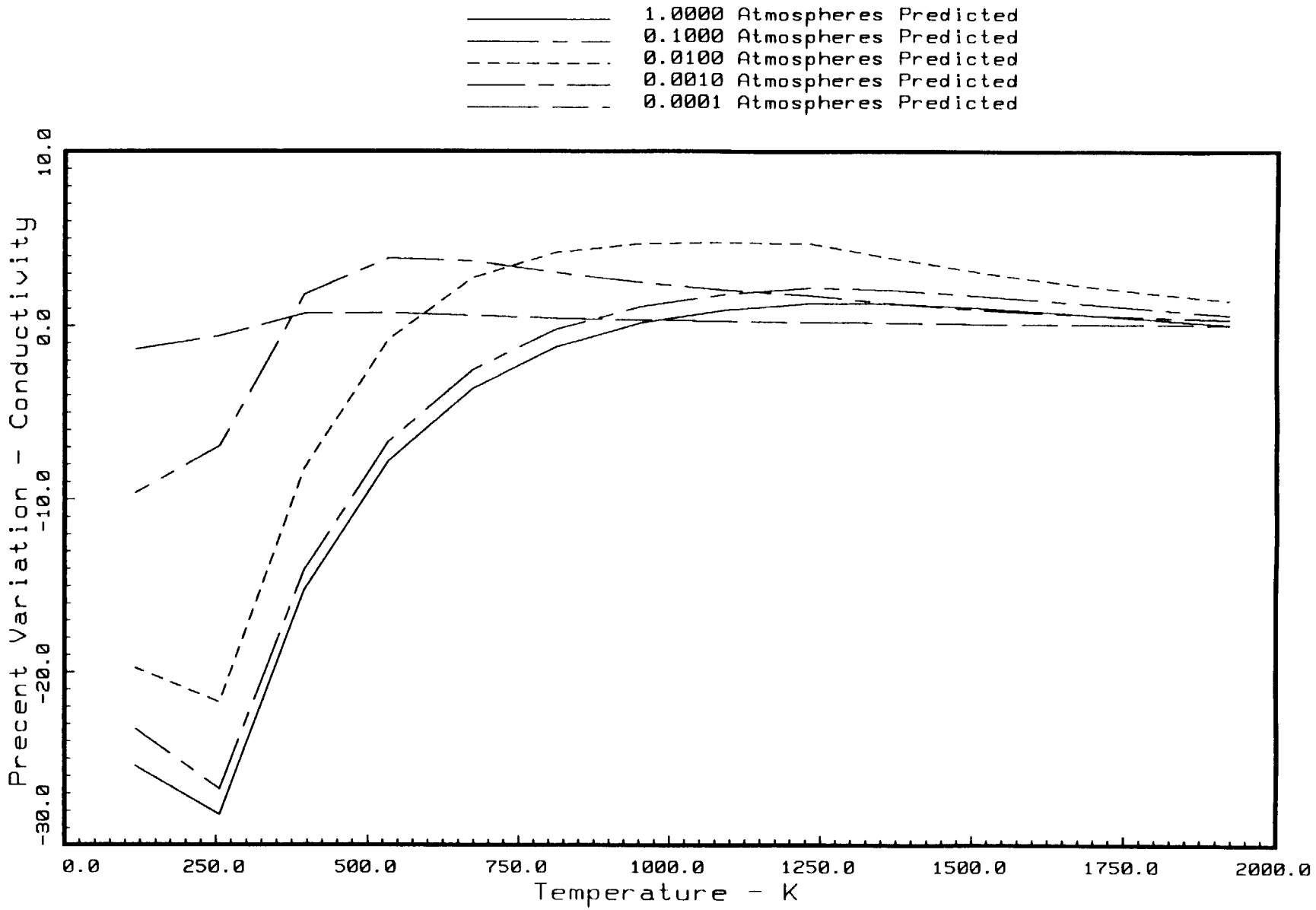

Fig. 55 Percent Variation in Predicted HTP-6 Conductivity in the Strong Direction in a C02 Atmosphere vs. Predicted Values in Air.

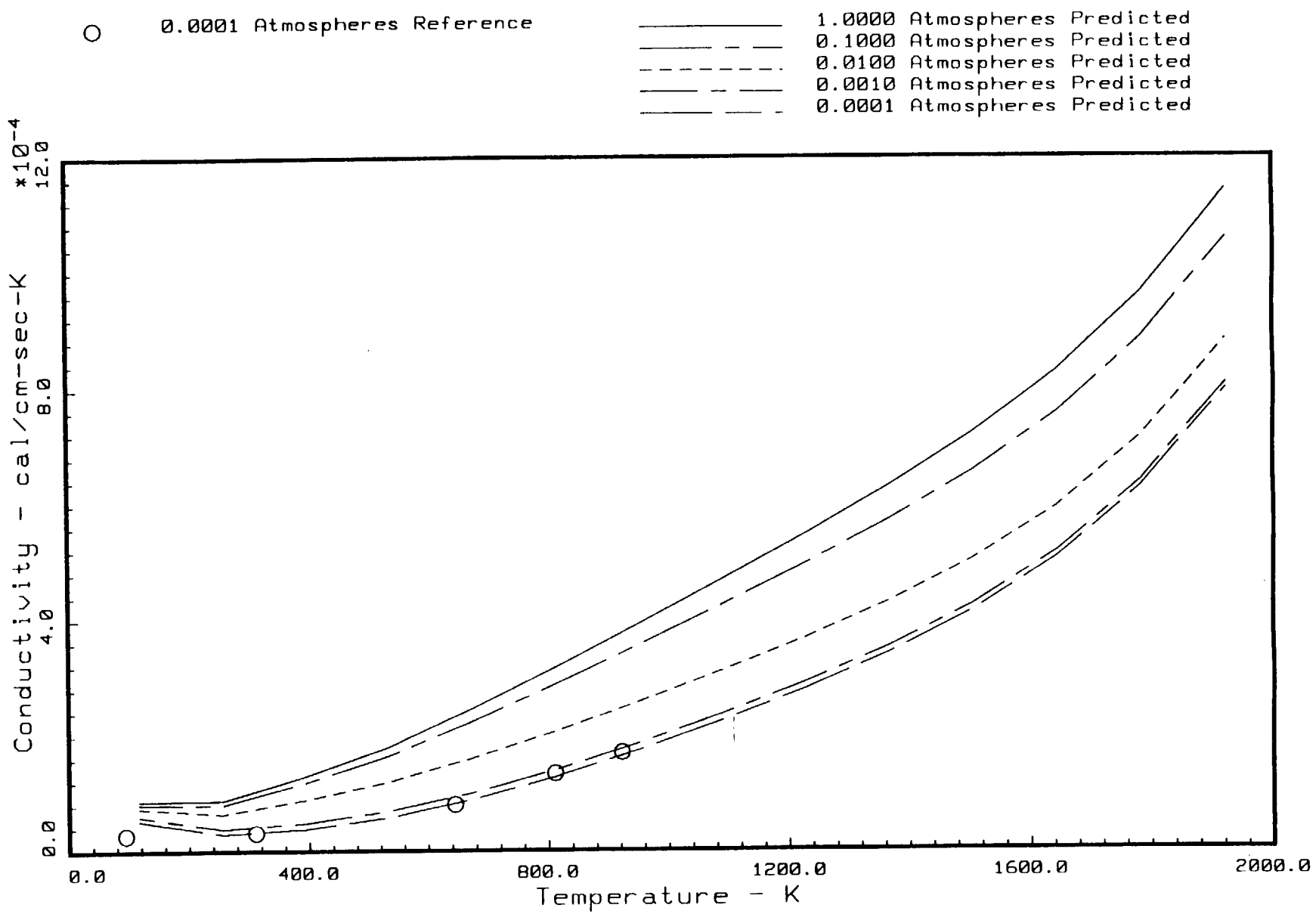

Fig. 56 Predicted HTP-9 Conductivity in the Weak Direction in a C02 Atmosphere vs. Baseline Values in Air.

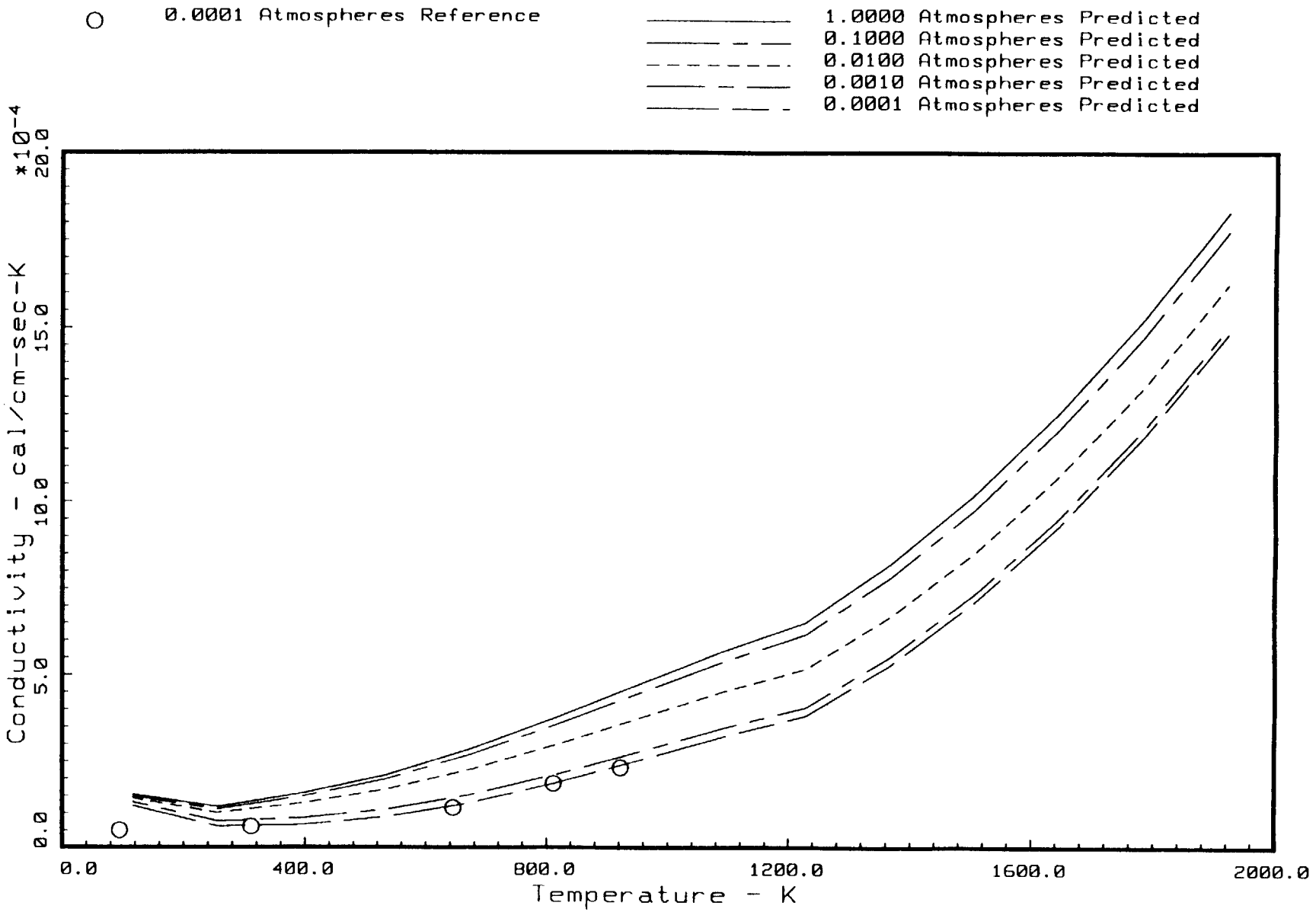

Fig. 57 Predicted HTP-9 Conductivity in the Strong Direction in a C02 Atmosphere vs. Baseline Values in Air.

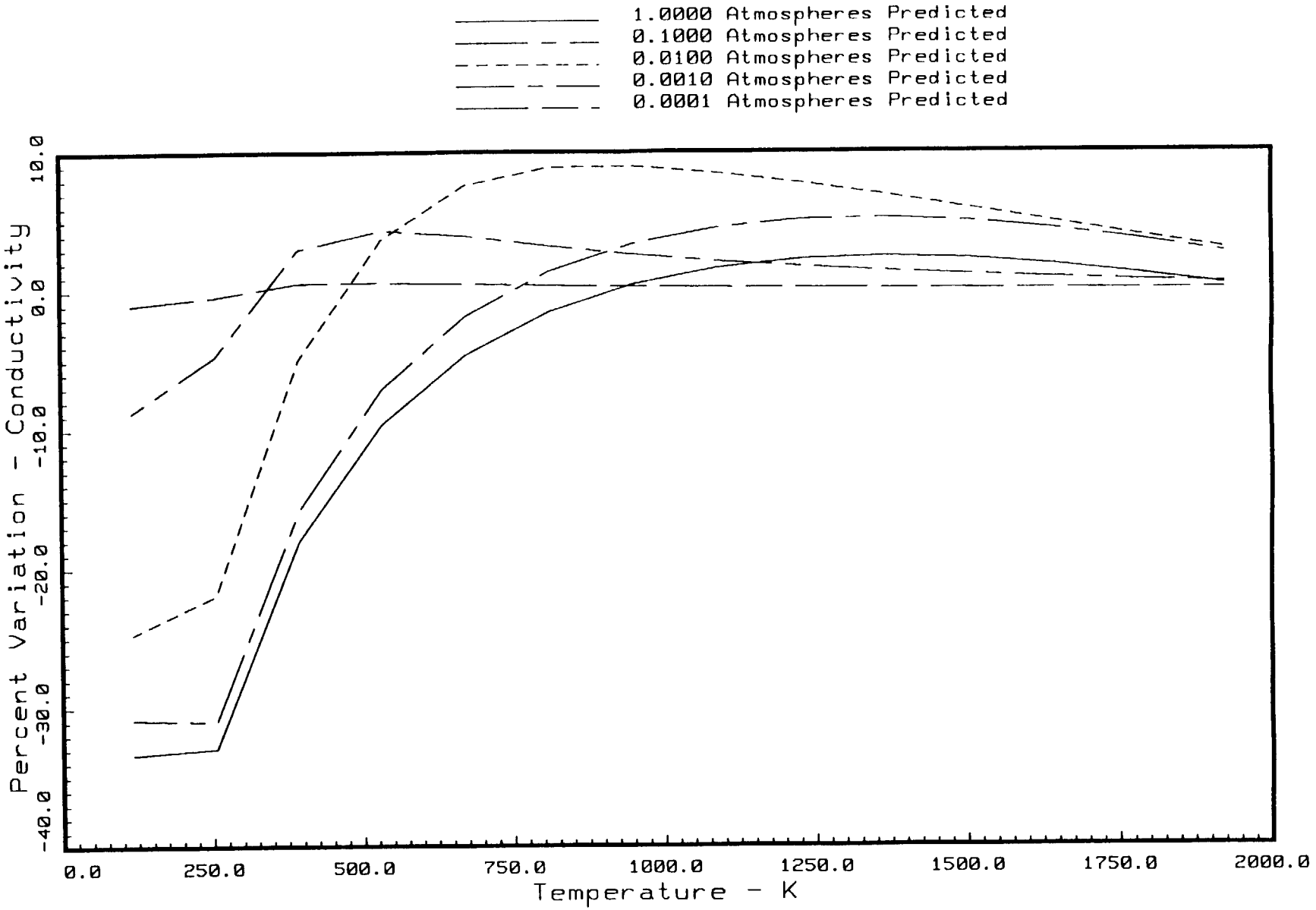

Fig. 58 Percent Variation in Predicted HTP-9 Conductivity in the Weak Direction in a C02 Atmosphere vs. Predicted Values in Air.

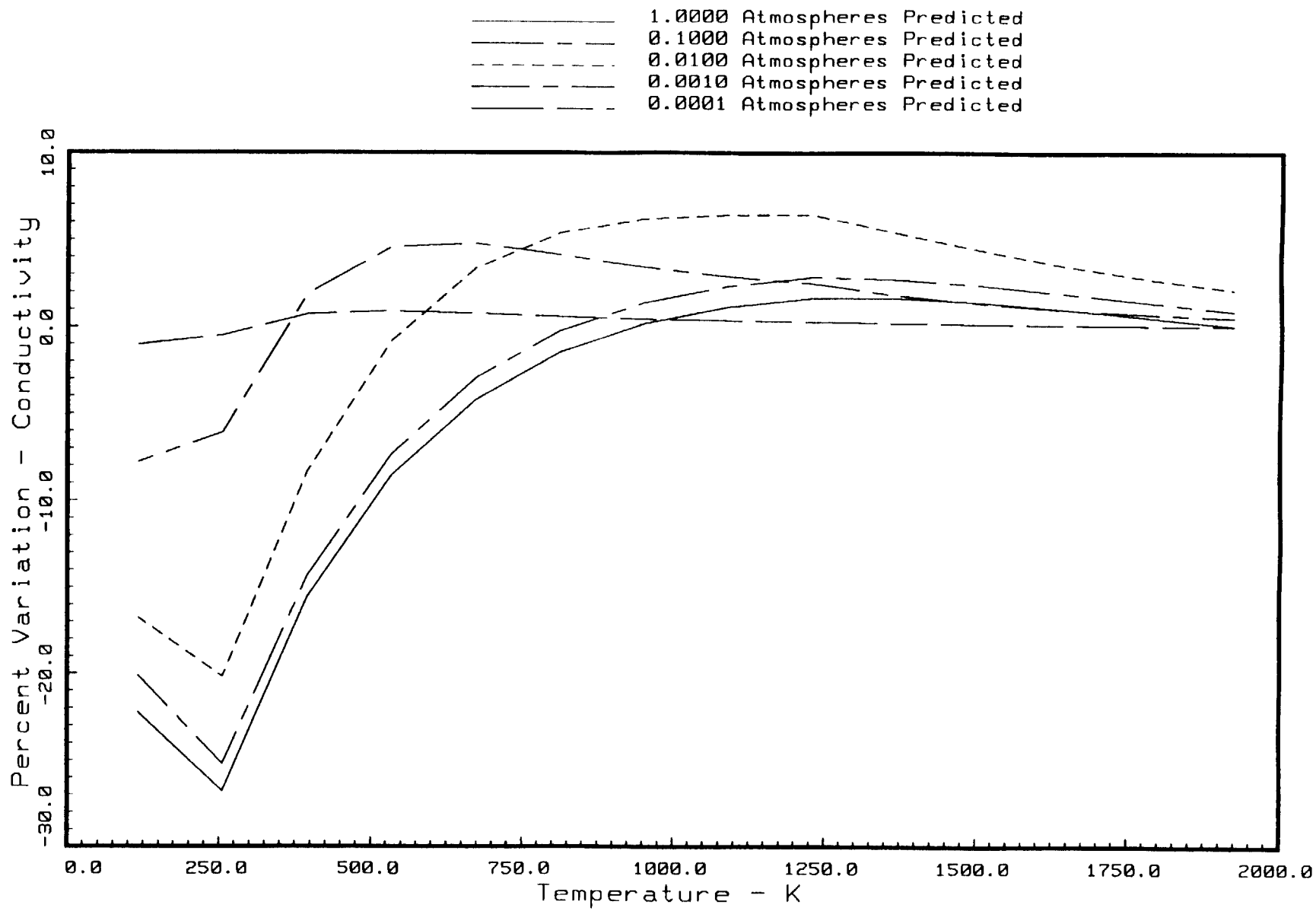

Fig. 59 Percent Variation in Predicted HTP-9 Conductivity in the Strong Direction in a C02 Atmosphere vs. Predicted Values in Air.

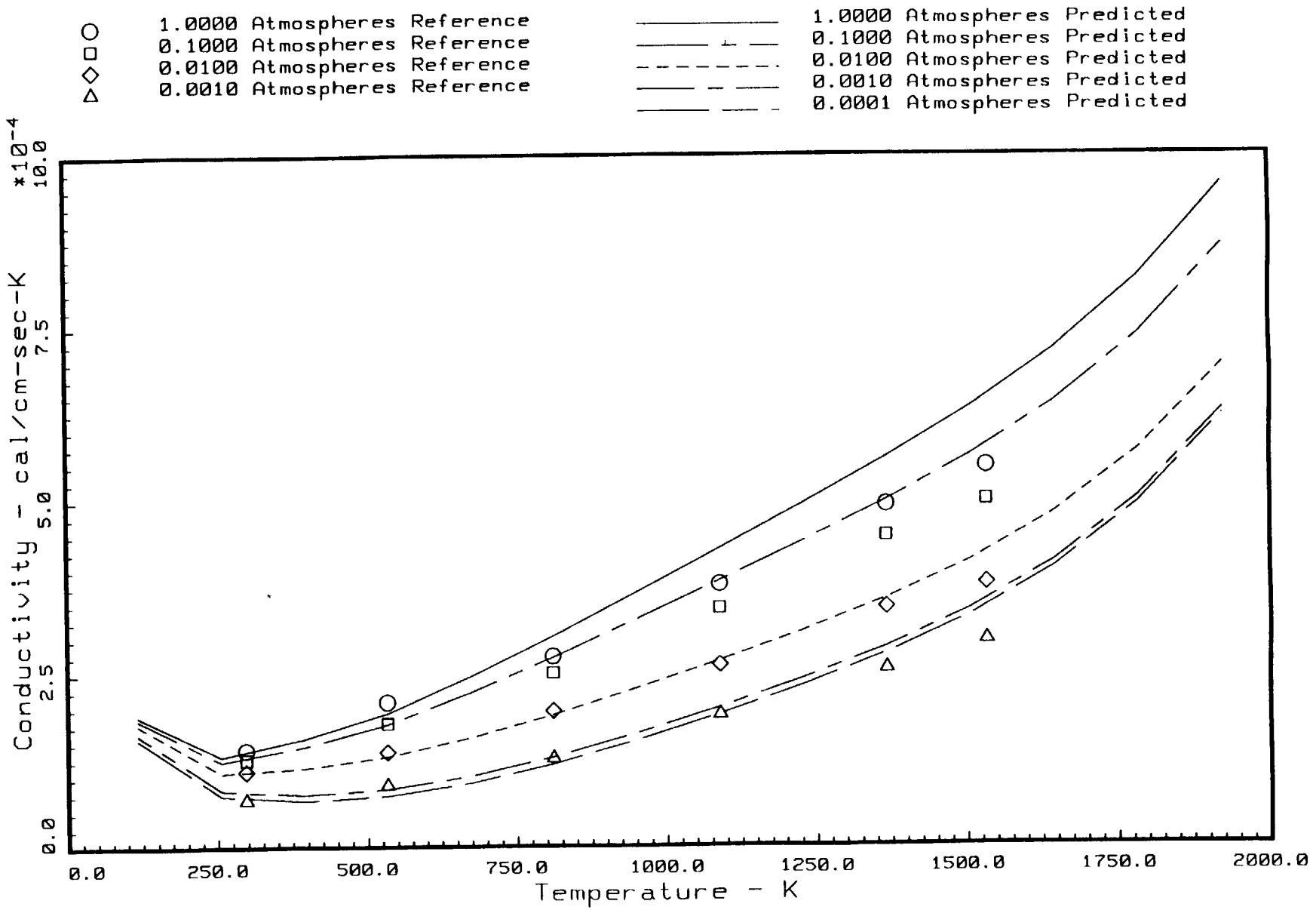

Fig. 60 Predicted HTP-12 Conductivity in the Weak Direction in a C02 Atmosphere vs. Baseline Values in Air.

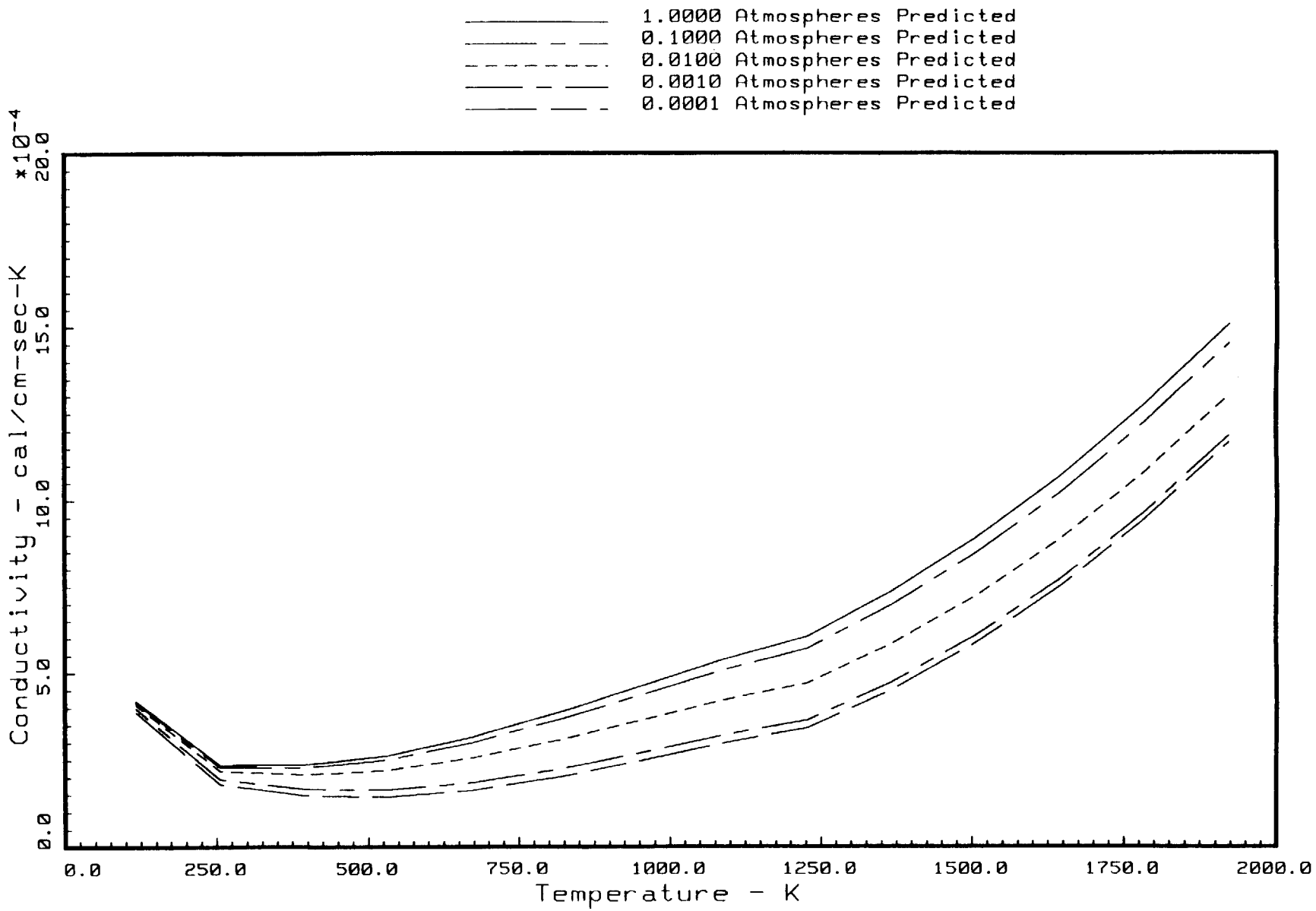

Fig. 61 Predicted HTP-12 Conductivity in the Strong Direction in a C02 Atmosphere.

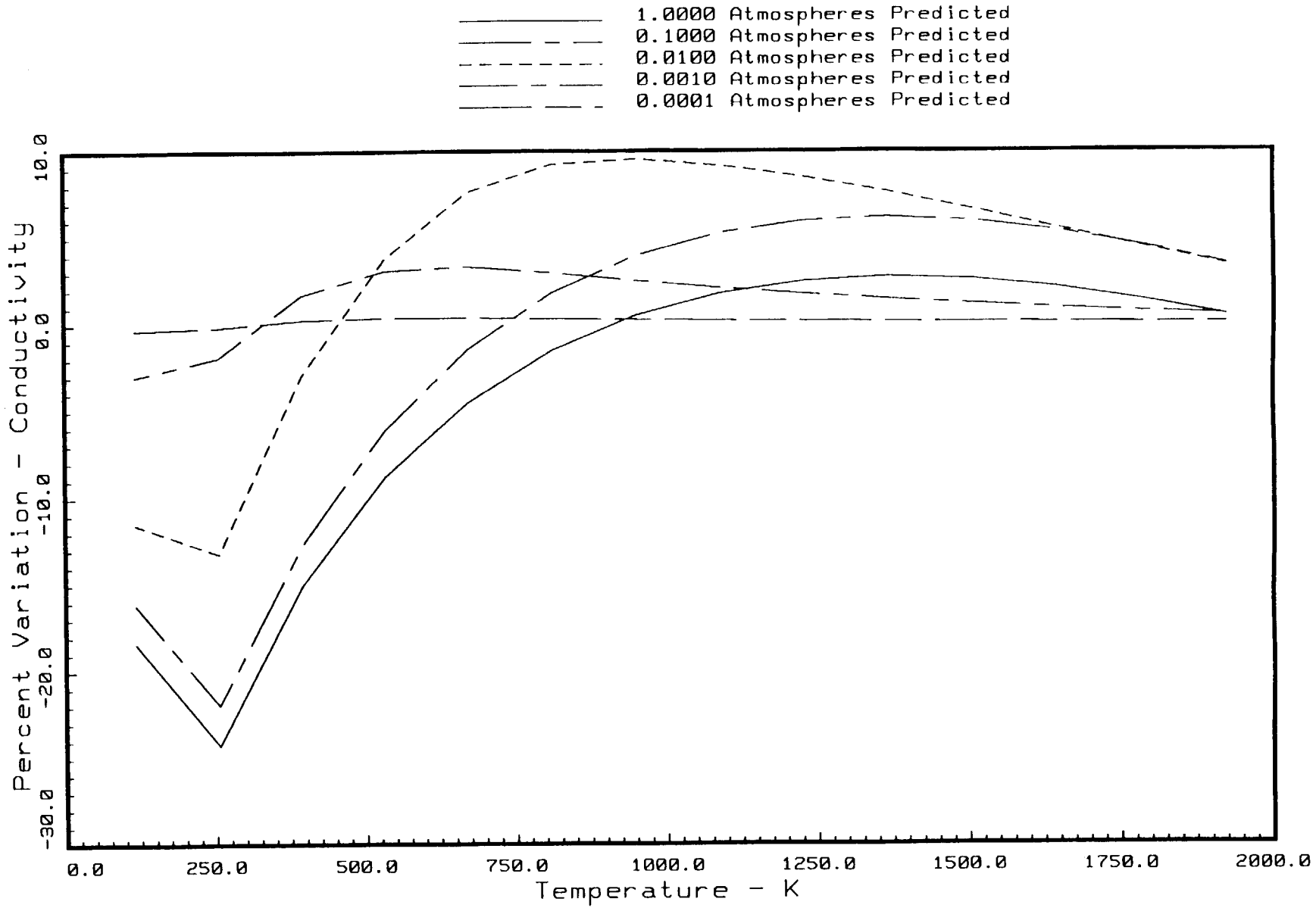

Fig. 62 Percent Variation in Predicted HTP-12 Conductivity in the Weak Direction in a C02 Atmosphere vs. Predicted Values in Air.

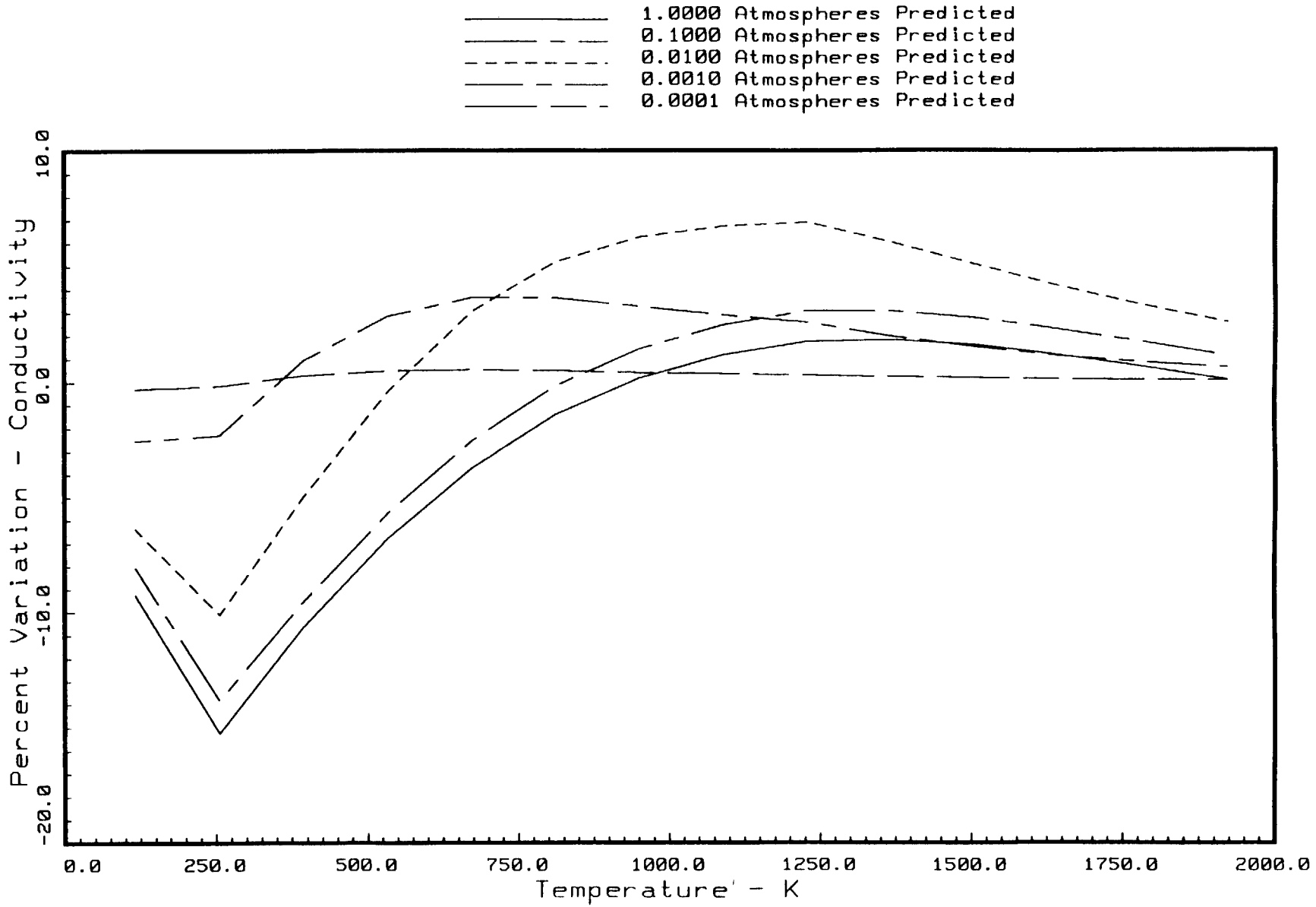

Fig. 63 Percent Variation in Predicted HTP-12 Conductivity in the Strong Direction in a C02 Atmosphere vs. Predicted Values in Air.

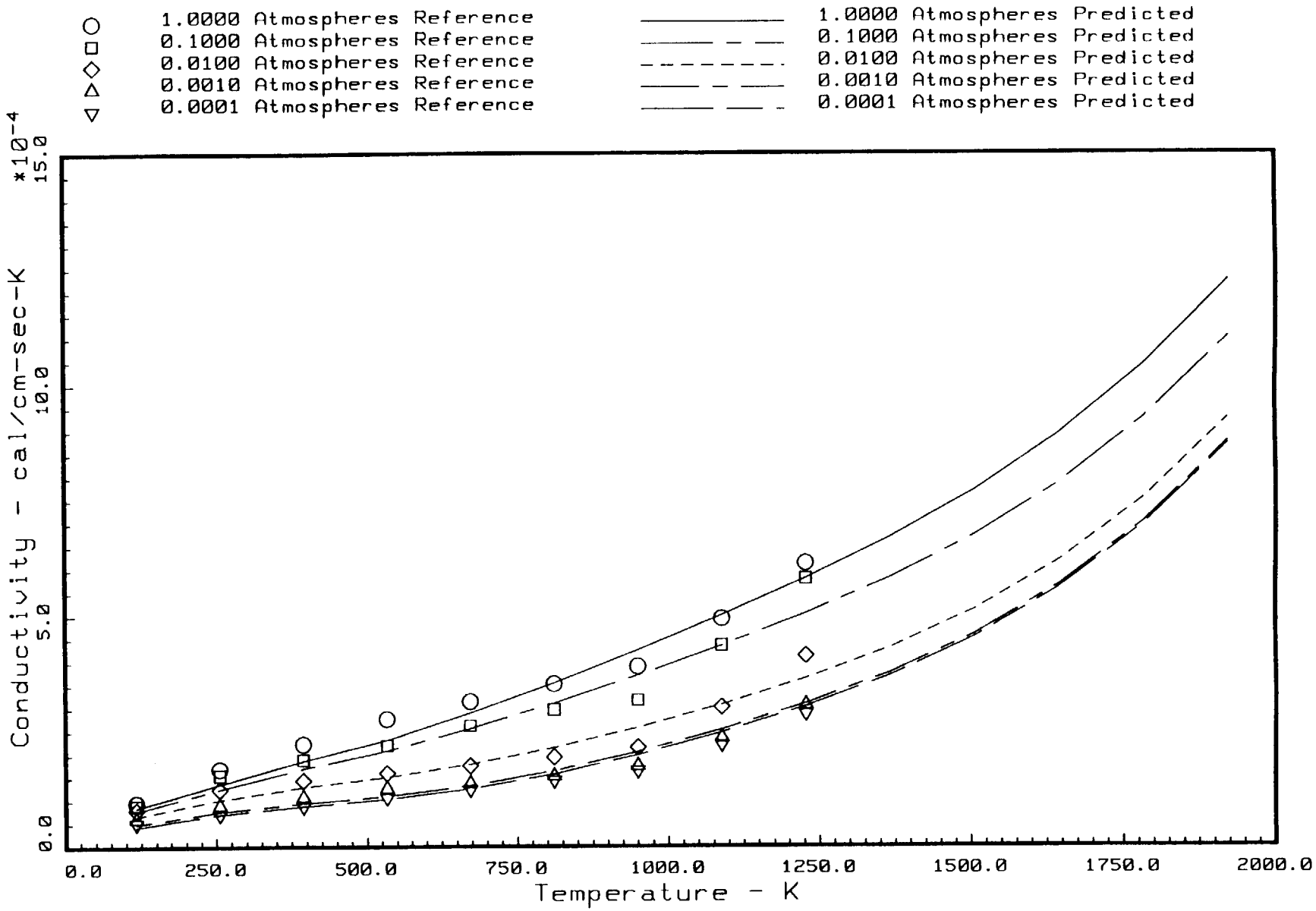

Fig. 64 Predicted LI-2200 Conductivity in the Weak Direction in a C02 Atmosphere vs. Baseline Values in Air.

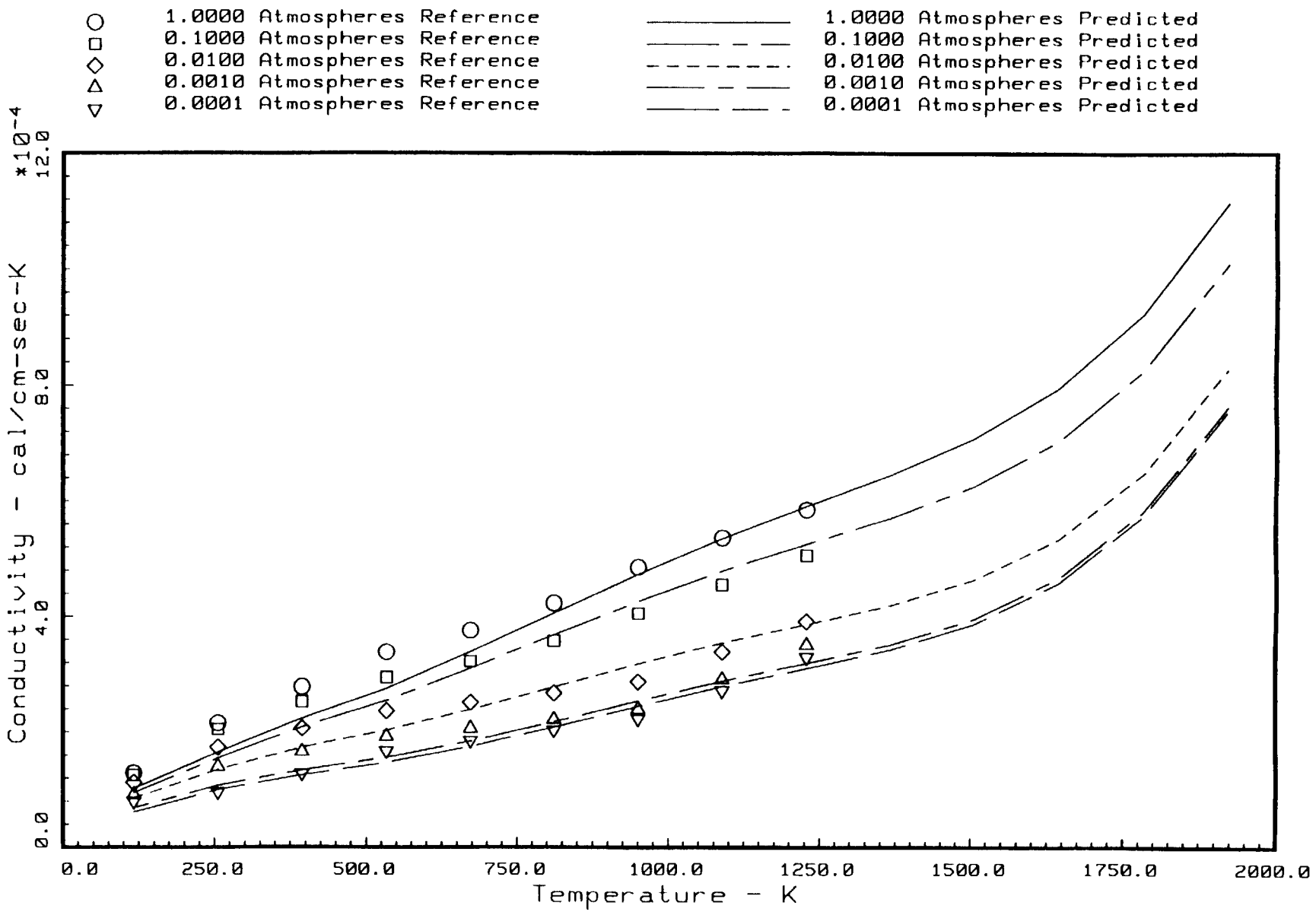

Fig. 65 Predicted LI-2200 Conductivity in the Strong Direction in a C02 Atmosphere vs. Baseline Values in Air.

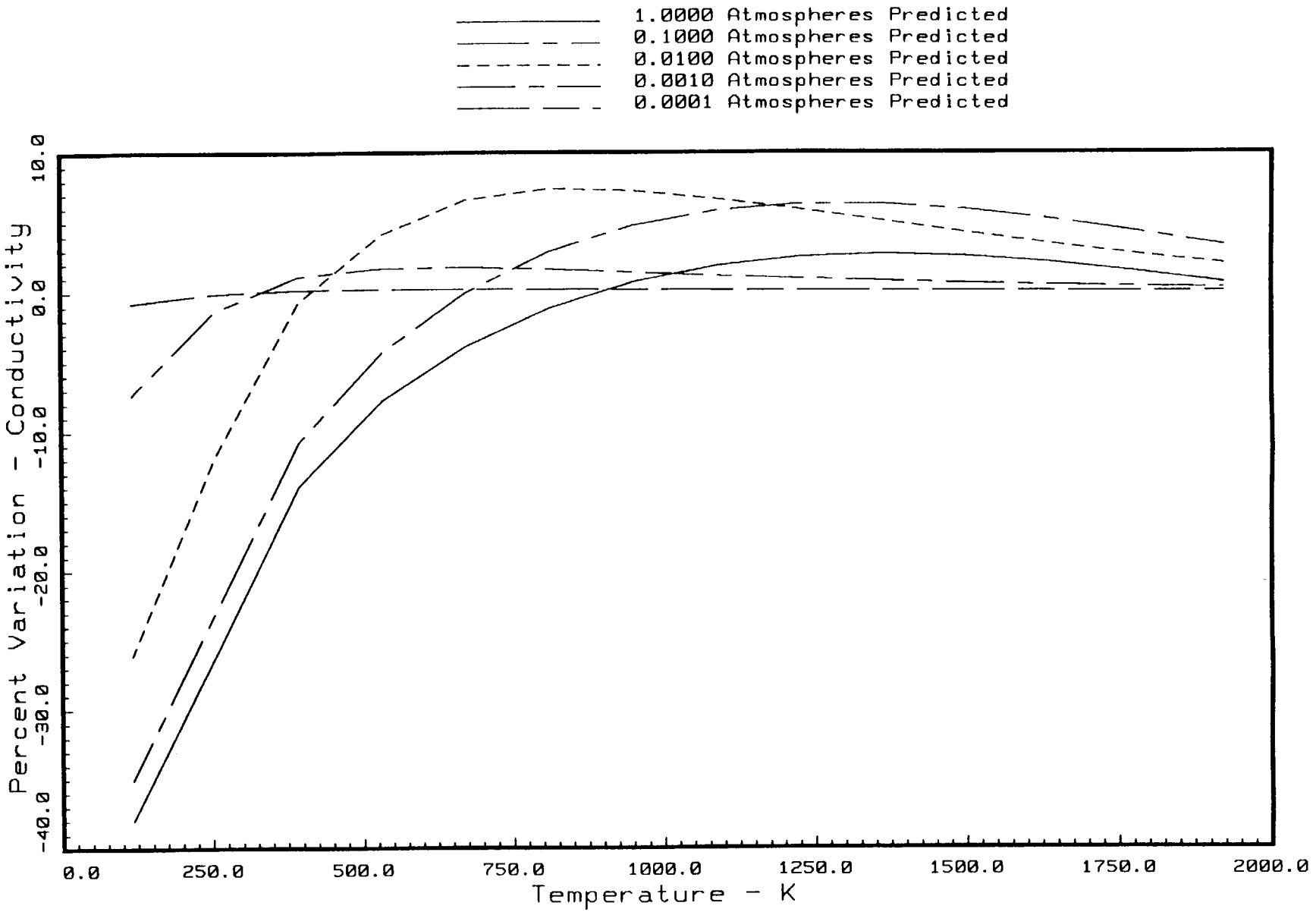

Fig. 66 Percent Variation in Predicted LI-2200 Conductivity in the Weak Direction in a C02 Atmosphere vs. Predicted Values in Air.

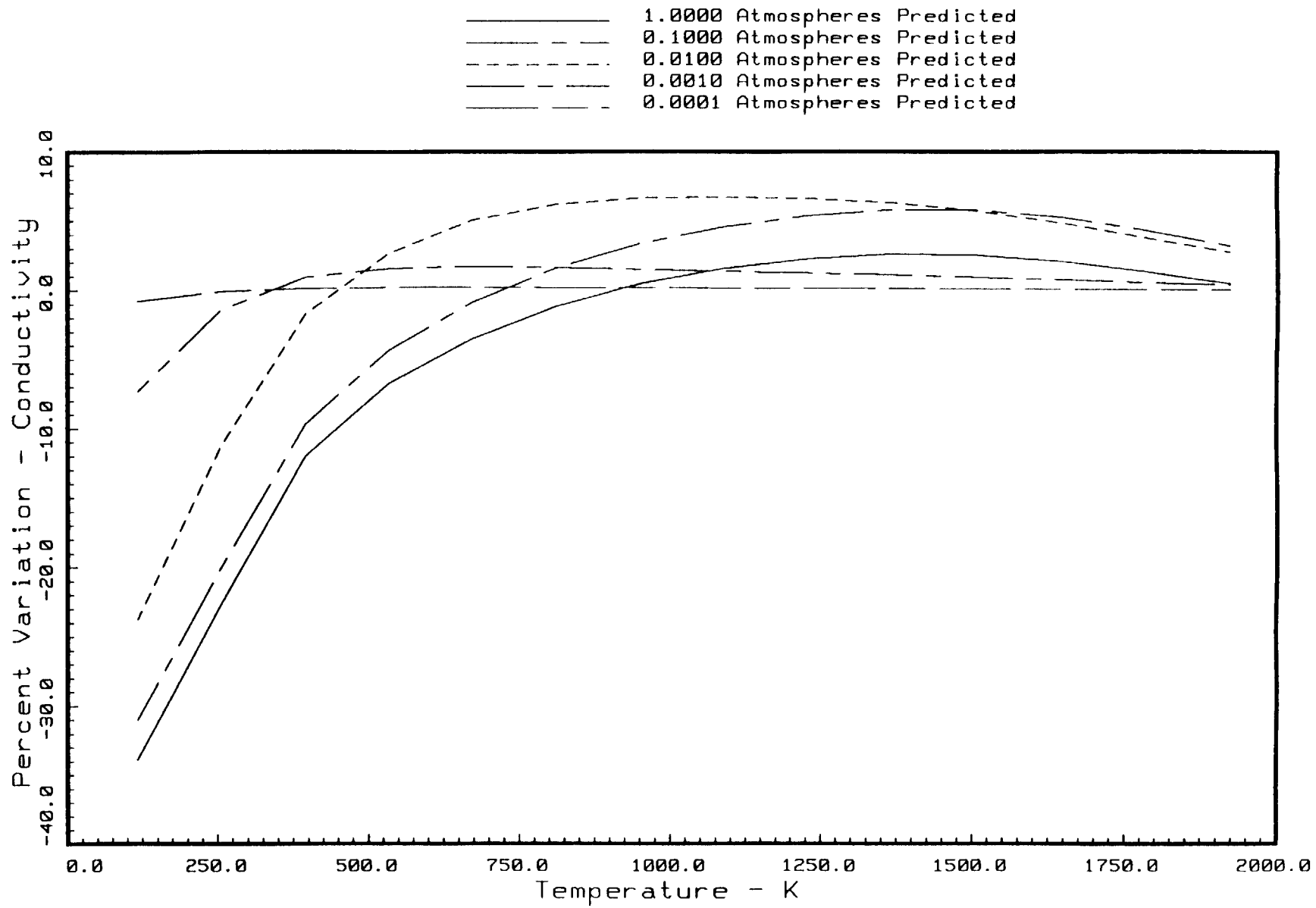

Fig. 67 Percent Variation in Predicted LI-2200 Conductivity in the Strong Direction in a C02 Atmosphere vs. Predicted Values in Air.

Appendix A

Sketch of Calculation Procedure for Conductivity Prediction

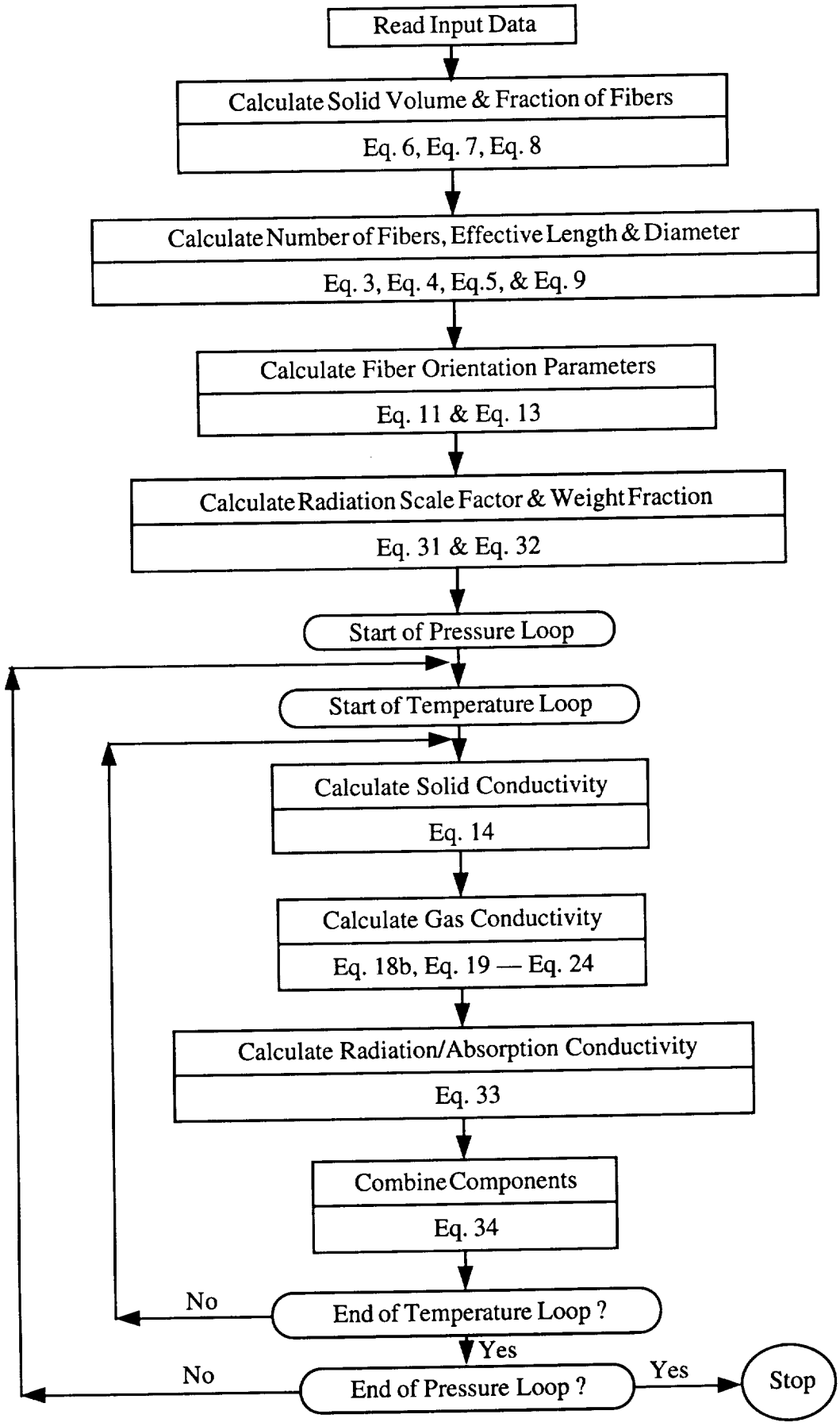

Sketch of Calculation Procedure for Conductivity Prediction

Appendix B

Morphological, Emissivity, and Conductivity Data

For
LI-900,
FRCI-12,
HTP-6, HTP-9, HTP-12,
and
LI-2200
in Air

Table B1 - Morphological and Emissivity Data for LI-900

Total Density	0.1442 gm/cm^3
Angle Between Fibers	100.0°

Fiber Data

	Silica	Alumina	Nextel	SiC
Content (%)	100.00	0.00	0.00	0.00
Diameter (microns)	1.40	3.00	11.00	75.00
Length (cm)	1.27	1.27	1.27	0.0075
Density (gm/cm^3)	2.20	3.97	2.79	3.10
Index of Refraction	1.487	1.768	1.642	

	Weak Direction	Strong Direction
Tensile Strength (N/m^2)	σ_w = 1.655 X 10^5	σ_{st} = 4.619 X 10^5
Gas Conduction Factor	f_g = 1.04799	
Solid Binding Efficiency Factors		
	η_w' = 0.45513	η_{st}' = 0.38492
	η_w = 0.11893	η_{st} = 0.28434

Temperature		Emissivity	
°F	°C	ε_w	ε_{st}
-250.00	-156.33	0.48726	0.33424
0.00	-17.44	0.44736	0.37798
250.00	121.44	0.41163	0.41818
500.00	260.33	0.38007	0.45484
750.00	399.22	0.35268	0.48796
1000.00	538.11	0.32946	0.51754
1250.00	677.00	0.31041	0.54357
1500.00	815.89	0.29553	0.56607
1750.00	954.78	0.28481	0.58502
2000.00	1093.67	0.27827	0.60043
2250.00	1232.56	0.27629	0.61032
2500.00	1371.44	0.27769	0.62063
2750.00	1510.33	0.28266	0.62462
3000.00	1649.22	0.29378	0.62666

Table B1 - Base Line Conductivity Data for LI-900

LI-900 Experimental Base Line Conductivity Values - Weak Direction

Conductivity - cal/cm-sec-°C X 10^{-4}
Pressure - Atmospheres

T (°C)	1.0000	0.1000	0.0100	0.0010	0.0001
-156.33	0.96315	0.89288	0.62005	0.31003	0.20668
-17.44	1.13676	1.03342	0.75646	0.41337	0.31003
121.44	1.40959	1.30624	0.93008	0.51671	0.38030
260.33	1.78988	1.65347	1.14090	0.69033	0.51671
399.22	2.20739	2.03377	1.34345	0.89288	0.72339
538.11	2.71996	2.48021	1.62040	1.13676	0.96315
677.00	3.23254	2.99692	2.03377	1.44679	1.27317
815.89	3.89393	3.61697	2.55048	1.89736	1.71961
954.78	4.67106	4.38170	3.17053	2.52155	2.34380
1093.67	5.62181	5.24978	3.89393	3.23254	3.03412
1260.33	6.90325	6.40721	4.79507	4.21636	3.99314
1371.44	8.01934	7.39929	5.74582	5.08443	4.79507
1538.11	10.00351	9.17678	7.44063	6.69657	6.36587
1649.22	11.98768	10.83025	9.05277	8.10202	7.85400

LI-900 Experimental Base Line Conductivity Values - Strong Direction

Conductivity - cal/cm-sec-°C X 10^{-4}
Pressure - Atmospheres

T (°C)	1.0000	0.1000	0.0100	0.0010	0.0001
-156.33	1.24010	1.07476	0.90941	0.53738	0.45471
-17.44	1.61214	1.36412	1.15743	0.74406	0.62005
121.44	1.94283	1.69481	1.36412	0.95075	0.82674
260.33	2.35620	2.10818	1.73615	1.24010	1.07476
399.22	2.89358	2.64556	2.10818	1.65347	1.44679
538.11	3.63764	3.34828	2.60422	2.14952	2.02550
677.00	4.58839	4.29903	3.43096	2.93491	2.72823
815.89	5.78716	5.45646	4.50571	3.96834	3.67898
954.78	7.23394	6.90325	5.78716	5.16710	4.91908
1093.67	9.13544	8.76341	7.44063	6.69657	6.32453
1260.33	11.90501	11.28495	9.92084	9.13544	8.80474

Table B1 - Analytical Conductivity Data for LI-900

LI-900 Analytically Predicted Conductivity Values - Weak Direction

Conductivity - cal/cm-sec-°C X 10^{-4}
Pressure - Atmospheres

T (°C)	1.0000	0.1000	0.0100	0.0010	0.0001
-156.33	0.91928	0.79541	0.59884	0.27820	0.15955
-17.44	1.27043	1.12163	0.77718	0.37390	0.27981
121.44	1.57019	1.38793	0.90154	0.46501	0.38259
260.33	1.90632	1.67493	1.04563	0.58789	0.51182
399.22	2.37396	2.06103	1.26309	0.77732	0.70368
538.11	2.89302	2.49479	1.54613	1.04571	0.97467
677.00	3.47029	2.98452	1.90285	1.39622	1.32777
815.89	4.11069	3.53612	2.33760	1.83011	1.76412
954.78	4.82879	4.16471	2.86334	2.35827	2.29459
1093.67	5.65571	4.90158	3.50901	3.00820	2.94664
1232.56	6.63995	5.79507	4.32050	3.82480	3.76514
1371.44	7.84337	6.90659	5.35689	4.86637	4.80839
1510.33	9.33644	8.30590	6.68565	6.19987	6.14333
1649.22	11.19937	10.07229	8.38396	7.90203	7.84668

Analytically Predicted Conductivity Values - Strong Direction

Conductivity - cal/cm-sec-°C X 10^{-4}
Pressure - Atmospheres

T (°C)	1.0000	0.1000	0.0100	0.0010	0.0001
-156.33	1.11599	1.00145	0.86133	0.57497	0.37509
-17.44	1.60663	1.48424	1.25559	0.81221	0.62740
121.44	1.97227	1.83776	1.50730	0.96281	0.79097
260.33	2.37195	2.21383	1.76595	1.14251	0.97878
399.22	2.97350	2.76619	2.16724	1.46041	1.29873
538.11	3.74719	3.48890	2.74250	1.97590	1.81780
677.00	4.73001	4.41944	3.53203	2.72316	2.56930
815.89	5.94535	5.58150	4.56071	3.72236	3.57295
954.78	7.42297	7.00494	5.85846	4.99986	4.85484
1093.67	9.20771	8.73456	7.46944	6.59704	6.45618
1232.56	11.35374	10.82432	9.44649	8.56456	8.42752
1371.44	13.90729	13.32008	11.83403	10.94511	10.81149
1510.33	16.88747	16.24048	14.64904	13.75430	13.62363
1649.22	20.28137	19.57201	17.87623	16.97569	16.84747

Table B2 - Morphological and Emissivity Data for FRCI-12

Total Density	0.1922 gm/cm^3
Angle Between Fibers q	100.0°

Fiber Data

	Silica	Alumina	Nextel	SiC
Content (%)	75.66	0.00	21.34	3.00
Diameter (microns)	1.40	3.00	11.00	75.00
Length (cm)	1.27	1.27	1.27	0.0075
Density (gm/cm^3)	2.20	3.97	2.79	3.10
Index of Refraction	1.487	1.768	1.642	

	Weak Direction	Strong Direction
Tensile Strength (N/m^2)	σ_w = 5.585 X 10^5	σ_{st} = 1.772 X 10^6
Gas Conduction Factor	f_g = 1.06574	
Solid Binding Efficiency Factors		
	η_w' = 0.30993	η_{st}' = 0.17315
	η_w = 0.07239	η_{st} = 0.13271

Emissivity

Temperature °F	Temperature °C	Silica ε_w	Silica ε_{st}	Mullite ε_w	Mullite ε_{st}
-250.00	-156.33	0.48726	0.33424	0.35025	0.77844
0.00	-17.44	0.44736	0.37798	0.31131	0.63547
250.00	121.44	0.41163	0.41818	0.27441	0.50734
500.00	260.33	0.38007	0.45484	0.23957	0.39405
750.00	399.22	0.35268	0.48796	0.20677	0.29561
1000.00	538.11	0.32946	0.51754	0.17603	0.21201
1250.00	677.00	0.31041	0.54357	0.14734	0.14326
1500.00	815.89	0.29553	0.56607	0.12069	0.08935
1750.00	954.78	0.28481	0.58502	0.09610	0.05029
2000.00	1093.67	0.27827	0.60043	0.07356	0.02607
2250.00	1232.56	0.27629	0.61032	0.05307	0.01669
2500.00	1371.44	0.27769	0.62063	0.03463	0.02216
2750.00	1510.33	0.28266	0.62462	0.01824	0.04248
3000.00	1649.22	0.29378	0.62666	0.00390	0.07763

Table B2 - Base Line Conductivity Data for FRCI-12

FRCI-12 Experimental Base Line Conductivity Values - Weak Direction

Conductivity - cal/cm-sec-°C X 10^{-4}
Pressure - Atmospheres

T (°C)	1.0000	0.1000	0.0100	0.0010	0.0001
-111.89	0.86105	0.82674	0.72339	0.44768	0.34434
24.22	1.34345	1.27441	0.96439	0.58574	0.44768
260.33	2.10115	1.89447	1.34345	0.82674	0.68908
482.56	2.96261	2.68689	1.79112	1.20580	0.99911
704.78	4.06465	3.54794	2.44590	1.72251	1.58444
927.00	5.44282	4.68470	3.30695	2.68689	2.58355

FRCI-12 Experimental Base Line Conductivity Values - Strong Direction

Conductivity - cal/cm-sec-°C X 10^{-4}
Pressure - Atmospheres

T (°C)	1.0000	0.1000	0.0100	0.0010	0.0001
-111.89	1.41248	0.00000	1.06773	0.00000	0.62005
24.22	1.75682	0.00000	1.37776	0.00000	0.79243
260.33	2.68689	0.00000	1.96350	0.00000	1.13676
482.56	3.65128	0.00000	2.58355	0.00000	1.58444
704.78	4.71943	0.00000	3.23791	0.00000	2.48021
927.00	6.44152	0.00000	4.34037	0.00000	3.61697

Table B2 - Analytical Conductivity Data for FRCI-12

FRCI-12 Analytically Predicted Conductivity Values - Weak Direction

Conductivity - cal/cm-sec-°C X 10^{-4}
Pressure - Atmospheres

T (°C)	1.0000	0.1000	0.0100	0.0010	0.0001
-156.33	1.07017	0.94651	0.75054	0.43252	0.31550
-17.44	1.37985	1.23146	0.88940	0.49141	0.39899
121.44	1.69932	1.51784	1.03611	0.60643	0.52562
260.33	2.10400	1.87387	1.25158	0.80166	0.72713
399.22	2.66813	2.35704	1.56842	1.09116	1.01903
538.11	3.28877	2.89303	1.95588	1.46438	1.39480
677.00	3.94750	3.46491	2.39677	1.89931	1.83226
815.89	4.61949	4.04883	2.86569	2.36748	2.30286
954.78	5.28287	4.62348	3.33917	2.84342	2.78106
1093.67	5.92529	5.17665	3.80268	3.31119	3.25090
1232.56	6.54671	5.70815	4.25362	3.76719	3.70877
1371.44	7.15925	6.22964	4.70131	4.22003	4.16325
1510.33	7.78657	6.76409	5.16650	4.68990	4.63453
1649.22	8.46687	7.34880	5.68436	5.21158	5.15738

FRCI-12 Analytically Predicted Conductivity Values - Strong Direction

Conductivity - cal/cm-sec-°C X 10^{-4}
Pressure - Atmospheres

T (°C)	1.0000	0.1000	0.0100	0.0010	0.0001
-156.33	1.32073	1.20433	1.05063	0.74926	0.57714
-17.44	1.69723	1.56920	1.31016	0.87259	0.72245
121.44	2.09109	1.94615	1.57201	1.05614	0.91986
260.33	2.58264	2.40827	1.90662	1.33278	1.20460
399.22	3.24048	3.00939	2.34805	1.71137	1.58578
538.11	3.94909	3.65886	2.84549	2.16671	2.04455
677.00	4.68543	4.33435	3.37886	2.67260	2.55418
815.89	5.44401	5.03084	3.94369	3.22020	3.10554
954.78	6.26263	5.78634	4.57747	3.84383	3.73280
1093.67	7.24277	6.70232	5.38055	4.64149	4.53384
1232.56	8.22013	7.61433	6.18694	5.44537	5.34081
1371.44	9.87180	9.19908	7.67160	6.92905	6.82723
1510.33	11.78677	11.04501	9.42110	8.67804	8.57858
1649.22	13.96012	13.14653	11.42793	10.68395	10.58645

Table B3 - Morphological and Emissivity Data for HTP-6

Total Density 0.0961 gm/cm^3
Angle Between Fibers θ 100.0°

Fiber Data

	Silica	Alumina	Nextel	SiC
Content (%)	76.44	21.56	0.00	2.00
Diameter (microns)	1.40	3.00	11.00	38.00
Length (cm)	1.27	1.27	1.27	0.0038
Density (gm/cm^3)	2.20	3.97	2.79	3.10
Index of Refraction	1.487	1.768	1.642	

	Weak Direction	Strong Direction
Tensile Strength (N/m^2)	σ_w = 3.172 X 10^5	σ_{st} = 9.101 X 10^5
Gas Conduction Factor	f_g = 0.95047	
Solid Binding Efficiency Factors		
	η_w' = 0.12574	η_{st}' = 0.08136
	η_w = 0.03208	η_{st} = 0.06060

Temperature		Emissivity			
		Silica		Mullite	
°F	°C	ε_w	ε_{st}	ε_w	ε_{st}
-250.00	-156.33	0.48726	0.33424	0.76325	0.85642
0.00	-17.44	0.44736	0.37798	0.65822	0.85642
250.00	121.44	0.41163	0.41818	0.56163	0.73885
500.00	260.33	0.38007	0.45484	0.47348	0.62126
750.00	399.22	0.35268	0.48796	0.39378	0.50367
1000.00	538.11	0.32946	0.51754	0.32252	0.38606
1250.00	677.00	0.31041	0.54357	0.25970	0.26843
1500.00	815.89	0.29553	0.56607	0.20533	0.15079
1750.00	954.78	0.28481	0.58502	0.15940	0.03314
2000.00	1093.67	0.27827	0.60043	0.12192	0.03314
2250.00	1232.56	0.27629	0.61032	0.09287	0.03314
2500.00	1371.44	0.27769	0.62063	0.07228	0.03314
2750.00	1510.33	0.28266	0.62462	0.06012	0.03314
3000.00	1649.22	0.29378	0.62666	0.05641	0.03314

Table B3 - Base Line Conductivity Data for HTP-6

HTP-6 Experimental Base Line Conductivity Values - Weak Direction

Conductivity - cal/cm-sec-°C X 10^{-4}
Pressure - Atmospheres

T (°C)	1.0000	0.1000	0.0100	0.0010	0.0001
-179.67	0.91313				0.27654
21.44	1.35709				0.30135
48.67	1.45010				0.36500
373.11	2.55586				0.90941
538.11	3.68600				1.46415
641.44	4.44371				2.00153
810.33	5.71151				3.29331
979.22	7.85400				5.13279

Table B3 - Analytical Conductivity Data for HTP-6

HTP-6 Analytically Predicted Conductivity Values - Weak Direction

Conductivity - cal/cm-sec-°C X 10^{-4}
Pressure - Atmospheres

T (°C)	1.0000	0.1000	0.0100	0.0010	0.0001
-156.33	1.21648	1.10462	0.94058	0.63457	0.49095
-17.44	1.28346	1.15424	0.86298	0.43746	0.31564
121.44	1.64211	1.48845	1.06401	0.57670	0.46711
260.33	2.17296	1.98121	1.41594	0.88610	0.78359
399.22	2.91482	2.65696	1.92361	1.34816	1.24836
538.11	3.75392	3.42665	2.53763	1.93426	1.83761
677.00	4.66523	4.26632	3.23541	2.61597	2.52257
815.89	5.63133	5.15927	3.99991	3.37234	3.28213
954.78	6.65398	6.10765	4.83204	4.20156	4.11436
1093.67	7.76436	7.14271	5.76136	5.13123	5.04682
1232.56	9.03271	8.33458	6.85599	6.22804	6.14615
1371.44	10.57773	9.80155	8.23216	7.60713	7.52747
1510.33	12.57596	11.71959	10.06373	9.44156	9.36381
1649.22	15.27227	14.33280	12.59272	11.97268	11.89653

HTP-6 Analytically Predicted Conductivity Values - Strong Direction

Conductivity - cal/cm-sec-°C X 10^{-4}
Pressure - Atmospheres

T (°C)	1.0000	0.1000	0.0100	0.0010	0.0001
-156.33	1.62589	1.51938	1.39036	1.11955	0.91668
-17.44	1.48196	1.36834	1.15577	0.71982	0.52514
121.44	1.84181	1.71694	1.40585	0.85839	0.67435
260.33	2.45881	2.31190	1.88609	1.25061	1.07377
399.22	3.38310	3.19050	2.61805	1.89251	1.71740
538.11	4.49521	4.25521	3.53850	2.74723	2.57566
677.00	5.72747	5.43881	4.58316	3.74443	3.57723
815.89	6.97213	6.63381	5.64588	4.77323	4.61069
954.78	8.08085	7.69199	6.57867	5.68199	5.52409
1093.67	10.46712	10.02675	8.79445	7.88075	7.72727
1232.56	13.36862	12.87560	11.52973	10.60373	10.45434
1371.44	16.82342	16.27628	14.82091	13.88551	13.73977
1510.33	20.85386	20.25066	18.68832	17.74492	17.60235
1649.22	25.46404	24.80226	23.13375	22.18256	22.04261

Table B4 - Morphological and Emissivity Data for HTP-9

Total Density	0.1442 gm/cm^3
Angle Between Fibers θ	100.0°

Fiber Data

	Silica	Alumina	Nextel	SiC
Content (%)	76.44	21.56	0.00	2.00
Diameter (microns)	1.40	3.00	11.00	38.00
Length (cm)	1.27	1.27	1.27	0.0038
Density (gm/cc)	2.20	3.97	2.79	3.10
Index of Refraction	1.487	1.768	1.642	

	Weak Direction	Strong Direction
Tensile Strength (N/m^2)	σ_w = 4.619 X 10^5	σ_{st} = 1.558 X 10^6
Gas Conduction Factor	f_g = 1.06574	
Solid Binding Efficiency Factors		
	η_w' = 0.10802	η_{st}' = 0.06989
	η_w = 0.02390	η_{st} = 0.05443

Temperature		Emissivity			
		Silica		Mullite	
°F	°C	ε_w	ε_{st}	ε_w	ε_{st}
-250.00	-156.33	0.48726	0.33424	0.76325	0.85642
0.00	-17.44	0.44736	0.37798	0.65822	0.85642
250.00	121.44	0.41163	0.41818	0.56163	0.73885
500.00	260.33	0.38007	0.45484	0.47348	0.62126
750.00	399.22	0.35268	0.48796	0.39378	0.50367
1000.00	538.11	0.32946	0.51754	0.32252	0.38606
1250.00	677.00	0.31041	0.54357	0.25970	0.26843
1500.00	815.89	0.29553	0.56607	0.20533	0.15079
1750.00	954.78	0.28481	0.58502	0.15940	0.03314
2000.00	1093.67	0.27827	0.60043	0.12192	0.03314
2250.00	1232.56	0.27629	0.61032	0.09287	0.03314
2500.00	1371.44	0.27769	0.62063	0.07228	0.03314
2750.00	1510.33	0.28266	0.62462	0.06012	0.03314
3000.00	1649.22	0.29378	0.62666	0.05641	0.03314

Table B4 - Base Line Conductivity Data for HTP-9

HTP-9 Experimental Base Line Conductivity Values - Weak Direction

Conductivity - cal/cm-sec-°C X 10^{-4}
Pressure - Atmospheres

T (°C)	1.0000	0.1000	0.0100	0.0010	0.0001
-178.56					0.28493
38.11					0.32007
371.44					0.80532
538.11					1.33679
649.22					1.69427

HTP-9 Experimental Base Line Conductivity Values - Strong Direction

Conductivity - cal/cm-sec-°C X 10^{-4}
Pressure - Atmospheres

T (°C)	1.0000	0.1000	0.0100	0.0010	0.0001
-178.56					0.49720
38.11					0.60889
371.44					1.15301
538.11					1.85325
649.22					2.31478

Table B4 - Analytical Conductivity Data for HTP-9

HTP-9 Analytically Predicted Conductivity Values - Weak Direction

Conductivity - cal/cm-sec-°C X 10^{-4}
Pressure - Atmospheres

T (°C)	1.0000	0.1000	0.0100	0.0010	0.0001
-156.33	1.32105	1.19609	1.00530	0.67958	0.54846
-17.44	1.31645	1.16952	0.83704	0.41616	0.31073
121.44	1.59151	1.41475	0.94258	0.47985	0.38707
190.89	1.76840	1.57403	1.03520	0.56061	0.47223
260.33	1.99907	1.77720	1.16157	0.67110	0.58525
399.22	2.58350	2.28454	1.49735	0.97246	0.88919
538.11	3.22804	2.84839	1.90580	1.36161	1.28118
677.00	3.91461	3.45201	2.37057	1.81687	1.73929
815.89	4.63059	4.08367	2.87882	2.32193	2.24710
954.78	5.37708	4.74496	3.43032	2.87423	2.80197
1093.67	6.17584	5.45775	4.04478	3.49183	3.42195
1232.56	7.07547	6.27051	4.76835	4.21972	4.15198
1371.44	8.15731	7.26411	5.67962	5.13563	5.06976
1510.33	9.54144	8.55798	6.89577	6.35605	6.29181
1649.22	11.39373	10.31711	8.57963	8.04335	7.98044

HTP-9 Analytically Predicted Conductivity Values - Strong Direction

Conductivity - cal/cm-sec-°C X 10^{-4}
Pressure - Atmospheres

T (°C)	1.0000	0.1000	0.0100	0.0010	0.0001
-156.33	1.99108	1.87428	1.73450	1.44834	1.23830
-17.44	1.62825	1.50447	1.27978	0.83162	0.63504
121.44	1.85906	1.72425	1.40098	0.84603	0.66235
260.33	2.29893	2.14168	1.70343	1.06388	0.88835
399.22	2.99147	2.78606	2.19825	1.46899	1.29525
538.11	3.81261	3.55744	2.82278	2.02823	1.85807
677.00	4.71038	4.40427	3.52841	2.68687	2.52108
815.89	5.60646	5.24850	4.23838	3.36340	3.20226
954.78	6.39732	5.98668	4.84946	3.95089	3.79437
1093.67	8.04659	7.58235	6.32465	5.40948	5.25736
1232.56	10.03602	9.51708	8.14447	7.21738	7.06932
1371.44	12.39334	11.81822	10.33490	9.39875	9.25432
1510.33	15.13476	14.50149	12.91008	11.96625	11.82496
1649.22	18.26339	17.56940	15.87075	14.91940	14.78073

Table B5 - Morphological and Emissivity Data for HTP-12

Total Density 0.1922 gm/cm^3
Angle Between Fibers θ 100.0°

Fiber Data

	Silica	Alumina	Nextel	SiC
Content (%)	76.44	21.56	0.00	2.00
Diameter (microns)	1.40	3.00	11.00	38.00
Length (cm)	1.27	1.27	1.27	0.0038
Density (gm/cm^3)	2.20	3.97	2.79	3.10
Index of Refraction	1.487	1.768	1.642	

	Weak Direction	Strong Direction
Tensile Strength (N/m^2)	σ_w = 6.067 X 10^5	σ_{st} = 2.206 X 10^6
Gas Conduction Factor	f_g = 1.06574	
Solid Binding Efficiency Factors	η_w' = 0.26164	η_{st}' = 0.16928
	η_w = 0.05413	η_{st} = 0.13426

Temperature		Emissivity			
		Silica		Mullite	
°F	°C	ε_w	ε_{st}	ε_w	ε_{st}
-250.00	-156.33	0.48726	0.33424	0.76325	0.85642
0.00	-17.44	0.44736	0.37798	0.65822	0.85642
250.00	121.44	0.41163	0.41818	0.56163	0.73885
500.00	260.33	0.38007	0.45484	0.47348	0.62126
750.00	399.22	0.35268	0.48796	0.39378	0.50367
1000.00	538.11	0.32946	0.51754	0.32252	0.38606
1250.00	677.00	0.31041	0.54357	0.25970	0.26843
1500.00	815.89	0.29553	0.56607	0.20533	0.15079
1750.00	954.78	0.28481	0.58502	0.15940	0.03314
2000.00	1093.67	0.27827	0.60043	0.12192	0.03314
2250.00	1232.56	0.27629	0.61032	0.09287	0.03314
2500.00	1371.44	0.27769	0.62063	0.07228	0.03314
2750.00	1510.33	0.28266	0.62462	0.06012	0.03314
3000.00	1649.22	0.29378	0.62666	0.05641	0.03314

Table B5 - Base Line Conductivity Data for HTP-12

HTP-12 Experimental Base Line Conductivity Values - Weak Direction

Conductivity - cal/cm-sec-°C X 10^{-4}
Pressure - Atmospheres

T (°C)	1.0000	0.1000	0.0100	0.0010	0.0001
24.22	1.41248	1.27441	1.10245	0.68908	
260.33	2.10115	1.79112	1.37776	0.89577	
538.11	2.75593	2.51452	1.96350	1.27441	
815.89	3.78935	3.44460	2.61786	1.89447	
1093.67	4.92611	4.47802	3.44460	2.54924	
1260.33	5.47713	4.99473	3.78935	2.96261	

Table B5 - Analytical Conductivity Data for HTP-12

HTP-12 Analytically Predicted Conductivity Values - Weak Direction

Conductivity - cal/cm-sec-°C X 10^{-4}
Pressure - Atmospheres

T (°C)	1.0000	0.1000	0.0100	0.0010	0.0001
-156.33	2.36065	2.23612	2.03776	1.71828	1.60216
-17.44	1.75332	1.60345	1.25723	0.85919	0.76770
121.44	1.86318	1.67947	1.19249	0.76384	0.68392
260.33	2.13265	1.89937	1.27116	0.82307	0.74939
399.22	2.58427	2.26880	1.47368	0.99894	0.92765
538.11	3.10122	2.69982	1.75597	1.26750	1.19874
677.00	3.65890	3.16937	2.09459	1.60055	1.53430
815.89	4.23868	3.65982	2.47029	1.97580	1.91195
954.78	4.83698	4.16816	2.87786	2.38603	2.32443
1093.67	5.47026	4.71100	3.33151	2.84410	2.78455
1232.56	6.17785	5.32750	3.86799	3.38577	3.32806
1371.44	7.02378	6.08126	4.54853	4.07154	4.01546
1510.33	8.09906	7.06256	5.46116	4.98893	4.93425
1649.22	9.52708	8.39386	6.72623	6.25789	6.20436

HTP-12 Analytically Predicted Conductivity Values - Strong Direction

Conductivity - cal/cm-sec-°C X 10^{-4}
Pressure - Atmospheres

T (°C)	1.0000	0.1000	0.0100	0.0010	0.0001
-156.33	4.70351	4.58876	4.44920	4.16465	3.96445
-17.44	2.81393	2.69162	2.46522	2.02501	1.84000
121.44	2.67386	2.53982	2.21354	1.67293	1.50098
260.33	2.84055	2.68339	2.24162	1.62234	1.45851
399.22	3.29849	3.09267	2.50170	1.79885	1.63701
538.11	3.91489	3.65871	2.92195	2.15906	2.00076
677.00	4.62122	4.31343	3.43712	2.63162	2.47753
815.89	5.33397	4.97360	3.96516	3.12985	2.98019
954.78	5.96291	5.54909	4.41606	3.56015	3.41487
1093.67	7.22975	6.76157	5.51084	4.64081	4.49968
1232.56	8.75187	8.22820	6.86558	5.98571	5.84840
1371.44	10.55651	9.97587	8.50574	7.61861	7.48472
1510.33	12.65702	12.01743	10.44256	9.54936	9.41842
1649.22	15.05190	14.35080	12.67220	11.77297	11.64448

Table B6 - Morphological and Emissivity Data for LI-2200

Total Density	0.3524 gm/cm^3
Angle Between Fibers θ	100.0°

	Fiber Data			
	Silica	Alumina	Nextel	SiC
Content (%)	98.00	0.00	0.00	2.00
Diameter (microns)	1.40	3.00	11.00	75.00
Length (cm)	1.27	1.27	1.27	0.0075
Density (gm/cm^3)	2.20	3.97	2.79	3.10
Index of Refraction	1.487	1.768	1.642	

	Weak Direction	Strong Direction
Tensile Strength (N/m^2)	σ_w = 5.033 X 10^5	σ_{st} = 1.241 X 10^6
Gas Conduction Factor	f_g = 1.59464	
Solid Binding Efficiency Factors		
	η_w' = 0.42537	η_{st}' = 0.24154
	η_w = 0.12371	η_{st} = 0.17130

Temperature		Emissivity	
°F	°C	ε_w	ε_{st}
-250.00	-156.33	0.48726	0.99031
0.00	-17.44	0.44736	0.84486
250.00	121.44	0.41163	0.71393
500.00	260.33	0.38007	0.59734
750.00	399.22	0.35268	0.49566
1000.00	538.11	0.32946	0.40831
1250.00	677.00	0.31041	0.33549
1500.00	815.89	0.29553	0.27719
1750.00	954.78	0.28481	0.23342
2000.00	1093.67	0.27827	0.20417
2250.00	1232.56	0.27629	0.19190
2500.00	1371.44	0.27769	0.18925
2750.00	1510.33	0.28266	0.20119
3000.00	1649.22	0.29378	0.23243

Table B6 - Base Line Conductivity Data for LI-2200

Experimental Base Line Conductivity Values - Weak Direction

Conductivity - cal/cm-sec-°C X 10^{-4}
Pressure - Atmospheres

T (°C)	1.0000	0.1000	0.0100	0.0010	0.0001
-156.33	0.96604	0.90404	0.80855	0.61220	0.52332
-17.44	1.69026	1.55385	1.24755	0.89742	0.70851
121.44	2.23012	1.89116	1.44307	1.08302	0.87923
260.33	2.76791	2.18589	1.59726	1.26573	1.06153
399.22	3.14615	2.61910	1.75682	1.37238	1.23597
538.11	3.52355	2.96013	1.93539	1.52285	1.42529
677.00	3.89972	3.16475	2.14579	1.73904	1.63653
815.89	4.93644	4.35359	3.01221	2.34586	2.20036
954.78	6.13852	5.80038	4.12335	3.05727	2.85679

Experimental Base Line Conductivity Values - Strong Direction

Conductivity - cal/cm-sec-°C X 10^{-4}
Pressure - Atmospheres

T (°C)	1.0000	0.1000	0.0100	0.0010	0.0001
-156.33	1.28806	1.25209	1.12395	0.90900	0.79615
-17.44	2.15324	2.04328	1.73243	1.39966	0.96273
121.44	2.78321	2.52733	2.06188	1.65471	1.28103
260.33	3.38342	2.94608	2.36405	1.91720	1.67042
399.22	3.76082	3.22303	2.50915	2.06147	1.85106
538.11	4.23496	3.58060	2.67449	2.21896	2.03377
677.00	4.85253	4.05638	2.86836	2.39630	2.22806
815.89	5.36676	4.55491	3.38714	2.91425	2.72120
954.78	5.85453	5.05921	3.92328	3.51528	3.29868

Table B6 - Analytical Conductivity Data for LI-2200

LI-2200 Analytically Predicted Conductivity Values - Weak Direction

Conductivity - cal/cm-sec-°C X 10^{-4}
Pressure - Atmospheres

T (°C)	1.0000	0.1000	0.0100	0.0010	0.0001
-156.33	1.37958	1.20261	0.90911	0.54165	0.44316
-17.44	1.84187	1.62480	1.16273	0.78228	0.71392
121.44	2.16711	1.90160	1.30586	0.93517	0.87874
260.33	2.50487	2.17113	1.44803	1.08250	1.03190
399.22	3.01146	2.56265	1.67711	1.29992	1.25121
538.11	3.58476	3.01764	1.99471	1.61414	1.56733
677.00	4.22365	3.53724	2.39906	2.01992	1.97493
815.89	4.91710	4.11181	2.87717	2.50221	2.45894
954.78	5.66958	4.74650	3.43077	3.06149	3.01980
1093.67	6.51465	5.47502	4.09041	3.72742	3.68716
1232.56	7.51354	6.35823	4.91404	4.55739	4.51841
1371.44	8.74168	7.47086	5.97376	5.62306	5.58521
1510.33	10.27325	8.88607	7.34037	6.99494	6.95806
1649.22	12.18066	10.67498	9.08287	8.74181	8.70573

LI-2200 Analytically Predicted Conductivity Values - Strong Direction

Conductivity - cal/cm-sec-°C X 10^{-4}
Pressure - Atmospheres

T (°C)	1.0000	0.1000	0.0100	0.0010	0.0001
-156.33	1.54861	1.37959	1.12117	0.74169	0.61533
-17.44	2.13029	1.93314	1.52006	1.09322	1.00219
121.44	2.54015	2.30767	1.75984	1.32497	1.24886
260.33	2.94711	2.66096	1.97810	1.53680	1.46812
399.22	3.51100	3.12821	2.27164	1.80697	1.74059
538.11	4.10969	3.62686	2.61728	2.14137	2.07741
677.00	4.70950	4.12493	2.98204	2.50242	2.44083
815.89	5.26922	4.58224	3.32363	2.84494	2.78561
954.78	5.78021	4.99072	3.63139	3.15640	3.09918
1093.67	6.29049	5.39849	3.95076	3.48095	3.42565
1232.56	6.90780	5.91303	4.38654	3.92250	3.86893
1371.44	7.78604	6.68766	5.08953	4.63119	4.57913
1510.33	9.10908	7.90540	6.24035	5.78715	5.73640
1649.22	11.09502	9.78328	8.05382	7.60484	7.55516

Appendix C

Predicted Conductivity Data

For
LI-900,
FRCI-12,
HTP-6, HTP-9, HTP-12,
and
LI-2200
in CO_2

Table C1 - Analytical Conductivity Data for LI-900 in CO_2

LI-900 Analytically Predicted Conductivity Values in CO_2 - Weak Direction

Conductivity - cal/cm-sec-°C X 10^{-4}
Pressure - Atmospheres

T (°C)	1.0000	0.1000	0.0100	0.0010	0.0001
-156.33	0.49029	0.43763	0.36489	0.22624	0.15473
-17.44	0.84578	0.76972	0.60894	0.35724	0.27871
121.44	1.28952	1.17304	0.86483	0.47829	0.38450
260.33	1.71809	1.55749	1.09329	0.61410	0.51492
399.22	2.25702	2.02721	1.37578	0.81141	0.70748
538.11	2.84618	2.54254	1.70941	1.08449	0.97885
677.00	3.48876	3.10833	2.10443	1.43771	1.33215
815.89	4.18607	3.72746	2.56695	1.87290	1.76858
954.78	4.94915	4.41239	3.11131	2.40133	2.29903
1093.67	5.80564	5.19209	3.76749	3.05071	2.95099
1232.56	6.80060	6.11283	4.58227	3.86608	3.76934
1371.44	7.99250	7.23418	5.61534	4.90583	4.81239
1510.33	9.44843	8.62431	6.93475	6.23698	6.14707
1649.22	11.24532	10.36108	8.61810	7.93632	7.85013

LI-900 Analytically Predicted Conductivity Values in CO_2 - Strong Direction

Conductivity - cal/cm-sec-°C X 10^{-4}
Pressure - Atmospheres

T (°C)	1.0000	0.1000	0.0100	0.0010	0.0001
-156.33	0.68608	0.63610	0.58174	0.47073	0.36348
-17.44	1.17967	1.11355	1.00824	0.76641	0.62453
121.44	1.68818	1.59595	1.39849	0.97866	0.79526
260.33	2.17897	2.06115	1.75777	1.18867	0.98596
399.22	2.85006	2.68755	2.24478	1.52611	1.30758
538.11	3.69200	3.48330	2.89540	2.05414	1.82761
677.00	4.73817	4.48243	3.74880	2.80924	2.57961
815.89	6.00836	5.70538	4.82938	3.81292	3.58347
954.78	7.52873	7.17896	6.16694	5.09231	4.86533
1093.67	9.34058	8.94505	7.80571	6.68930	6.46647
1232.56	11.49452	11.05484	9.79872	8.65489	8.43746
1371.44	14.03325	13.55161	12.19064	11.03201	10.82095
1510.33	16.97239	16.45152	14.99871	13.83643	13.63250
1649.22	20.29555	19.73868	18.20789	17.05184	16.85566

Table C2 - Analytical Conductivity Data for FRCI-12 in CO_2

FRCI-12 Analytically Predicted Conductivity Values in CO_2 - Weak Direction

Conductivity - cal/cm-sec-°C X 10^{-4}
Pressure - Atmospheres

T (°C)	1.0000	0.1000	0.0100	0.0010	0.0001
-156.33	0.64412	0.59155	0.51900	0.38134	0.31076
-17.44	0.95943	0.88356	0.72375	0.47508	0.39790
121.44	1.42198	1.30592	1.00034	0.61948	0.52749
260.33	1.91820	1.75835	1.29881	0.82736	0.73017
399.22	2.55273	2.32409	1.67957	1.12458	1.02275
538.11	3.24261	2.94061	2.11668	1.50239	1.39889
677.00	3.96584	3.58758	2.59514	1.93995	1.83654
815.89	4.69405	4.23816	3.09128	2.40940	2.30722
954.78	5.40187	4.86842	3.58298	2.88561	2.78541
1093.67	6.07351	5.46387	4.05677	3.35283	3.25516
1232.56	6.70554	6.02227	4.51086	3.80762	3.71287
1371.44	7.30673	6.55352	4.95527	4.25868	4.16716
1510.33	7.89742	7.07898	5.41123	4.72625	4.63819
1649.22	8.51256	7.63454	5.91437	5.24516	5.16075

FRCI-12 Analytically Predicted Conductivity Values in CO_2 - Strong Direction

Conductivity - cal/cm-sec-°C X 10^{-4}
Pressure - Atmospheres

T (°C)	1.0000	0.1000	0.0100	0.0010	0.0001
-156.33	0.89397	0.84348	0.78489	0.66447	0.56840
-17.44	1.27502	1.20684	1.08788	0.83919	0.72036
121.44	1.81109	1.71369	1.48755	1.07218	0.92316
260.33	2.39316	2.26609	1.91916	1.37194	1.21006
399.22	3.12004	2.94281	2.44107	1.76512	1.59249
538.11	3.89647	3.66677	3.00682	2.22957	2.05196
677.00	4.69581	4.41222	3.59626	2.74099	2.56196
815.89	5.50902	5.17096	4.20521	3.29159	3.11347
954.78	6.37037	5.97808	4.87168	3.91631	3.74071
1093.67	7.37784	6.93231	5.69653	4.71350	4.54159
1232.56	8.36366	7.86662	6.51428	5.51564	5.34829
1371.44	10.00147	9.45536	8.00038	6.99649	6.83436
1510.33	11.87682	11.28475	9.74184	8.74166	8.58527
1649.22	13.98140	13.34710	11.73153	10.74285	10.59261

Table C3 - Analytical Conductivity Data for HTP-6 in CO_2

HTP-6 Analytically Predicted Conductivity Values in CO_2 - Weak Direction

Conductivity - cal/cm-sec-°C X 10^{-4}
Pressure - Atmospheres

T (°C)	1.0000	0.1000	0.0100	0.0010	0.0001
-156.33	0.80340	0.75535	0.69410	0.56765	0.48441
-17.44	0.86636	0.79907	0.66551	0.41315	0.31408
121.44	1.36268	1.26250	1.00217	0.59205	0.46971
260.33	1.98341	1.84809	1.44751	0.91952	0.78787
399.22	2.79541	2.60354	2.03050	1.39272	1.25361
538.11	3.70343	3.45152	2.70599	1.98562	1.84340
677.00	4.67883	4.36458	3.45239	2.67134	2.52864
815.89	5.70063	5.32289	4.25381	3.42978	3.28831
954.78	6.76704	6.32572	5.11215	4.25960	4.12053
1093.67	7.90572	7.40174	6.05783	5.18870	5.05286
1232.56	9.18346	8.61869	7.15975	6.28397	6.15198
1371.44	10.71551	10.09269	8.53476	7.66069	7.53302
1510.33	12.67501	11.99775	10.35726	9.49200	9.36901
1649.22	15.30346	14.57612	12.86971	12.01933	11.90132

HTP-6 Analytically Predicted Conductivity Values in CO_2 - Strong Direction

Conductivity - cal/cm-sec-°C X 10^{-4}
Pressure - Atmospheres

T (°C)	1.0000	0.1000	0.0100	0.0010	0.0001
-156.33	1.21229	1.16576	1.11561	1.01172	0.90427
-17.44	1.06353	1.00207	0.90446	0.66989	0.52199
121.44	1.56038	1.47468	1.29001	0.87379	0.67901
260.33	2.26646	2.15696	1.87102	1.29905	1.08163
399.22	3.25985	3.10886	2.68985	1.96238	1.72711
538.11	4.43978	4.24590	3.68744	2.83097	2.58643
677.00	5.73498	5.49740	4.79809	3.83695	3.58856
815.89	7.03409	6.75263	5.91492	4.87083	4.62224
954.78	8.18524	7.86026	6.88961	5.78183	5.53561
1093.67	10.59832	10.23078	9.13501	7.98054	7.73858
1232.56	13.50752	13.09888	11.88768	10.70156	10.46526
1371.44	16.94738	16.49963	15.18418	13.97971	13.75017
1510.33	20.93674	20.45239	19.04502	17.83402	17.61210
1649.22	25.47622	24.95823	23.47220	22.26521	22.05161

Table C4 - Analytical Conductivity Data for HTP-9 in CO_2

HTP-9 Analytically Predicted Conductivity Values in CO_2 - Weak Direction

Conductivity - cal/cm-sec-°C X 10^{-4}
Pressure - Atmospheres

T (°C)	1.0000	0.1000	0.0100	0.0010	0.0001
-156.33	0.87376	0.82036	0.74938	0.61082	0.53302
-17.44	0.88007	0.80422	0.64973	0.39202	0.30500
121.44	1.30136	1.18708	0.89101	0.48913	0.38447
260.33	1.80065	1.64502	1.19705	0.69324	0.58215
399.22	2.45410	2.23255	1.59961	1.00082	0.88407
538.11	3.16609	2.87443	2.05999	1.39223	1.27333
677.00	3.91551	3.55106	2.56429	1.84775	1.72878
815.89	4.68668	4.24817	3.10182	2.35236	2.23466
954.78	5.47755	4.96502	3.67404	2.90431	2.78880
1093.67	6.30652	5.72120	4.30189	3.52211	3.40944
1232.56	7.21855	6.56281	5.03221	4.25077	4.14141
1371.44	8.29094	7.56819	5.94371	5.16754	5.06185
1510.33	9.63922	8.85386	7.15297	6.38790	6.28617
1649.22	11.42414	10.58146	8.82153	8.07247	7.97493

HTP-9 Analytically Predicted Conductivity Values in CO_2 - Strong Direction

Conductivity - cal/cm-sec-°C X 10^{-4}
Pressure - Atmospheres

T (°C)	1.0000	0.1000	0.0100	0.0010	0.0001
-156.33	1.53045	1.47940	1.42485	1.31457	1.20317
-17.44	1.18496	1.11781	1.01391	0.77188	0.62249
121.44	1.56222	1.46919	1.27595	0.85279	0.65845
260.33	2.09288	1.97481	1.67864	1.10155	0.88592
399.22	2.85300	2.69070	2.25789	1.52509	1.29192
538.11	3.74098	3.53315	2.95751	2.09584	1.85361
677.00	4.70339	4.44934	3.72973	2.76372	2.51777
815.89	5.66096	5.36064	4.49980	3.45132	3.20526
954.78	6.50982	6.16373	5.16745	4.05584	3.81218
1093.67	8.18957	7.79882	6.67527	5.51755	5.27815
1232.56	10.19073	9.75697	8.51619	7.32739	7.09364
1371.44	12.53750	12.06290	10.71640	9.50983	9.28280
1510.33	15.24255	14.72981	13.29026	12.07770	11.85823
1649.22	18.30535	17.75767	16.23865	15.03061	14.81938

Table C5 - Analytical Conductivity Data for HTP-12 in CO_2

HTP-12 Analytically Predicted Conductivity Values in CO_2 - Weak Direction

Conductivity - cal/cm-sec-°C X 10^{-4}
Pressure - Atmospheres

T (°C)	1.0000	0.1000	0.0100	0.0010	0.0001
-156.33	1.90288	1.84997	1.77652	1.63786	1.56780
-17.44	1.31930	1.24275	1.08066	0.83138	0.75506
121.44	1.57585	1.45844	1.14868	0.76800	0.67714
260.33	1.93765	1.77566	1.31034	0.84008	0.74416
399.22	2.45902	2.22714	1.57531	1.02257	0.92211
538.11	3.04384	2.73740	1.90504	1.29397	1.19190
677.00	3.66459	3.28064	2.27902	1.62789	1.52594
815.89	4.29962	3.83677	2.68029	2.00318	1.90244
954.78	4.94222	4.40055	3.10536	2.41332	2.31455
1093.67	5.60555	4.98645	3.56968	2.87153	2.77526
1232.56	6.32546	5.63156	4.11076	3.41364	3.32026
1371.44	7.16222	6.39730	4.79007	4.09984	4.00965
1510.33	8.20269	7.37155	5.69537	5.01689	4.93012
1649.22	9.56564	8.67404	6.94607	6.28343	6.20026

HTP-12 Analytically Predicted Conductivity Values in CO_2 - Strong Direction

Conductivity - cal/cm-sec-°C X 10^{-4}
Pressure - Atmospheres

T (°C)	1.0000	0.1000	0.0100	0.0010	0.0001
-156.33	4.20096	4.15087	4.09662	3.98634	3.87924
-17.44	2.36110	2.29494	2.19043	1.95067	1.80909
121.44	2.37236	2.28026	2.08498	1.66897	1.48601
260.33	2.63293	2.51551	2.21597	1.65195	1.44974
399.22	3.16061	2.99882	2.56169	1.84886	1.63078
538.11	3.84480	3.63719	3.05674	2.22177	1.99563
677.00	4.61549	4.36126	3.63685	2.70379	2.47450
815.89	5.38789	5.08691	4.22175	3.21184	2.98267
954.78	6.07077	5.72349	4.72381	3.65566	3.42893
1093.67	7.36710	6.97457	5.84892	4.73882	4.51621
1232.56	8.90004	8.46389	7.22261	6.08487	5.86764
1371.44	10.69347	10.21588	8.87072	7.71792	7.50704
1510.33	12.75729	12.24096	10.80475	9.64802	9.44424
1649.22	15.08642	14.53458	13.02100	11.87018	11.67413

Table C6 - Analytical Conductivity Data for LI-2200 in CO_2

LI-2200 Analytically Predicted Conductivity Values in CO_2 - Weak Direction

Conductivity - cal/cm-sec-°C X 10^{-4}
Pressure - Atmospheres

T (°C)	1.0000	0.1000	0.0100	0.0010	0.0001
-156.33	0.85538	0.78112	0.67168	0.50176	0.43967
-17.44	1.36136	1.25190	1.02643	0.77183	0.71320
121.44	1.86549	1.69679	1.29631	0.94548	0.87999
260.33	2.30980	2.07755	1.50810	1.10086	1.03389
399.22	2.89369	2.56139	1.78759	1.32323	1.25364
538.11	3.54313	3.10490	2.14191	1.64034	1.56999
677.00	4.25312	3.70577	2.57241	2.04772	1.97772
815.89	5.00885	4.35160	3.06823	2.53074	2.46178
954.78	5.81108	5.04523	3.63261	3.09009	3.02262
1093.67	6.68975	5.81851	4.29714	3.75557	3.68993
1232.56	7.70253	6.73076	5.12056	4.58466	4.52109
1371.44	8.92137	7.85542	6.17555	5.64908	5.58775
1510.33	10.41704	9.26459	7.53335	7.01938	6.96044
1649.22	12.25860	11.02852	9.26331	8.76437	8.70793

LI-2200 Analytically Predicted Conductivity Values in CO_2 - Strong Direction

Conductivity - cal/cm-sec-°C X 10^{-4}
Pressure - Atmospheres

T (°C)	1.0000	0.1000	0.0100	0.0010	0.0001
-156.33	1.02357	0.95163	0.85495	0.68762	0.61049
-17.44	1.64786	1.54612	1.34937	1.07775	1.00117
121.44	2.23582	2.08465	1.72987	1.33769	1.25058
260.33	2.74839	2.54557	2.03076	1.56080	1.47086
399.22	3.38829	3.10109	2.38657	1.83796	1.74393
538.11	4.06175	3.68556	2.77982	2.17651	2.08109
677.00	4.73126	4.26341	3.18007	2.53991	2.44468
815.89	5.35178	4.79140	3.54697	2.88355	2.78953
954.78	5.91095	5.25879	3.87131	3.19521	3.10308
1093.67	6.45311	5.71142	4.19965	3.51924	3.42948
1232.56	7.08235	6.25474	4.63764	3.95965	3.87262
1371.44	7.94901	7.04033	5.33675	4.66668	4.58264
1510.33	9.23344	8.24968	6.47812	5.82052	5.73969
1649.22	11.15026	10.09848	8.27700	7.63565	7.55820

REPORT DOCUMENTATION PAGE

Form Approved
OMB No. 0704-0188

1. AGENCY USE ONLY *(Leave blank)*	2. REPORT DATE	3. REPORT TYPE AND DATES COVERED
	January 1993	Technical Paper

4. TITLE AND SUBTITLE
Prediction of Rigid Silica Based Insulation Conductivity

5. FUNDING NUMBERS
551-74-11-31

6. AUTHOR(S)
Stanley D. Williams and Donald M. Curry

7. PERFORMING ORGANIZATION NAME(S) AND ADDRESS(ES)
Lyndon B. Johnson Space Center
Houston, Texas 77058

8. PERFORMING ORGANIZATION REPORT NUMBER
S-687

9. SPONSORING / MONITORING AGENCY NAME(S) AND ADDRESS(ES)
National Aeronautics and Space Administration
Washington, D.C. 20546

10. SPONSORING / MONITORING AGENCY REPORT NUMBER
NASA TP-3276

11. SUPPLEMENTARY NOTES
Williams: Lockheed Engineering & Sciences Co., Houston, TX; Curry: Lyndon B. Johnson Space Center, Houston, TX.

12a. DISTRIBUTION / AVAILABILITY STATEMENT
Unclassified - Unlimited

Subject Category 34

12b. DISTRIBUTION CODE

13. ABSTRACT *(Maximum 200 words)*
A method is presented for predicting the thermal conductivity of low density, silica based fibrous insulators. It is shown that the method can be used to extend data values to the upper material temperature limits from those obtained from test data. It is demonstrated that once the conductivity is accurately determined by the analytical model the conductivity for other atmospheres can be predicted. The method is similar to that presented by previous investigators, but differs significantly in the contribution due to gas and internal radiation.

14. SUBJECT TERMS	15. NUMBER OF PAGES
Thermal Conductivity, Rigid Silica Insulation, Conductivity Prediction Technique	132
	16. PRICE CODE: A07

17. SECURITY CLASSIFICATION OF REPORT	18. SECURITY CLASSIFICATION OF THIS PAGE	19. SECURITY CLASSIFICATION OF ABSTRACT	20. LIMITATION OF ABSTRACT
Unclassified	Unclassified	Unclassified	Unlimited

National Aeronautics and
Space Administration
Code JTT
Washington, D.C.
20546-0001

Official Business

Penalty for Private Use, $300

BULK RATE
POSTAGE & FEES PAID
NASA
Permit No. G-27

POSTMASTER: If Undeliverable (Section 158 Postal Manual) Do Not Return